UNIVERSITY OF COPENHAGEN
NIELS BOHR INSTITUTE

SDC
The university partnership
Denmark – China

THE CISS EFFECT

PhD thesis
Sakse Dalum
December 30, 2019

Supervisor: Per Hedegård

This thesis has been submitted to the PhD School of The Faculty of Science, University of Copenhagen

THE CISS EFFECT

ABSTRACT

In recent years, a wide range of experiments have been done that show spin selectivity of electrons after they have passed through a layer of chiral molecules. This effect has been termed chiral-induced spin selectivity (CISS) and is the subject of this thesis. Several attempts have been made to explain the effect theoretically, but no consensus on the origin or mechanism has emerged. In this thesis, we derive a mathematical framework that aims to provide a foundation for a correct treatment of the effect. From simple arguments involving time reversal symmetry, the so-called no-polarisation theorem emerges. In essence, it says that the system must start in a non-thermal distribution, i. e. a distribution where states with the same energy are unequally populated. Some of the experiments involve transient effects, and we show that the same formalism that is used in steady state can be generalised in such a way that it can be used to make statements about the transient behaviour. In experiments involving magnetic leads, another phenomenon emerges. In this case, the equilibrium distribution of a magnetic lead coupled to a non-magnetic lead through a layer of chiral molecules changes non-trivially, when the magnetisation is flipped. Therefore, when a bias is applied, the system behaves differently for different orientations of the magnetic field.

The theory is investigated further by studying models of organic molecules. Here it is found that the polarisation can only reach a sizeable value, if the molecular spectrum contains levels that are close in energy, compared to the size of the coupling to the leads. It is shown that accidental degeneracies appear in the spectrum of polyacetylene, when the bonds between neighbouring atoms are twisted in such a way that it forms a helix. These degeneracies are shown to be a general feature of twisted chains of p-like orbitals. Similar features are shown to be present in a model of helicene.

DANSK RESUMÉ

I de seneste år har en lang række eksperimenter vist en udvælgelse af elektroner på baggrund af deres spin, efter de har bevæget sig gennem kirale molekyler. Denne effekt kaldes kiralinduceret spinselektivitet (eng.: chiral-induced spin selectivity, CISS) og er emnet for denne afhandling. Effekten har været forsøgt forklaret teoretisk af flere omgange, men der er endnu ikke opnået enighed omkring dens oprindelse eller mekanisme. I denne afhandling vil vi udlede en matematisk model, der forsøger at danne grundlag for en korrekt analyse af effekten. Fra simple argumenter vedrørende tidsomvendingssymmetri fremkommer et teorem, der sætter strenge krav til, hvilken form en teori for spin polarisering af elektroner kan tage. Grundessensen i teoremet er, at et system skal starte i en utermisk fordeling, dvs. en fordeling hvori tilstande med ellers samme energi ikke fremkommer med samme sandsynlighed. Nogle af eksperimenterne måler også transiente effekter og vi viser, at den samme formalisme, som vi har udviklet til at beskrive forventningsværdier i steady state, kan udvides til også at omfatte denne transiente opførsel. Et nyt fænomen gør sig imidlertid gældende for eksperimenter, der involverer magnetiske kontakter. I dette tilfælde viser vi, at for en magnetisk kontakt, der er koblet til en almindelig kontakt gennem et lag af kirale molekyler, skifter ligevægtstilstanden på en utriviel måde, når magnetfeltet ændres. Når en spænding påføres mellem de to kontakter, vil der derfor ikke løbe den samme strøm for de to magnetfeltsretninger.

Teorien udforskes dernæst ved at studere modeller af organiske molekyler. Hertil vises det, at der kun fremkommer en betydelig polarisering, såfremt at molekylets spektrum indeholder molekylære tilstande, hvis energier er forholdsvis tæt på hinanden, sammenlignet med størrelsen af koblingen til kontakterne. Det vises derudover, at udartninger forekommer i spektrummet for polyacetylen, når båndene mellem atomerne i kæden vrides, så molekylet tager form af en helix. Disse udartninger er en generel egenskab for vredet kæder af p-agtige orbitaler. Lignende egenskaber vises at gøre sig gældende for en model af helicen.

ACKNOWLEDGEMENTS

First of all I would like to thank my supervisor, Per Hedegård, for providing me with the opportunity and idea to start this project. It has been a tough journey sometimes, but your positive attitude towards science and research has given me inspiration to continue in the face of the many setbacks I have experienced.

I would also like to thank professor Xiaohui Qiu for hosting me during my stays in Beijing at the Nanoscience Center at the University of Chinese Academy of Science. Thank you to Junbo, Qin and Liang for our discussions and for including me in your lunch and dinner group during my stays. Also thanks to the other SDC PhD and Master students, in particular Christian, Christina, Joshua, Marina and Nina for our many discussions about the ups and downs of PhD life. Thanks to Jingtao Lü for hosting me during my three month stay in Wuhan at the Huazhong University of Science and Technology.

I have thoroughly enjoyed my time in the Condensed Matter Theory group in Copenhagen. During the hardest times, I could always look forward to having good food and discussions in the lunch club, and I would of course like to thank all present and past members. Thank you to Morten and Ida for good tea times in Vibenshuset, and a special thanks to Jens Rix for good company and helpful discussions about almost anything, both in Copenhagen and during our stays in China.

I would not have been able to complete this project without my family and friends who have provided me with moral support. In particular, I would like to thank Guiping for her love and support throughout this journey.

Finally, I would like to thank the Sino-Danish Center for Education and Research (SDC) for financing this project and providing me with the opportunity to spend twelve months of research in China.

CONTENTS

APPENDIX

LIST OF FIGURES

LIST OF TABLES

THESIS OVERVIEW

This thesis is a monograph of work that has been done between 2016 and 2019 on the subject of the chiral-induced spin selectivity effect (CISS). Many of the results presented here were published in Nano Letters in the summer of 2019[1], and part of the aim of this thesis is to give a more comprehensive and detailed description of those results. The thesis also contains results that have not yet been published. These include the results presented in the sections 2.4.3, 3.1.4, 3.1.5, 3.2.3, 4.2, and 4.3.

The thesis is divided into four chapters. The first chapter serves as an introduction to the history and concepts of chirality and as a comprehensive overview of most of the experiments related to the CISS effect. Section 1.1 is meant to provide the reader who is unfamiliar with the concept of chirality in chemistry with enough understanding to follow any arguments related hereto. In section 1.2 we delve into the experimental and theoretical history that lead to the discovery of the CISS effect. This is followed up in section 1.3 by a structured summary and discussion of most of the related experiments done in the past decade.

In chapter 2 we introduce the mathematical formalism that we use throughout the thesis. It starts in section 2.1 with a brief discussion of statistical averages and the density matrix and how to get an effective single-particle theory from a many-particle problem. In section 2.2 and 2.3 we introduce the scattering and initial state picture, respectively. These two pictures provide two different ways of describing transport through molecules. However, when considering steady state transport, they both reduce to the same effective equations. In section 2.4 we derive a general formula for the particle current in steady state, but also show that the same formalism can be generalised to encompass transient effects as well, if one includes a kind of virtual lead, related to the time-dependence. Section 2.5 extends this formalism to include spin currents and magnetic leads, and we arrive at general formulas for both the spin and particle currents for any number of magnetic or non-magnetic leads.

In chapter 3 we use the fact that the atomic spin-orbit coupling in organic molecules is weak. This allows us to derive an equation for the particle current in section 3.1 that is valid for weak spin-orbit interactions, in which the spin degrees of freedom have been traced out. It shows that if the electrons start in a thermal initial distribution, the particle current is the same when the polarisation is flipped. This is referred to as the no-polarisation theorem. If the electrons are not thermal, we can form a useful vector quantity that we call the $\vec{D}$-vector, which quantifies the direction along which the polarisation is largest. This construct is then used to show that the electrons that are photoexcited have different escape rates depending on their spin, which is consistent with the experiments. In section 3.2 the concept is extended to include the spin current. Here we find that the $\vec{D}$-vector has a partner, the $\vec{C}$-vector which describes precession of the spin as it moves through the molecule. These two constructs are used to understand a number of experiments, and the no-polarisation theorem is revisited in this regard. Finally, it is shown that when chiral molecules are sandwiched between a magnetic lead and a normal lead, the induced magnetisation in the normal lead due to the magnetic lead is not simply anti-symmetric, when the magnetic field is flipped, due to the presence of the chiral molecules. This non-trivial effect forms the basis for understanding experiments involving magnetic leads.

The thesis concludes with numerical models of organic molecules in chapter 4. In section 4.1 we study a model of twisted polyacetylene. It is found that the $\vec{D}$-vector only reaches a magnitude comparable to the values obtained in experiments, when the molecular spectrum contains almost degenerate levels. This is supported by considerations of the mathematical formula for the $\vec{D}$-vector, and it is found that at these degeneracies, the polarisation grows linearly with the length of the molecule. This result is consistent with experiments in which the length of the molecules was varied. Finally, in section 4.3 we find that the analysis carries over to a model of helicene, where the $\vec{D}$-vector is again enhanced near degeneracies.

1

INTRODUCTION

> *"I call any geometrical figure, or group of points,* chiral, *and say that it has chirality, if its image in a plane mirror, ideally realized, cannot be brought to coincide with itself. Two equal and similar right hands are homochirally similar. Equal and similar right and left hands are heterochirally similar or 'allochirally' similar (but heterochirally is better). These are also called 'enantiomorphs,' after a usage introduced, I believe, by German writers. Any chiral object and its image in a plane mirror are heterochirally similar."* — Lord Kelvin[2]

Symmetries play a fundamental role in many branches of science, their absence doubly so. In this thesis, we shall study the *lack* of so-called mirror symmetries and its effect on electrons at the molecular level. Before delving into the depths of the theory, we start off with a brief introduction to the relevant nomenclature.

1.1 CHIRALITY

In general, systems which lack mirror symmetry are referred to as *chiral*, named after the Greek word for hand, $\chi\epsilon\iota\rho$ (kheir), a term which was coined by Lord Kelvin and introduced into the literature in 1894 (the quote at the beginning of this chapter). The reason for this name originates with the everyday observation that, in some sense, the left and right hand of a person are similar. However, no matter how one orients one hand, it cannot be made to superpose upon the other. There is a similarity, though, which comes from the fact that when looked at in a mirror, the left hand would appear to have become a right and vice versa. That is, a mirrored left hand will superpose upon a right. We thus say that the *chirality* (or handedness) of a hand changes when looked at in a mirror. An object, such as the head of a person (in its most idealised form), however, does not have a handedness to it. In other words, a mirrored head will readily superpose upon its unmirrored self, and as such, we refer to it as *achiral*.

These notions are easily extended to the molecular level. I. e. some molecules exhibit handedness (chiral molecules) while others do not (achiral molecules). This is illustrated in Figure 1.1. The two molecules with opposite chirality are referred to as *enan-*

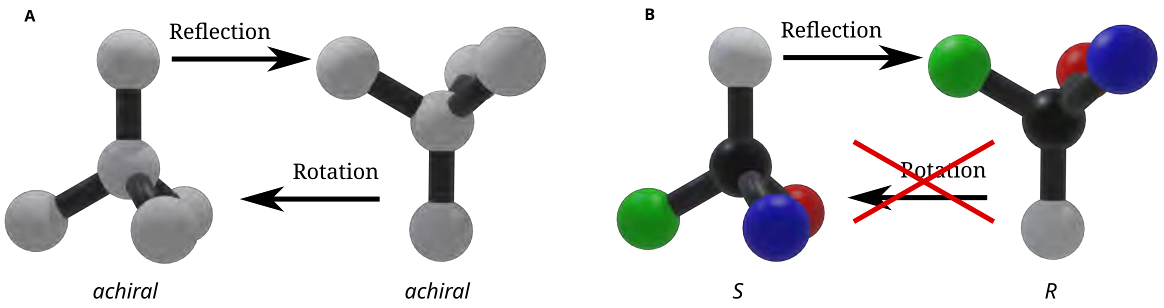

Figure 1.1: (A) An achiral molecule. After a mirror reflection, there exists a proper rotation that brings the molecule back to its original configuration. (B) A chiral molecule. By colouring the balls, there exists no proper rotation which brings the molecule back after a mirror reflection. If the masses of the balls are ordered as $m_{\text{white}} < m_{\text{red}} < m_{\text{green}} < m_{\text{blue}}$, the Cahn-Ingold-Prelog sequence rules would assign the names S and R to the enantiomers, as indicated by the letters below.

tiomers, a name derived from the Ancient Greek word for opposite, *ένᾰντῐ́ος* (enantíos). As with the naming convention of which side is right and which is left, there is some degree of arbitrariness as to how to name the two enantiomers of a given chiral molecule. One convention for this dates back to the discovery of chiral molecules by Louis Pasteur in 1848[3]. At the time, it was known from experiments by Jean Baptiste Biot in 1815, that certain organic compounds could rotate the polarisation of a beam of light either left or right, a property known as optical activity[3]. Pasteur found that by growing crystals of synthetically produced compounds, the faces of the crystal structures rotated either left or right, although the chemical formulæ of the compounds were the same. By dissolving the crystals and shining light on them, he was able to establish a connection between the shape of the crystals and the optical activity of the compounds. Because they did not have the necessary techniques or equipment at the time to determine the structure of the molecules, the two enantiomers were assigned different names based on their optical activity. According to this convention, one takes the cross-product of the incoming and outgoing polarisations, and if it is parallel to the light propagation, it is denoted D, and if it is anti-parallel, L. This notation comes from latin for right and left, *dexter* and *lævus*, respectively.

A more recent convention for naming enantiomers in organic chemistry are the so-called Cahn-Ingold-Prelog sequence rules[4]. In this convention, one can assign a handedness (or lack thereof) to each carbon atom in a molecule based on the distribution of the most massive atoms around it. The letters below the models in Figure 1.1B indicate the names that these rules would assign to the two enantiomers of the central carbon atom (black ball). The handedness is determined by using the common mnemonic conventions of the right-hand rule. That is, one orients the molecule such that the lightest side-group, in this case the white ball, points away from the viewer. If remaining side-groups are ordered in a counter-clockwise manner, from lowest to highest mass, the enantiomer is right-handed and assigned the letter R, from latin, *rectus*. If they are ordered in a clockwise manner, they are assigned S, again from latin, *sinister*, meaning left. In more complex molecules, there may be several carbon atoms, so-called *stereocentres*, for which a handedness can be defined. The various configurations are known as *stereoisomers*. The enantiomer of a given chiral molecule is thus the stereoisomer for which the handedness of each stereocentre has been flipped. Finally, when the molecule has a so-called helical or axial chirality, i. e. the molecule looks like a screw, the enantiomers are denoted M and P for *minus* and *plus*, respectively. This is the case for the class of molecules known as helicenes, that we are going to encounter later.

Mathematically, a mirror reflection followed by a rotation is known as an improper rotation. Note that if the rotation axis is in the mirror plane, it is equivalent to simply rotating the mirror by half the angle around that axis. Thus, it is sufficient to consider only rotations around an axis that is perpendicular to the mirror plane to describe all improper rotations. We denote improper rotations by the symbol, S_n, after the German word for mirror, *Spiegel*. The subscript, n, denotes the fraction of a full turn by which it rotates around the rotation axis, i. e. the angle of rotation is given as $\theta = 2\pi/n$. We can now say that a molecule, denoted m, is achiral if there exists an improper rotation such that $S_n m = m$. On the other hand, if no such improper rotation exists, it is chiral. The set of all operators, S_1, describe all possible mirror planes, typically denoted σ, while the S_2's are the set of all point inversions, denoted i.

1.2 HISTORY

When Pasteur discovered the chirality of molecules in 1848, he also discovered that naturally occuring tartaric acid were all of the D-type[5]. Later on, it was found that several other molecules involved in organic life on Earth are chiral. An example of this is DNA, which in living organisms is found to form a right-handed double helix. Another example is the amino acids that make up the proteins in living cells, which are all-but-one enantiomers of the L-type. The question of why is often referred to as the asymmetry of life. In 1961, Ulbricht and Vester, tried to shed some light on the problem[6]. Previous experiments at the time had found that by exposing molecules to circularly polarised UV light, the decay rate of the two enantiomers differed. Since Lee and Yang had shown that the β-decay of atomic nuclei produced spin polarised electrons, a discovery for which they were awarded the Nobel Prize in 1957, it was suggested that the asymmetry of life could find its origin in the circularly polarized *bremsstrahlung* emitted by these electrons. Thus, Ulbricht and Vester set out to test this hypothesis by exposing various chiral molecules to bremsstrahlung from β-decay, but found no significant result. In 1968, however, an article was published in the magazine Nature in which the author, Garay, had obtained positive results[7]. Garay had observed a significant difference in the decay of the two enantiomers of the amino acid tyrosine, when left together with the radioactive isotope, Strontium-90. Although a mechanism could not be determined, it was suggested that, perhaps, it was not the bremsstrahlung, but the polarised electrons themselves which were the source of the differential decay. This hypothesis was first confirmed by a subsequent experiment in 1975 by a group at Stanford using a linear accelerator[8], but was later disputed in a more extensive study in 1979[9].

These experiments inspired Farago, in 1980, to study the general problem of electron scattering from chiral molecules using symmetry arguments[10]. Farago found that there was nothing, in principle, which prohibited the scattered electrons from becoming spin polarised, if the target was chiral, but did not predict the magnitude of the effect, leaving it for experiments to determine. In particular, Farago proposed that there should be a spin asymmetry in the transmission of a beam of electrons with opposite spin polarisation, given by the equation:

$$A(P) = \frac{I(P) - I(-P)}{I(P) + I(-P)}, \tag{1.1}$$

where A is the asymmetry factor, P is the polarisation of the incoming electron beam in one orientation and I is the beam intensity. This effect was termed *electron dichroism*. Although the first follow up experiment could not measure any significant polarisation[11], in 1987, Campbell and Farago reported on a study[12] of gas-phase chiral molecules (the two enantiomers of camphor, $C_{10}H_{16}O$) in which the effect was of the order of $\sim 10^{-4}$ for beams with incoming polarisation, $P \approx 0.28$. The measured effect was small, but significant according to their error estimates.

Eight years later, in 1995, attempts to reproduce these results with more accurate equipment were unsuccessful, and concluded that the results for camphor in Campbell and Farago's experiments must have had been due to systematic errors[13]. In the same study, however, they found a significant effect for a compound containing the much heavier element, Ytterbium, known as $\mathrm{Yb(hfc)}_3$, chemical formula $C_{42}H_{45}F_{21}O_6Yb$, and thus claimed to have made the first true experimental verification of electron dichroism. The effect they measured was still of the order $\sim 10^{-4}$, and was supported further by experiments done by the same group for similar compounds, published in 1997[14].

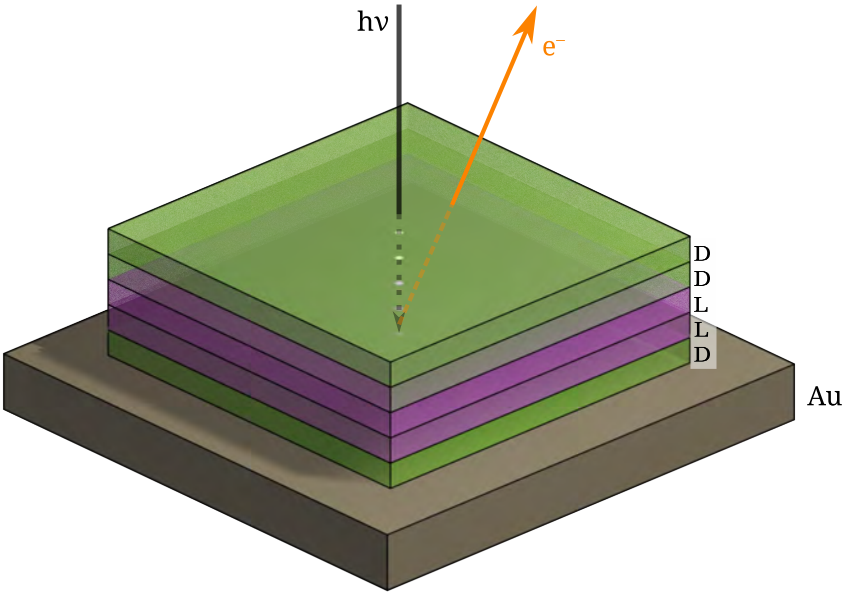

Figure 1.2: Illustration of the experimental setup of Ray et al. (1999). The figure shows a 1D2L2D sandwich, illuminated by a laser which ejects electrons from the gold surface. To reach the detector, the electrons must travel through all five layers of the sandwich.

Intuitively, and supported by a theoretical investigation into scattering from chiral molecules using a continuum model[15], the polarisation of scattered electrons were expected to depend on the scattering angle. Thus, it was suggested that experiments on highly oriented molecules, rather than the random orientation that the molecules had in the gas phase, could lead to a significant enhancement of the effect. This inspired Ron Naaman and David Waldeck to attempt to show this effect by studying the scattering of electrons through sandwiches of self-assembled monolayers (SAMs) of the chiral molecule stearoyl lysine[16]. The experimental setup for this is sketched out in Figure 1.2. Note that stearoyl lysine is an organic compound with no heavy elements. The results, published in 1999, suggested that the polarisation effect of these highly oriented molecules indeed was much larger[17]. They measured an asymmetry of $|A| \approx 0.12$ for a polarization of $P \approx 0.18$ of the incoming electrons, three orders of magnitude larger than previous studies, for homochiral sandwiches. In addition, for heterochiral sandwiches, i. e. layers of SAMs with opposite chirality, they found a decrease in the total quantum yield.

To understand this last result, we can use a very crude model with differential transmission of spin species through a single chiral monolayer. Let,

$$t_{D,\uparrow} = t_{L,\downarrow} = t_{(+)}, \quad t_{L,\uparrow} = t_{D,\downarrow} = t_{(-)}, \tag{1.2}$$

where, for instance, $t_{D,\uparrow}$ is the transmission probability through a D-layer for an electron with spin up, and $t_{(\pm)}$ is the transmission probability of an electron with spin favoured or unfavoured by the layer, respectively. Note that in this crude model, we are assuming that the spin is not rotated during transmission, and that electrons that are not transmitted are, in a sense, lost. The relative intensity of the transmission of an initially unpolarised electron beam, through a sandwich of N_D layers of D-enantiomers and N_L layers of L-enantiomers is thus given by:

$$\frac{I(N_D, N_L)}{I_0} = \frac{t_{(+)}^{N_D} t_{(-)}^{N_L} + t_{(-)}^{N_D} t_{(+)}^{N_L}}{2}. \tag{1.3}$$

Now, since $t_{(+)}$ is the expected relative intensity of a transmitted electron beam for fully polarised ($P = 1$) electrons, we can relate the ideal asymmetry of a single layer to the spin transmissions, through:

$$A = \frac{t_{(+)} - t_{(-)}}{t_{(+)} + t_{(-)}} = \frac{f-1}{f+1}, \quad \text{where} \quad f = \frac{t_{(+)}}{t_{(-)}}. \tag{1.4}$$

The relative beam intensity of a sandwich with a variable composition of layers to one with only D-monolayers is then found to be:

$$\frac{I(N_D, N_L)}{I(N_D + N_L, 0)} = \frac{f^{N_D} + f^{N_L}}{f^{N_D + N_L} + 1}. \tag{1.5}$$

Using the reported experimental values of the relative quantum yield of 5L and 3D2L sandwiches, we extract an asymmetry factor of a single layer of $|A| \approx 0.2$, for fully polarised electrons. Note that this value is smaller than the one reported in their paper, where they used the transmission cross-section rather than the intensity to arrive at a larger asymmetry factor of 0.7.

In 2002 results were reported by the same group for SAMs of polyalanine with lengths of 16 to 22 amino acids[18]. In this study, it was found that the polarisation not only changed sign with the handedness of the amino acids, but also changed when the other end of the peptide was connected to the substrate. It was thus proposed that the mechanism was related to the electric dipole of the peptides and consequent charge transfer from the SAM to the substrate. This seemed further supported by results in 2003 which showed that the contact potential difference (CPD) varied and changed sign as a function of temperature, and that the spin polarisation was correlated with this sign inversion of the CPD[19]. Thirteen years later, further studies into this effect found that the change in CPD was caused by a major structural change of the peptides at these temperatures, which led to a sign flip of the dipole[20].

The same group published studies on DNA in 2006, in which they compared SAMs of single-stranded DNA (ssDNA) and double-stranded DNA (dsDNA)[21]. While it was found that dsDNA also exhibited significant asymmetry in the transmission of electrons with opposite polarisation, ssDNA did not show any measurable effect. This was attributed to the highly unorganised layers formed by ssDNA which lack the rigid structural backbone of dsDNA. This was followed up in 2011 with a paper in the magazine Science that sparked a greater interest in the general field[22]. In this paper, they directly measured the spin of the electrons after they had passed through a SAM of dsDNA, and confirmed that there was a large polarisation of the transmitted electrons, even for an unpolarised laser beam. The effect was found to depend roughly linearly on the length of the DNA molecules and reached as high as 60% for the longest chains, 78 base pairs long. A complementary study was published the same year with conduction measurements through dsDNA adsorbed on a magnetised nickel substrate[23]. Each dsDNA molecule was connected to a single 10 nm gold nanoparticle on the other end, and an AFM tip was used to ensure that transport was measured through a single molecule-nanoparticle complex. Although they could not determine the polarisation of the transmitted electrons, they measured a significant difference in the current when the substrate was magnetised either towards or away from the dsDNA. This effect was attributed to an effective spin-dependent barrier of about 1 eV. Combined, the experiments were taken as evidence that transmission through chiral molecules is spin-dependent, which led Ron Naaman & David H. Waldeck to coin the term *chiral-induced spin selectivity* (CISS) for the effect, distinguishing it from Farago's electron dichroism.

Three different theoretical models were proposed in the immediate aftermath of the two papers mentioned above[24–26]. Common to all three was the reliance on some form of *spin-orbit coupling* (SOC). This coupling can be understood by considering the potential energy of a magnetic moment, $\vec{\mu}$ in a magnetic field, $\vec{B}$,

$$V = -\vec{\mu} \cdot \vec{B}. \tag{1.6}$$

If the electron orbits a nucleus, it carries two magnetic moments: one related to its intrinsic spin, $\vec{\mu}_S$, and one related to its charge as it orbits the nucleus, $\vec{\mu}_L$. Now, in the rest frame of the electron, where it has zero angular orbital momentum, it will appear as if the positively charged nucleus is orbiting the electron. From the point of view of the electron, this is itself a source of a magnetic field with a coupling to its spin angular momentum of the form in Eq. (1.6). Thus, in the laboratory rest frame, we find an effective coupling between the spin and orbital components of its magnetic moment,

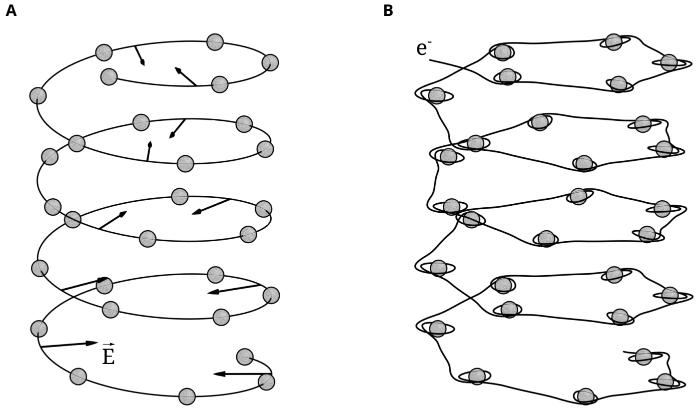

Figure 1.3: (A) Model of the chiral electric field felt by an electron moving through a helix due to the electron seeing a higher concentration of nuclei towards the helix centre. (B) As the electron moves through the helix, the strongest electric fields it experiences, and thus the strongest source of spin-orbit coupling, are those it sees when orbiting the nuclei.

which we refer to as the *atomic* spin-orbit coupling. Mathematically, the interaction is described by:

$$H_{\mathrm{SO}} = \frac{2\lambda}{\hbar^2}\vec{L}\cdot\vec{S}, \tag{1.7}$$

where λ is a constant describing the interaction strength, $\vec{L}$ and $\vec{S}$ are the electronic angular momentum and spin operators, respectively, and $\hbar$ is the reduced Planck's constant. For the p-orbitals in a carbon atom, λ is around 6 meV.

This idea can be extended to an electron moving in any electrostatic field, and one finds a spin-orbit interaction of the form:

$$H_{\mathrm{SO}} = \frac{e\hbar}{4mc^2}(\vec{v}\times\vec{E})\cdot\vec{\sigma}, \tag{1.8}$$

where e is the elementary charge, c is the speed of light, m is the mass of the electron, $\vec{v}$ its velocity, and $\vec{E}$ is the electric field. Considering the shape of a helix or cylinder, there is an electric field pointing from the edge towards the centre. This is illustrated in Figure 1.3A. An electron moving along a helical pathway in such an electric field would experience an energy splitting dependent on whether its spin was aligned parallel or anti-parallel with the helix. This is also known as a Rashba-type spin-orbit interaction. Now, the photoexcited electrons in the experiments have kinetic energy of about 1 eV, which corresponds to a velocity of

$$v = \sqrt{\frac{2E_{\mathrm{kin}}}{m}} \approx 0.2\% \text{ the speed of light.}$$

The electric field of a single charge at a distance of 1 Å is $|E| \approx 1.4 \times 10^{11}$ V/m. This scales as r^{-2} and is thus much weaker for atoms further away. In addition, the cores of those atoms are screened by bound electrons which means that, effectively, they do not present a full unscreened charge for the propagating electron. Even in a gratuitous model, where the helix does present an effective charge, 1 Å away, we find an energy splitting of:

$$\Delta E_{\mathrm{SO}} \approx \frac{e\hbar}{mc} \times (1.4 \times 10^{8}\ \mathrm{V/m}) \approx 56\,\mu\mathrm{eV}.$$

This effect is thus more than a hundred times weaker than the atomic SOC of a carbon atom.

In two of the theoretical models that followed the papers in 2011, the spin-orbit interaction used was of the type above—an electron moving in the electric field of a helix. In order to reach reasonable values for the spin polarisation, such models have to assume much larger values for the spin-orbit coupling than what the calculation above gives. Thus, for the model to have explanatory power, one has to account for how such an effect can be enhanced. We shall not attempt to do so here. Instead, we shall make the claim that any model which attempts to explain the experiments on spin selectivity must use the atomic SOC as its basis, which is shown illustratively in Figure 1.3B. This fact was also pointed out by Medina et al.[26] in their paper, in which they studied scattering of a normalised electron wave packet from a helix of six carbon atoms with atomic SOC. In their study, they could reach polarisations up to 1% for specific parameters of the model, without tuning the SOC parameter. Their model, however, could only handle a few atoms.

1.3 REVIEW OF CISS EXPERIMENTS

Inspired by the initial reports, a wealth of new experiments on the CISS effect started to emerge. In this section, rather than list the experiments in chronological order, as was done in the previous section, we shall group them according to the experimental methods used in an attempt to systematise them. Because the experiments use many different methods in which electrons are transported through molecules in both directions, we shall adopt the notation P, for parallel, when an electron is travelling in the direction that its spin is pointing and AP, for antiparallel, when it points in the opposite direction.

Broadly speaking, the experiments can be categorised into four different classes: photoemission, photoexcitation, transport and electrochemistry. They each characterise different aspects of spin polarised transport through chiral molecules at different energy scales. To compare these experiments, we will outline the different experimental methods in the following subsections, and summarise the results in tables with the relevant measured quantities. It is worth noting at this point that some molecules have been studied using several different experimental methods, as well as by different groups. These experiments are largely consistent in the sense that the sign of the polarisation always changes when the opposite enantiomer is used. The different methods have different ways of calculating the polarisation, however, and thus the sign is not always the same for the same molecule across experiments. At the end of this section, we shall remark upon the most striking features across the various methods.

1.3.1 *Photoemission*

In the first class, we find most of the experiments discussed in the previous section. Here, a laser is shun at a substrate (typically copper, silver or gold) to excite electrons above its work function, which is generally around 5 eV[27]. The HOMO states of the molecules being studied are typically a few eV below the Fermi level, and thus their ionization energy is generally around 7 eV. This thus leaves a window in between for the laser energy, where one ensures that electrons are excited to the vacuum level only from the substrate. After the electrons have been excited to the vacuum level, they are slowly accelerated through a weak electric field and brought to the analyser.

Photoemission experiments generally come in two forms. The first makes use of the fact that when shun upon by circularly polarised light, the photoelectrons emitted from a gold substrate are spin polarised. For a bare, single crystal, this polarisation is around 15% and changes sign when the circular polarisation of the light changes[22]. Thus, when the substrate is covered by organised chiral molecules, exciting photoelectrons in the substrate produces a polarised beam of electrons which passes through the molecular layer. By using a time-of-flight spectrometer, the kinetic energy distribution and total intensity of the transmitted electron beams can be analysed and compared. The experimental results of these kinds of photoemission experiments, with an asymmetry factor calculated using in Eq. (1.1), are summarised in Table 1.1.

In the second form, the electrons are analysed by using a Mott polarimeter. The technique, first proposed in the late 1920's by Nevill Mott and Niels Bohr[28] as a way to measure the existence of spin in free electrons, uses the fact that the scattering angle of electrons from heavy atoms depends on their spin component orthogonal to their direction of motion[29]. By accelerating the electrons to 10–300 keV and bending the beam by 90° using an electrostatic lens, the electrons are then shot directly at a thin gold foil target and scattered into detectors placed at equal angles from the foil. This is shown

Table 1.1: Asymmetry factor measured in photoemission experiments of the first kind given in percentages. Unless otherwise indicated, the experiments were performed at room temperature.

Year	Author(s)	Molecule	Substrate	asymmetry
1999	Ray et al.[17]	5L-stearoyl lysine	Au	11
		5D-stearoyl lysine		−13
2002	Carmeli et al.[18]	C-terminated poly(D-alanine)	Au	−9
		N-term. poly(D-alanine)		10
2003	Carmeli et al.[19]	C-term. poly(L-alanine)	Au	9
		C-term. poly(L-alanine)[a]		−11
2006	Ray et al.[21]	ssDNA	Au	0
		dsDNA		−8
2011	Göhler et al.[22]	50-bp dsDNA	Au	−7

[a] this experiment was conducted at 250K

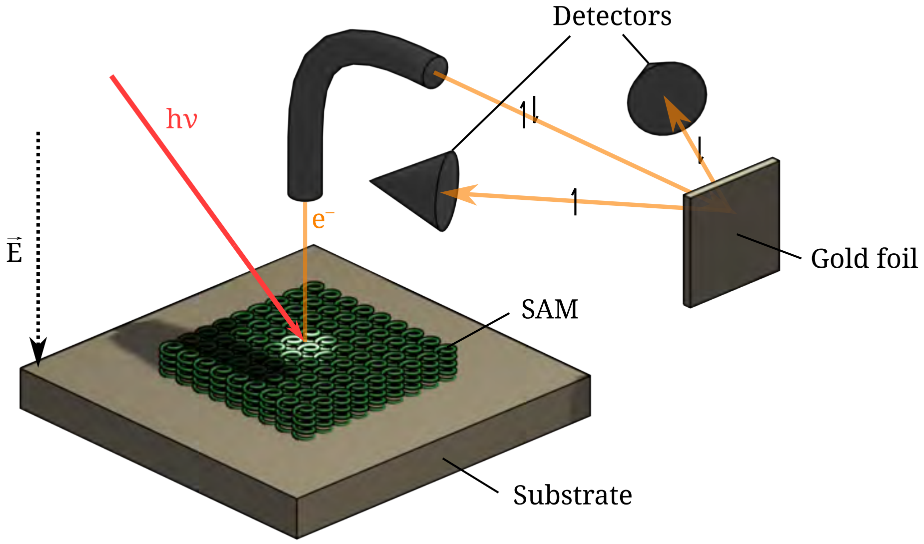

Figure 1.4: Model of the photoemission experiments analysed using a Mott polarimeter. Electrons are excited in the substrate using a laser and then accelerated up and bent by 90° before experiencing spin-dependent scattering from a gold foil.

Table 1.2: Polarisation measured in photoemission experiments for different polarisations of light. All polarisations are given as percentages.

Year	Author(s)	Molecule	Substrate	ccw.	lin.	cw.
2011	Göhler et al.[22]	50-bp[a] dsDNA	Au(111)	−29	−31	−35
		40-bp dsDNA	Au(poly.[b])	−40	−38	−35
		50-bp dsDNA		−39	−36	−32
		78-bp dsDNA		−61	−57	−55
2013	Mishra et al.[30]	Bacteriorhodopsin	Au(poly.)	8	14	17
			Al(poly.)	15	15	15
2015	Kettner et al.[31]	AL5 oligopeptide	Au(poly.)	−17	−11	−6
		AL6 oligopeptide		−20	−14	−10
		AL7 oligopeptide		−22	−18	−14
2018	Kettner et al.[27]	M-helicene	Cu(332)	−6	−7	−6
		P-helicene		11	12	12
		M-helicene	Ag(110)	−7	−9	−12
		P-helicene		6	7	6
		M-helicene	Au(111)	22	−8	−35
		P-helicene		34	8	−16
2019	Ghosh et al.[32]	L-CuO film (20 nm)	Au(111)	–	−12	–
		D-CuO film (20 nm)		–	4	–

[a] bp stands for base pair.
[b] poly. stands for polycrystalline

in Figure 1.4. A comparison of the beam intensity into the two detectors thus gives an asymmetry factor as before. By calibrating the detectors against a known source of spin, one can thus measures the polarisation of the beam to a high accuracy. This method allows direct detection of the polarisation of the electron beam along one axis, but does not provide the energy resolution that one gets from time-of-flight measurements. Experiments of this kind are summarised in Table 1.2.

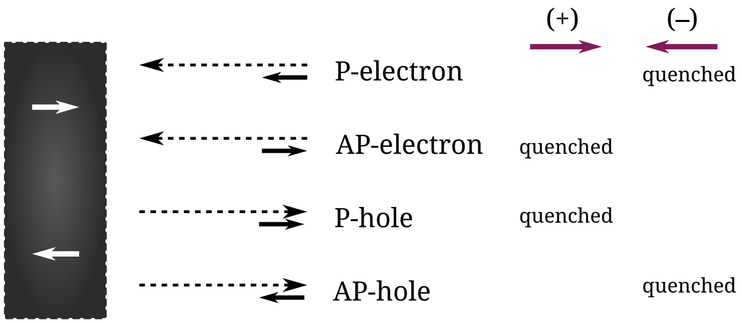

Figure 1.5: The various configurations of electron and hole transport in photoexcitation experiments. The dashed arrow indicate the direction in which the electron moves, and the small arrow indicates its direction of spin, either parallel or anti-parallel to its motion. On the right, the magnetic field direction for which the photoluminescence is quenched is indicated for each configuration.

1.3.2 *Photoexcitation*

Although similar sounding to photoemission, the photoexcitation experiments use a lower energy laser in the range of visible light to excite an electron-hole pair in a chromophore (a nanoparticle or dye) attached to a chiral molecule. If transport of the electron or hole is affected by its spin, this will influence various properties of the system. Three different kinds of photoexcitation experiments exist. In the first kind, the photoluminescence of the system is measured, i. e. the system is excited with a laser at a specific energy and its emission spectrum due to recombination is recorded. The molecules are adsorbed on a thin ferromagnetic substrate, typically nickel, and because some of the excited electrons or holes will be transported to the substrate, the emission spectrum will be quenched, as the energy will dissipate in the substrate instead. By putting the substrate close to a permanent magnet, it becomes magnetised perpendicular to the plane, and thus the density of states and therefore coupling of the molecule to the substrate depends on spin.

Note that there are two competing mechanisms at play in these experiments related to the charge carriers. One effect is the preferred transport of either electrons or holes while the other is the preferred transport of spin. If transport is dominated by P-electrons, that is, spin-down electrons transported from the chromophore to the substrate, the intensity will be most quenched by a downward pointing magnetic field, as illustrated in Figure 1.5. Similarly, AP-electrons will show higher quenching with an upward pointing magnetic field. On the other hand, if transport is dominated by holes, the quenching effects are reversed.

Table 1.3: Laser energy and polarisation in photoexcitation experiments measured using photoluminescence.

Year	Author(s)	Molecule	Energy [eV]	Pol. (%)
2016	Mondal et al.[33]	Ala8-CdSe	2.4	-10
2016	Roy et al.[34]	Bacteriorhodopsin	2.4	-17
2017	Abendroth et al.[35]	dsDNA-PDI	2.3	0.2

The quantity we are interested in is the polarisation of the transported electrons, for comparison with other experiments. Assuming a crude model in which an electron is either transported to the substrate or recombines with its hole partner, the intensity of the photoluminescence can be related to the probability for an electron to be transported to the substrate through:

$$\frac{I}{I_0} = 1 - t, \tag{1.9}$$

where t is the transmission probability, I is the photoluminescence intensity and I_0 is the intensity one would measure for the bare molecule, uncoupled to the substrate. Note that, by definition, $I_0 \geq I$, but it is otherwise an undetermined quantity from the experiments. Assuming I_0 to be spin-independent, the transmission polarisation can then be calculated as:

$$P = \frac{t_{\mathrm{P}} - t_{\mathrm{AP}}}{t_{\mathrm{P}} + t_{\mathrm{AP}}} = \frac{I_{\mathrm{AP}} - I_{\mathrm{P}}}{2I_0 - I_{\mathrm{P}} - I_{\mathrm{AP}}}. \tag{1.10}$$

Since the experiments do not provide a measure for I_0, we have to guess its value. Typically, the polarisation reported in these experiments is defined as:

$$P = \frac{I_+ - I_-}{I_+ + I_-}. \tag{1.11}$$

This is equivalent to choosing $I_0 = I_{\mathrm{P}} + I_{\mathrm{AP}}$ and assuming that electrons are the charge carriers, in which case $I_{\mathrm{AP}} = I_+$, i. e. the intensity with the magnet pointing up. If the charge carriers are holes, however, $I_{\mathrm{AP}} = I_-$, and the sign of the polarisation changes. The measured polarisations for experiments of this kind a listed in Table 1.3. Unfortunately, these experiments do not provide a way to measure the type of carrier. This problem can be overcome by the second kind of photoexcitation experiments, described below.

The second kind of experiments are rather similar, but instead of coupling the molecules directly to the nickel substrate, a silver and dielectric (AlO_x) layer is put in between. To balance out the current flow from the molecules to the silver during steady state, an electrostatic potential builds up which involves charge transfer between the nickel and

Table 1.4: Laser energy and polarisation in photoexcitation experiments of the second kind.

Year	Author(s)	Molecule	Carriers	Energy [eV]	Pol. (%)
2013	Kumar et al.[36]	30-bp dsDNA	holes	2.3	0.8
		40-bp dsDNA			1.2
		50-bp dsDNA			1.6
2014	Carmeli et al.[37]	Photosystem I	holes	1.9	−8.0
		Photosystem I[a]	electrons		4.0

[a] in this experiment, the substrate was connected to the opposite end of the molecule.

silver layers across the dielectric. This potential can be measured by measuring the voltage between the two layers. As in the photoluminescence experiments, the voltage is reduced when it is easy for the electrons or holes to tunnel across the dielectric, which is proportional to the density of states in the magnet. Thus, we have to face the same problems related to quenching as mentioned above. In these experiments, though, the sign of the voltage indicates which type is the predominant charge carrier. If electrons are the primary ones, negative charge will accumulate in the silver layer leading to a negative voltage. On the other hand, if transport occurs mainly by holes, negative charge will flow away from the silver leading to a positive voltage. As before, we are faced with the issue of translating the voltage into a polarisation of the transmitted electrons. Thus, the polarisation in these experiments is by convention defined as

$$P = \frac{V_+ - V_-}{V_0}, \tag{1.12}$$

where V_+, V_- are the voltages for the magnetic field pointing either up or down, respectively, and V_0 is the voltage without a magnetic field. It is worth noting that experiments of this kind find an increase in polarisation as the temperature is decreased, likely due to temperature dependent loss of spin coherence in the substrate. Additionally, these experiments also show a roughly linear increase in the effect with the magnetic field strength.

In the third and final kind of photoexcitation experiments, no external magnet is applied. Rather, the molecules are adsorbed on a thin ferromagnetic substrate which becomes locally magnetised when spins are injected from the chiral molecules. This thin layer is put on top of a Hall probe which is used to measure the effective generated magnetic field, by calibrating the device against an externally applied one. Now, the magnetic field through the Hall bar for the external magnet is H_{ext}.Note that in these experiments, we can again not tell the difference between transport of P-electrons and AP-holes in the sign of the magnetic field.

To get an idea of how polarised the electrons in these experiments are, we now calculate the magnetic field resulting from a distribution of electrons lying in a plane. For simplicity, we choose a cylindrical coordinate system such that the plane is the xy-plane and the electrons are placed a distance a above the plane with their spin pointing in the positive z-direction. The magnetic moment of the electron's spin is given by $\vec{\mu} = g\mu_B\vec{S}/\hbar$, where μ_B is the Bohr magneton, g is the electron's spin g-factor and $\vec{S}$ is its spin. Now, $g \approx 2$, and for a spin-up electron, $S/\hbar = 1/2$, so the magnetic field from a single electron through the plane in the z-direction is:

$$B(r, z = 0) = \frac{\mu_B\mu_0}{4\pi}\left[\frac{3a^2/(a^2+r^2)-1}{(a^2+r^2)^{3/2}}\right], \tag{1.13}$$

where μ_0 is the vacuum permeability. Note that, since we are dealing with a dipole, the field measured at the plane is the same, independent of whether we place the spin above or below it. If we naïvely assume all the electrons to lie in an infinite plane with a constant dipole density, ρ_d, the field in the z-direction at any given point a distance a above or below the electrons is given by:

$$B = 2\pi\rho_d\int_0^\infty B(r)rdr = \rho_d\frac{\mu_B\mu_0}{2}\int_a^\infty\left[\frac{3a^2}{x^4}-\frac{1}{x^2}\right]dx = 0, \tag{1.14}$$

where we have made the substitution, $x = \sqrt{a^2+r^2}$ to solve the integral in the second equality. This result for an infinite plane is due to the demagnetising effects of the other electrons. Thus, such a simple model is not sufficient to describe the magnetic field from the electrons.

If we treat the electrons by their discrete nature, the magnetic field near a single dipole is not entirely cancelled, however. If we ignore the demagnetising effects of the other electrons, we get an upper bound for the field strength by evaluating Eq. (1.13) for $r = 0$, i. e. right below the dipole. In the experiments, the 2DEG is reported to lie about $20\,\text{nm}$ inside the substrate. There are impurity sites in the substrate, however, into which the electrons might tunnel, so in a gratuitous model, the electrons might get as close as $1\,\text{nm}$ to the 2DEG. With this assumption, the magnetic field from the injected electrons would be around

$$B_0 \sim 1\,\text{mT},$$

if we ignore the demagnetising effects of the other electrons, and assume that the electrons can tunnel to within $1\,\text{nm}$ of the 2DEG. Table 1.5 lists the effective H-field induced by the spins being transported through the molecules. We see that the results

Table 1.5: Laser energy and effective magnetic field in photoexcitation experiments using a Hall probe.

Year	Author(s)	Molecule	Energy [eV]	H_{eff} [mT]
2014	Ben Dor et al.[38]	AHPA-L	2.3	28.0
2016	Eckshtein-Levi et al.[20]	Polyala.-COOH (300K)	2.4	2.0
		Polyala.-COOH (120K)		−0.5
		Polyala.-PO_4 (300K)		7.0
		Polyala.-PO_4 (120K)		−0.8

for polyalanine are on the order of one mT, and are therefore not inconsistent with this mechanism. The experiment on AHPA-L experiment, on the other hand, is twenty times larger. Taking into account the fact that the density of molecules is reported to be around $10^{-13}\,\text{cm}^{-2}$, corresponding to one every ten square nanometres, it is implausible that the measured effective magnetic field could originate from the injected spin alone. Therefore, some other mechanism must be in play in the substrate which leads to an enhancement of the Hall effect. We discuss the possibility of such a mechanism a little later, but it is beyond the scope of this thesis to give a detailed explanation of this enhancement.

1.3.3 *Transport*

A third class of experiments is based on transport measurements. Here, a device is made which consists of chiral molecules sandwiched between two leads, one of them being ferromagnetic, i. e. nickel. This class of experiments come in two variations. In the first, a permanent magnet is used to magnetise the nickel and the current through the device as a function of bias voltage (I-V curve) is measured. Depending on the direction of the magnetic field and the chirality of the molecules, the current is either enhanced or suppressed. Unlike the photoexcitation experiments, the current here, typically on the order of a few nA, is proportional to the transmission probability, and because the bias is applied externally, there are no signs creeping in due to carrier type. Thus, the polarisation at a given bias voltage is generally given as:

$$P(V) = \frac{I_+ - I_-}{I_+ + I_-}. \tag{1.15}$$

The general idea is that transport between the two leads is dominated by the majority spin in the nickel, and thus if there is a difference in the transmission for different

Table 1.6: Gap difference and polarisation in transport experiments. A dash is used when the gap difference was not reported.

Year	Author(s)	Molecule	Gap diff. [eV]	Bias [V]	Pol. (%)
2011	Xie et al.[23]	26-bp dsDNA	1.1	1.5	−64
		40-bp dsDNA	1.2		−60
		50-bp dsDNA	1.0		−63
2015	Kettner et al.[31]	AL7 oligopeptide	0.5	1.5	−32
2016	Bloom et al.[39]	CdSe/L-cysteine	−0.15	−1.5	33
		CdSe/D-cysteine	0.2		−58
2016	Kiran et al.[40]	AL5 oligopeptide	–	1.0	−38
		AL7 oligopeptide	–		−49
		AL5 oligopeptide[a]	–		−6
		AL7 oligopeptide[a]	–		−17
2016	Kiran et al.[41]	M-helicene	–	1.0	−45
		P-helicene	–		49
2017	Aragonès et al.[42]	L-α-22AA-peptide	–	0.05	−60
		D-α-22AA-peptide	–		57
2018	Al-Bustami et al.[43]	AHPA-L	–	1.0	−22
2018	Tassinari et al.[44]	L-oligopeptide	–	1.5	68
		D-oligopeptide	–	1.5	−59
2019	Bullard et al.[45]	Pro_8	–	1.5	51
		$\mathrm{Pro}_8\mathrm{PZn}_1$	–		67
		$\mathrm{Pro}_8\mathrm{PZn}_2$	–		24
		$\mathrm{Pro}_8\mathrm{PZn}_3$	–		60

[a] these experiments were done by applying a 7 nN force on the molecules with the AFM tip during measurement

Table 1.7: Saturated polarisation in magnetoresistance transport experiments. Unless otherwise noted, experiments were reported to have been done using a constant current of 1 mA.

Year	Author(s)	Molecule	Pol. (%)
2014	Mathew et al.[46]	L-polyalanine	2.5
		L-cysteine	0.9
		D-cysteine	−4.2
		— (higher quality)	−10.0
2015	Mondal et al.[47]	PCT-L	1.5
2016	Bloom et al.[39]	CdSe/L-cysteine	−0.4
		CdSe/D-cysteine	0.3
2016	Kiran et al.[41]	M-helicene[a]	−0.7
		P-helicene[a]	0.7
2018	Varade et al.[48]	Bacteriorhodopsin	0.9

[a] these experiments were done using a constant current of 10 μA.

spin species through the chiral molecules, this will manifest itself as a difference in the current. In some of these experiments, the I-V curves show that the current is not just suppressed by a constant factor, due to a reduced number of carriers with the right spin type, but an apparent shift in the effective barrier for transport. This difference in the effective barrier, or gap in the molecular spectrum, is reported in early experiments of this type and listed in Table 1.6 alongside the calculated polarisation at a given bias voltage.

The second variation uses a similar setup, but measures the magnetoresistance of the device instead. That is, a constant current (typically around 1 mA) is passed through the system, and by measuring the voltage between the leads, the resistance of the device is obtained. By sweeping an external magnetic field, H, the magnetoresistance is defined as the relative resistance of the device at different magnetic fields:

$$\mathrm{MR}(H) = \frac{R(H) - R(H=0)}{R(H=0)}. \tag{1.16}$$

Note that we can relate the magnetoresistance to a polarisation of the kind in Eq (1.15) through the relationship:

$$P(H) = \frac{\mathrm{MR}(H) - \mathrm{MR}(-H)}{2 + \mathrm{MR}(H) + \mathrm{MR}(-H)} = \frac{R(H) - R(-H)}{R(H) + R(-H)}. \tag{1.17}$$

For brevity, we list the magnetoresistance experiments in Table 1.7 using the polarisation as calculated using Eq. (1.17) at magnetic fields for which the magnetoresistance has saturated. Note that the polarisations in these experiments are much lower then the ones in experiments of the first kind. This can be understood by considering the fact that the current through these systems are several orders of magnitudes larger, which corresponds to a much larger bias voltage and thus many more molecular orbitals are involved in transport. In addition, the sign of the polarisation changes for CdSe capped cysteine SAMs between the two methods. This hints towards the fact that the polarisation may not be the same at all energies. Finally, the CdSe capped cysteine SAMs show an opposite sign when compared to pure cysteine. This sign change was shown not to be an artifact of the experiment[39], and thus shows that the polarisation depends on properties of the full system, and not just the chiral cysteine molecules.

1.3.4 *Electrochemistry*

Rather similar to the transport experiments are the electrochemistry ones. These experiments use ions in a solution (an *electrolyte*) to physically "ferry" electrons from a so-called *counter electrode* to a *working electrode*, which in these experiments are molecules adsorbed on a substrate. A third electrode, the *reference electrode*, is used to measure the voltage across the molecules. On top of the SAM, a *redox couple*—a molecule or nanoparticle—sits at which the electron transfer happens, through reduction or oxidation. This is shown in Figure 1.6a. These experiments again come in three variations, the first of which uses a magnetised nickel substrate. In this kind, *cyclic voltammetry* is used to measure so-called cyclic voltammograms (CV curves). I. e. an electron current is generated by ramping the voltage up and down and measuring the current flowing between the counter electrode and the working electrode. As the voltage is changed, a reduction or oxidation process occurs at the working electrode which leads to peaks in the current. The CV curves for opposite magnetisations is compared to establish the presence of the CISS effect as in the transport case. Generally, the polarisation of the current at the reduction and oxidation peaks is reported, as defined in Eq. (1.15), and the values for different molecules are listed in Table 1.8. It is worth noting here that the table lists two papers in which the so-called wild-type bacteriorhodopsin embedded in a purple membrane was studied. Both papers share several authors and they reported to have used similar buffers, electrolytes, redox couples and magnetic fields, but show different CV curves and an order of magnitude difference in the polarisation.

The second variation also uses cyclic voltammetry, but the magnetic substrate is replaced by a Hall probe—a two-dimensional electron gas (2DEG) formed between

Table 1.8: Polarisation measured in electrochemistry experiments at the reduction and oxidation peaks (low and high voltages, respectively). Unless otherwise noted, the magnetic field strength was reported as 0.35 T.

Year	Author(s)	Molecule	Voltage [V]	Pol. (%)
2013	Mishra et al.[30]	Bacteriorhodopsin	0.8	14
			0.35	11
2015	Einati et al.[49]	Bacteriorhodopsin	0.11	3
			0.30	0.5
2015	Kettner et al.[31]	AL5 oligopeptide	0.12	16
			0.29	4
		AL6 oligopeptide	0.12	21
			0.29	8
		AL7 oligopeptide	0.12	12
			0.29	9
2015	Mondal et al.[50]	L-Cys-TBO	−0.02	8
			0.16	9
		D-Cys-TBO	−0.06	−5
			0.19	−6
2016	Mondal et al.[33]	Ala8	0.05	−7
			0.32	−5
		Ala8-CdSe[a]	0.05	4
			0.32	4
2016	Zwang et al.[51]	16-bp dsDNA-MB	−0.23	5
		17-bp dsDNA-NB	−0.20	4
2018	Gazzotti et al.[52]	L-tartaric acid	0.33	−21
			0.51	−9
		D-tartaric acid	0.52	15
			0.65	26

[a] these experiments were done under laser illumination

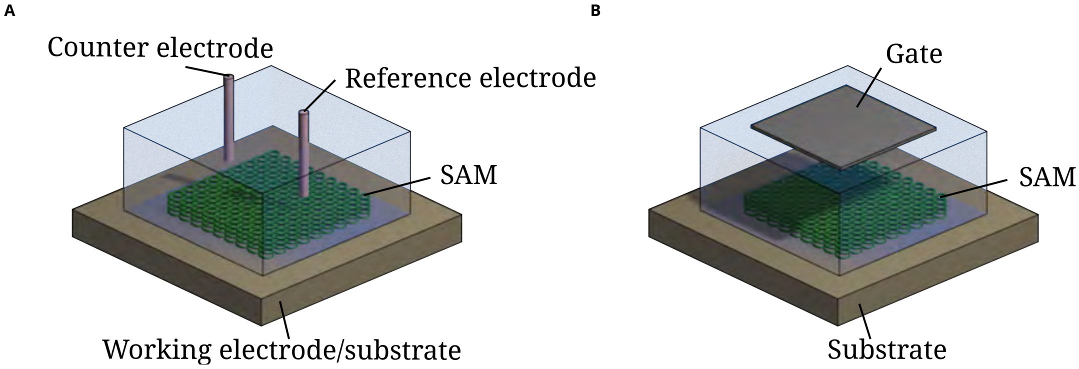

Figure 1.6: (A) Generic setup of the electrochemistry experiments. A current flows from the counter electrode through the electrolyte to a redox couple on top of the SAM, where a reaction occurs which transfers an electron or hole. The transferred electron or hole is then transferred to the substrate and the current is measured. The voltage between the reference electrode and the working electrode/substrate is measured simultaneously. (B) Setup where the counter and reference electrodes have been replaced by a gate, isolated from the electrolyte.

layers of AlGaN and GaN. As in the photoexcitation experiments, this allows direct detection of the induced magnetic field as a result of a spin polarised current. The 2DEG is again typically at a distance of about 20 nm below the SAM and the density of molecules is around $10^{13}\,\mathrm{cm}^{-2}$, and thus the analysis for photoexcited electrons on a Hall probe is valid here as well. The calculated effective magnetic field measured at specific bias voltages in experiments of this kind are listed in Table 1.9. Note that the values in these experiments are even larger than for the photoexcitation ones, corresponding to hundreds of fully polarised electrons per molecule, even at low bias voltages. These numbers do not make sense in the simple picture of just electrons being polarised by transport through the SAM, and thus some other effects must be at play which enhance the Hall response.

In the final variation, molecules are again adsorbed on a Hall probe, but instead of driving a current through the system, the counter electrode is replaced by a gate which is insulated from the electrolyte, as illustrated in Figure 1.6B. Such experiments display a transient magnetisation of the substrate as the gate voltage is switched on. This transient effect is attributed to polarised charge transfer from the chiral molecules to the substrate. Experiments of this type shows an increase of the magnetisation with an increase in the applied voltage, as well as the length of the molecules being used. Table 1.10 lists the peak value of the calculated effective H-field to generate the necessary magnetisation.

Table 1.9: Effective magnetic field at specific bias voltages in electrochemistry experiments without an external magnet.

Year	Author(s)	Molecule	V_{bias} [V]	H_{eff} [mT]
2017	Kumar et al.[53]	AL5 oligopeptide	0.2	27
		AL7 oligopeptide		35
		AL9 oligopeptide		113
2019	Bullard et al.[45]	$\text{Pro}_8{}^a$	0.2	−31
		$\text{Pro}_8\text{PZn}_1{}^a$		−28
		$\text{Pro}_8\text{PZn}_2{}^a$		−42
		$\text{Pro}_8\text{PZn}_3{}^a$		−27
2019	Mishra et al.[54]	20-bp dsDNA^a	0.6	121
		30-bp dsDNA^a		291
		40-bp dsDNA^a		369

a these experiments did not report the calibration of the Hall device to an external magnet, thus the field is calculated using calibration from other experiments with a similar setup

It is worth mentioning that in the paper by Smolinsky et al.[56], published in 2019, they reported a sustained magnetic field for as long as the gate voltage was applied. They suggested that a mechanism to explain this effect could be based on an RKKY interaction, mediated by the electrons in the 2DEG. For this model to make sense, the electrons have to pass through the 20 nm GaN layer and be captured by defects in the semiconductor near the 2DEG to allow for a significant interaction with the conducting electrons. This, incidentally, is also consistent with the high values of flux, corresponding to each molecule contributing several thousand electrons at a 20 nm distance from the 2DEG, as the flux per electron scales as the cubed inverse of its distance. To give credence to this model, we must consider the RKKY interaction between two spins in two dimensions:

$$V_{ij} \propto -J^2(\vec{S}_i \cdot \vec{S}_j) \int_1^\infty \frac{1}{2k_F r} \frac{J_1(2k_F r x)}{x\sqrt{x^2-1}} dx, \tag{1.18}$$

where J_1 is a Bessel function. For a doped semi-conductor where k_F is small, and assuming that the distance between impurities, r, is small as well, such that, $k_F r \ll 1$, the asymptotic behaviour of the integral tends to $\ln[2/k_F r]$, which is always positive for the values of $k_F r$ we are interested in[57]. This would suggest that the interaction is indeed ferromagnetic, which would explain the sustained magnetisation. Curiously, the same study also found spontaneous magnetisation without an applied gate voltage, as the chiral molecules were cooled down. It was suggested that the RKKY interaction was also responsible for this effect in conjunction with hybridisation of the molecular states with the states in the substrate. It awaits to be seen if experiments of this type are reproducible. The RKKY mechanism might also be responsible for the high magnetic fields measured in the other Hall probe experiments. An in-depth analysis of the RKKY interaction in the substrate and 2DEG, and its interplay with the molecules, however, is beyond the scope of this thesis.

1.3.5 *Other experiments*

There are a few other related experiments that fall outside the classification scheme above. One of the most notable ones is the one by Ben Dor et al.[58], in which they studied AHPA molecules adsorbed on a ferromagnet, and observed an induced magnetic moment related to the handedness of the molecules. The measured induced moment per molecule corresponded to around 300 Bohr magnetons, or 300 spins, similar in magnitude to the values extracted from the gated electrochemistry experiments. This result is consistent with the gated experiments, since during the adsorption charge is transferred between the SAM and the substrate to equilibrate their chemical potentials.

Another experiment, also by Ben Dor et al.[59], measures the transient behaviour of the resistance in a device of AHPA sandwiched between two gold electrodes, with a thin nickel layer on top. The the nickel layer is thin enough such that its easy axis is in the plane due to demagnetising effects discussed earlier. The idea of the experiment is that as a current flows through the chiral molecules, spin of one type will be injected into the nickel, magnetising it out of plane. Depending on the voltage applied, the preferred spin being transported through the SAM changes, which transfers opposite magnetic moments to the nickel. Due to temperature fluctuations, however, this effect is in competition with the fact that the magnetisation of the nickel will tend to relax towards the easy axis. Thus, after some time, an equilibrium magnetisation will be reached. Because of the competition, the effect is only significant for temperatures below 100K. When the ferromagnet is magnetised out of plane, the resistance through the device is either higher or lower, depending on whether the magnet is aligned parallel or antiparallel to the electrons' spin, and saturates around $600\,\mathrm{M\Omega}$ at 2.5K, with peak high and low resistances of $1600\,\mathrm{M\Omega}$ and $100\,\mathrm{M\Omega}$, respectively.

Finally, there are also a few of the papers already reported on, in which they do additional electrochemical measurements showing that the current and induced magnetisation depends on the handedness of the redox couple being used[46,47,53]. By using either S- or R-ferrocene, the ability of the redox couple to bind to the chiral molecules is different, and the electronic coupling between them is thus different for the two enantiomers.

1.3.6 *Additional remarks*

As noted in the beginning of this section, some of the experiments on similar molecules may seem inconsistent at first glance. For instance, the photoexcitation experiment on Ala8 shown in Table 1.3, using CdSe nanoparticles as the chromophore shows the opposite sign as compared to the electrochemistry experiments on Ala8, found in Table 1.8. Fortunately, the authors of these experiments also conducted electrochemistry experiments on Ala8 while simultaneously exciting electrons in the CdSe nanoparticles using a laser, which showed a change in sign when compared to the experiment without. Because the electrochemistry experiments happen at much lower voltages, and thus energies, this would suggest that the spin polarisation for electrons being transported through these systems depends on the energy of the electrons. The same is true for the experiments on the family of ALn $(n = 5, 6, 7, 9)$ molecules. In the low voltage electrochemistry experiments, these molecules show positive polarisation, while the higher energy experiments show negative polarisations. This again supports the idea that the polarisation direction is an energy-dependent phenomenon. As we shall see later, this is also what the theory we shall develop predicts.

For the photoexcitation experiments on dsDNA, although they find a positive polarisation, a different explanation is at play here. In this case, the predominant charge carriers are holes, and thus the polarisation of the electrons is negative. Thus, like the experiments on ALn, the experiments on dsDNA indicate that the spins are negatively polarised, with the exception of the negative voltage electrochemistry ones in Table 1.8. The dsDNA experiments, alongside the ALn experiments, also generally show an increase in the effect with an increase in length, which is again a feature that our theory has.

Finally, not all experiments show exactly symmetric results for the two enantiomers. This is mostly due to the fact that the methods used to synthesise them differs, resulting in more pure films of one kind than the other and is generally not something one should worry about.

Table 1.10: Peak effective magnetic fields measured at specific gate voltages in electrochemistry experiments without an external magnet.

Year	Author(s)	Molecule	V_{gate} [V]	H_{eff} [mT]
2017	Kumar et al.[55]	L-AL5 oligopeptide	2	−0.2
		D-AL5 oligopeptide		0.2
		L-AL5 oligopeptide	10	−0.6
		D-AL5 oligopeptide		0.4
2019	Bullard et al.[45]	$\text{Pro}_8{}^a$	2	0.4
		$\text{Pro}_8\text{PZn}_1{}^a$		−1.6
		$\text{Pro}_8\text{PZn}_2{}^a$		−1.9
		$\text{Pro}_8\text{PZn}_3{}^a$		−3.1
		$\text{Pro}_8{}^a$	10	−0.6
		$\text{Pro}_8\text{PZn}_1{}^a$		−5.3
		$\text{Pro}_8\text{PZn}_2{}^a$		−7.4
		$\text{Pro}_8\text{PZn}_3{}^a$		−7.4
2019	Mishra et al.[54]	20-bp dsDNA[a]	2	21
		30-bp dsDNA[a]		0.5
		40-bp dsDNA[a]		1.6
		20-bp dsDNA[a]	10	4.7
		30-bp dsDNA[a]		6.7
		40-bp dsDNA[a]		8.1
2019	Smolinsky et al.[56]	AHPA-L	0.3	23.3
			−0.2	−43.4

[a] these experiments did not report the calibration of the Hall device to an external magnet, thus the field is calculated using calibration from other experiments with a similar setup

2

FORMALISM

We saw in the previous chapter that quite a few experiments over the past decade had found a significant spin polarisation of electrons transported through chiral molecules, an effect termed chiral-induced spin selectivity (CISS). We also noted that the theoretical treatments of these experiments all made use of a spin-orbit coupling to explain the effect, but that any theory which seeks explanatory power from the microscopic scale, had to use the atomic spin-orbit coupling as its basis. We pointed to three early theory papers, but the same is true for all subsequent CISS theory papers.

A large number of theoretical investigations into the CISS effect has been done using a Landauer-Büttiker like approach[24,25,60–68]. That is, two thermally equilibrated leads connected to the molecule at either end. The model systems are explicitly constructed for specific helical molecules, and provide valuable insight into the effects at play for that system. These models consistently find that in order to get a significant spin polarisation, it is necessary to introduce extra phenomenological leakage terms either via an extra physical lead or virtual Büttiker leads—a mathematical trick to model dephasing effects. This dephasing is argued to occur, for instance, by vibrations in the molecule and the environment. Other papers consider transport through a continuum helical potential[26,69–72], or assume spin-dependent transport through the system and derive properties of such systems[73,74], without going into details of how the spin-dependent transport arises in the first place.

Several unpublished *ab initio* studies of the CISS effect using the non-equilibrium Green's function (NEGF) formalism has found similar results. Namely, in order to enhance the effect to an appreciable level, one has to tune a phenomenological dephasing parameter. From a theoretical point of view, this is an unattractive feature of the models, which led us to explore the theoretical underpinnings of this result. This led to the formalism that we shall present in the following chapters, and which was published in the summer of 2019[1]. It bears resemblance to standard NEGF or Landauer transport theories but in this treatment we are careful not to throw the baby out with the bathwater, by making assumptions about the electron distributions. A strength of the approach presented is that the resulting equations can easily be adapted to by existing *ab initio* routines for transport calculation.

A notable feature of the formalism is a theorem which states that for two thermalised, non-magnetic leads, the spin polarisation vanishes analytically to first order in the spin-orbit coupling without dephasing effects or coupling to a third, external lead. This result arises from considerations of time-reversal symmetry, and explains why previous models found such small effects in the absence of dephasing. One of the proposed methods of introducing dephasing was via coupling to vibrations or phonons. As we shall see, a full treatment of the problem shows that the polarisation which results from the proposed dephasing (the self-energies of the electron-phonon interaction) is exactly cancelled by their corresponding so-called vertex corrections. The same theorem says that in a system with a single magnetic lead, there can be no difference in the measured current when the magnetisation of the lead is flipped. This result can also not be remedied by the introduction of vibrations. These findings significantly limit the space of possible theoretical models. We defer discussions of the implications of the theorem for the interpretation of the experiments until later. In the following sections, we shall instead lay the groundwork leading to the theorem above, and in the next chapter, we shall derive it.

2.1 STATISTICAL AVERAGES

Our first line of action is to discuss the types of models that we shall use. In experiments of the photoemission kind, the intensity of the laser is low enough that the experimenters report that only a single electron is emitted at a time. The illuminated point itself is wide enough that the excited electron is not necessarily localised underneath a single molecule, though. Thus, one could in principle imagine spatially varying interference effects resulting from such a multi-slit experiment. The detector covers a large area, though, and thus such spatially varying interference effects are cancelled out. Another effect to consider in this area is intermolecular couplings. Such couplings would lead to a broadening of the spectrum, depending on the transversal momentum of the electron. The distances between the molecules in the SAMs tend to be much greater than the distances between atoms in the molecules, though, and thus such broadening would lead to a rather small effect. Based on this analysis, we shall think of the photoemission experiments as a single electron travelling through a single molecule.

A similar argument can be made for the photoexcitation experiments. That is, the rate at which electrons are excited from the chromophore is slow enough, such that only one electron-hole pair is on the molecule at a time. Since the chromophores are generally locally coupled to just one molecule, transport of electrons again generally happens through just a single molecule. In the transport experiments, an AFM tip is put in contact with nanoparticles adsorbed on top of single molecules. The currents in these experiments are on the order of nA, which corresponds to around 10 to 100 electrons per nanosecond. A crude estimate for the time an electron stays on the molecule can be obtained from the uncertainty principle, $\Delta t = \hbar/2\Delta E$, which for $\Delta E = 1\,\text{meV}$ is one-third of a picosecond. Thus, it is probably fair to assume that there really is only one electron on the molecule at any one time in these experiments as well. In the electrochemistry experiments, the measured currents are on the order of a few µA, which can still be argued to be within the regime of one electron being transported at a time. Finally, in the magnetoresistance experiments, a constant current of 1 mA is used. Thus, those experiments might reach a regime where charging of the molecule plays a role, and so our treatment might not be entirely accurate in this case.

With that in mind, the experiments themselves are averaging over a lot of subsequent and parallel processes, and as such we are interested in calculating the statistical distribution of observables of this system. I. e. for the experiments involving magnets, we are interested in calculating the current through a molecule given different orientations of an external magnet, while for the photoemission experiments, we want the average orientation of spins that make it through. The mathematical tool that makes such a calculation possible is known as a density matrix, and for the sake of completeness, we begin with a brief discussion of its properties and how it comes about.

2.1.1 *The density matrix*

Let Ψ denote the quantum state of a many-body system and P_Ψ the *classical* probability that the system is prepared in the state Ψ. I. e. if one were to draw random states out of a jar, P_Ψ is the probability that one would draw the exact state Ψ. Note that in this sense, the states Ψ are not necessarily orthogonal by construction. We are, at this stage, not concerned with exactly how one obtains the probabilities, and simply assume that they are given to us. Then the average expectation value of an operator, $\hat{A}$, is given by the expectation values of the operator for a given state Ψ, weighted by the probability of having the system prepared in that state, summed over all possible system preparations. Mathematically, this is equivalent to:

$$\begin{aligned}\langle \hat{A} \rangle &= \sum_{\Psi} P_\Psi \langle \Psi | \hat{A} | \Psi \rangle = \sum_{\Psi} \sum_{\nu} P_\Psi \langle \Psi | \hat{A} | \nu \rangle \langle \nu | \Psi \rangle \\ &= \sum_{\nu} \langle \nu | \left(\sum_{\Psi} | \Psi \rangle P_\Psi \langle \Psi | \hat{A} \right) | \nu \rangle = \mathrm{tr}\left[\sum_{\Psi} | \Psi \rangle P_\Psi \langle \Psi | \hat{A} \right] = \mathrm{tr}\left[\hat{\rho} \hat{A} \right],\end{aligned} \tag{2.1}$$

where we have inserted a complete span of states, ν, and in the last equality, we have defined the density operator:

$$\hat{\rho} \equiv \sum_{\Psi} P_{\Psi} \left|\Psi\right\rangle \left\langle\Psi\right| . \tag{2.2}$$

Note that there is no requirement that the states in the basis, $\{\Psi\}$, are orthogonal to each other. In fact, if one knows nothing about the system, *a priori*, it is safe to say that given a sufficient number of states, Ψ, the basis will be overcomplete. This is not an issue, however, as there always exists a complete, orthonormal basis, $\{\nu\}$. Inserting it on either side, we find

$$\hat{\rho} = \sum_{\nu\nu'} \sum_{\Psi} \left|\nu\right\rangle \left\langle\nu|\Psi\right\rangle P_{\Psi} \left\langle\Psi|\nu'\right\rangle \left\langle\nu'\right| = \sum_{\nu\nu'} \rho_{\nu\nu'} \left|\nu\right\rangle \left\langle\nu'\right| , \tag{2.3}$$

where,

$$\rho_{\nu\nu'} = \sum_{\Psi} P_{\Psi} \left\langle\nu|\Psi\right\rangle \left\langle\Psi|\nu'\right\rangle . \tag{2.4}$$

Since P_{Ψ} is real, $\rho_{\nu\nu'} = \rho^{*}_{\nu'\nu}$ and thus ρ is Hermitian. Additionally, any Hermitian operator can be diagonalised, and since probabilities and hence P_{Ψ} is non-negative, ρ must be positive-semidefinite. Lastly, the probabilities must add up to unity, and thus:

$$1 = \sum_{\Psi} P_{\Psi} = \sum_{\Psi} P_{\Psi} \left\langle\Psi|\Psi\right\rangle = \sum_{\Psi} \sum_{\nu} P_{\Psi} \left\langle\Psi|\nu\right\rangle \left\langle\nu|\Psi\right\rangle = \sum_{\nu} \rho_{\nu\nu}, \tag{2.5}$$

where we have used Eq. (2.4) in the last equality. Note that Eq. (2.5) is equivalent to the statement, $\mathrm{tr}[\hat{\rho}] = 1$. This is a basis-independent statement, which thus further supports the statement that we do not have to care about the basis chosen to describe the density operator.

If all we are interested in are operators which count electrons, it suffices to treat only single particle operators. In the language of second quantisation, such operators and their statistical averages are given by:

$$\hat{A} = \sum_{ij} A_{ij} a_i^{\dagger} a_j, \quad \text{and} \quad \langle\hat{A}\rangle = \sum_{ij} A_{ij} \langle a_i^{\dagger} a_j\rangle, \tag{2.6}$$

where $a_i^{\dagger}$, a_j are creation and annihilation operators, and their average should be calculated using Eq. (2.1). Defining the single particle matrices in first quantisation:

$$A = \sum_{ij} A_{ij} \left|i\right\rangle \left\langle j\right| , \quad \rho = \frac{1}{N} \sum_{ji} \langle a_j^{\dagger} a_i\rangle \left|j\right\rangle \left\langle i\right| , \tag{2.7}$$

where $N = \sum_{ji} \langle a_j^{\dagger} a_i\rangle$ is the total number of particles in the system, we can rewrite the trace from Eq. (2.1) in our single particle space as:

$$\langle\hat{A}\rangle = N \sum_{ij} A_{ij} \rho_{ji} = N\, \mathrm{tr}[\rho A]. \tag{2.8}$$

This gives us an effective starting point for our formalism. Note that the trace of the single particle density matrix is also normalized to unity:

$$\mathrm{tr}[\rho] = \frac{1}{N}\sum_i \langle \hat{n}_i \rangle = 1. \tag{2.9}$$

The normalisation of N of this single particle density matrix is due to the fact that each electron can be in any one of the states described by the full density matrix. Note, however, that exchange statistics, such as the Pauli principle, *are* included in this definition. Such a feature of the statistics will be captured by the expectation values of the number operators, $\langle \hat{n}_i \rangle$. We shall refer to the trace without the hat over the operator, $\langle A \rangle = \mathrm{tr}[\rho A]$ as the *single particle expectation value* to distinguish it from the many-body expectation value, $\langle \hat{A} \rangle$.

2.1.2 *Thermal equilibrium*

For completeness, we briefly review the expectation values of particle counting operators in thermal equilibrium, as these will be used to treat special cases later on. In thermal equilibrium, we assume the system to have a well-defined energy, although it may statistically fluctuate in time, which implies that the density operator is diagonal in the eigenstates of the Hamiltonian. Moreover, the probability for the system to be initialised in an eigenstate ν is given by:

$$P_\nu = \frac{e^{-\beta E_\nu}}{\sum_{\nu'} e^{-\beta E_\nu}} \quad \Rightarrow \quad \hat{\rho} = \frac{e^{-\beta H}}{\mathrm{tr}[e^{-\beta H}]}. \tag{2.10}$$

For a Hamiltonian in a diagonal basis, $H = \sum_i \varepsilon_i \hat{n}_i$, the density operator factorizes as:

$$\hat{\rho} = \frac{e^{-\beta \sum_i \varepsilon_i \hat{n}_i}}{\mathrm{tr}\left[e^{-\beta \sum_i \varepsilon_i \hat{n}_i}\right]} = \frac{\bigotimes_i e^{-\beta \varepsilon_i \hat{n}_i}}{\mathrm{tr}\left[\bigotimes_i e^{-\beta \varepsilon_i \hat{n}_i}\right]} = \bigotimes_i \frac{e^{-\beta \varepsilon_i \hat{n}_i}}{\mathrm{tr}[e^{-\beta \varepsilon_i \hat{n}_i}]} = \bigotimes_i \hat{\rho}_i, \tag{2.11}$$

where $\bigotimes_i \hat{\rho}_i = \hat{\rho}_1 \otimes \hat{\rho}_2 \otimes \cdots \otimes \hat{\rho}_N$ represents the folded tensor product of the operators. Consequently, using the property of the trace that $\mathrm{tr}[\otimes_i \hat{\rho}_i] = \prod_i \mathrm{tr}[\hat{\rho}_i]$:

$$\langle \hat{n}_i \rangle = \mathrm{tr}\left[\hat{n}_i \bigotimes_i \hat{\rho}_i\right] = \mathrm{tr}[\hat{\rho}_i \hat{n}_i] \prod_{j \neq i} \underbrace{\mathrm{tr}\left[\hat{\rho}_j\right]}_{=1} = \mathrm{tr}[\hat{\rho}_i \hat{n}_i]. \tag{2.12}$$

To advance further, we must consider fermions and bosons separately.

FERMION STATISTICS If $\hat{n}_i$ is a fermionic number operator, $n_i \in \{0, 1\}$ and thus:

$$\langle \hat{n}_i \rangle = \frac{e^{-\beta \varepsilon_i}}{1 + e^{-\beta \varepsilon_i}} = \frac{1}{e^{\beta \varepsilon_i} + 1} = n_F(\varepsilon_i). \tag{2.13}$$

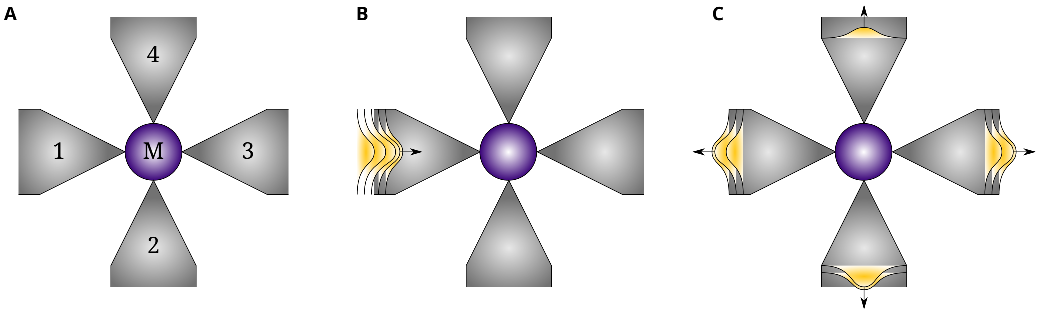

Figure 2.1: (A) General setup of the scattering problem with four leads (labelled 1-4) and a molecule (labelled M). The leads extend far out in the direction away from the molecule. In (B), an incoming wave packet (yellow) in the first lead hits the molecule and (**C**) scatters back into all of the leads with different amplitudes.

BOSON STATISTICS If $\hat{n}_i$ is a bosonic number, on the other hand, we define $\lambda_i = e^{-\beta\varepsilon_i}$:

$$\langle \hat{n}_i \rangle = \frac{\sum_{n_i} n_i e^{-\beta\varepsilon_i n_i}}{\sum_{n_i} e^{-\beta\varepsilon_i n_i}} = \frac{\lambda_i \partial_{\lambda_i} \sum_{n_i} \lambda_i^{n_i}}{\sum_{n_i} \lambda_i^{n_i}}, \tag{2.14}$$

where ∂_{λ_i} is the derivative operator w.r.t. λ_i. Noticing that, for $|\lambda_i| < 1$,

$$\frac{1}{1-\lambda_i} = 1 + \lambda_i(1 + \lambda_i(1 + \cdots)) = \sum_{n_i} \lambda_i^{n_i}, \tag{2.15}$$

we get:

$$\langle \hat{n}_i \rangle = (1-\lambda_i)\lambda_i \partial_{\lambda_i} \frac{1}{1-\lambda_i} = \frac{\lambda_i}{1-\lambda_i} = \frac{1}{e^{\beta\varepsilon_i} - 1} = n_B(\varepsilon_i). \tag{2.16}$$

Importantly, both of these distributions only depend on the energy of the single particle state, i. This fact will turn out to be crucial later, and we shall refer more loosely to distributions as being *thermal*, if the occupation number only depends on energy.

2.2 SCATTERING PICTURE

With the details of statistical averages and the density matrix out of the way, we now turn our attention to describing electron transport in molecules. We shall do this using two different approaches. The first, which is the focus of the current section, bears resemblance to the early experiments which looked at electron scattering from molecules in the gas phase. In this picture, electrons approach the molecule from afar and scatter into incoming and outgoing wave packets. The advantage of this picture is the vividness conjured up by the physical propagation of the electrons. As we shall see, the same line of thinking involved can also be used to describe photoemission experiments. The second approach, which we shall get into the details of in the next section, is subtly different and simply starts with a given density matrix and lets it evolve in time. Perhaps surprisingly, both approaches lead to the same equations for expectation values in steady state in the end, and thus we are free to choose either when interpreting the results and describing the experiments.

To get started, an abstract layout of the scattering problem is sketched out in Figure 2.1. In the figure, a molecule, indicated by a purple sphere and the letter M in the centre, is connected to by four leads. The actual number of leads is irrelevant to the theory and the four leads serves merely to illustrate that the number of leads is an arbitrary quantity in the theory that we develop. Even though it is not shown explicitly in Figure 2.1, we are, for the moment, going to assume that the leads extend very far in the direction away from the molecule.

Now, the Hamiltonian for such a system with N leads can be given in block-form as

$$H = \begin{pmatrix} H_1 & 0 & \cdots & 0 & H_{1M} \\ 0 & H_2 & \cdots & 0 & H_{2M} \\ \vdots & \vdots & \ddots & & \vdots \\ 0 & 0 & & H_N & H_{NM} \\ H_{M1} & H_{M2} & \cdots & H_{MN} & H_M \end{pmatrix}, \tag{2.17}$$

where H_n is the uncoupled Hamiltonian of the nth lead, H_M that of the free-standing molecule and H_{Mn} describe the coupling between the molecule and the nth lead. To simplify our language, we split the Hamiltonian into its block-diagonal and off-diagonal terms. For a system of four leads, this amounts to the two matrices:

$$H = \underbrace{\begin{pmatrix} H_1 & 0 & 0 & 0 & 0 \\ 0 & H_2 & 0 & 0 & 0 \\ 0 & 0 & H_3 & 0 & 0 \\ 0 & 0 & 0 & H_4 & 0 \\ 0 & 0 & 0 & 0 & H_M \end{pmatrix}}_{H_0} + \underbrace{\begin{pmatrix} 0 & 0 & 0 & 0 & H_{1M} \\ 0 & 0 & 0 & 0 & H_{2M} \\ 0 & 0 & 0 & 0 & H_{3M} \\ 0 & 0 & 0 & 0 & H_{4M} \\ H_{M1} & H_{M2} & H_{M3} & H_{M4} & 0 \end{pmatrix}}_{V}. \tag{2.18}$$

In other words, H_0 describes a system of the leads and molecules in isolation, and V describes the coupling between them.

We now consider an electronic wavepacket, Ψ, which has been prepared in one of the leads. For simplicity, let us say the first. The wavepacket is prepared far away from the molecule and in such a way that it moves towards it. This is shown in Figure 2.1B. At some point in time, which we denote t_0, the wavepacket reaches a point at which it starts to feel the molecule. As time evolves, the electron scatters off the molecule, some of the packet being transmitted through to the other leads and some being reflected back into the first lead, as illustrated in Figure 2.1c. Assuming the Hamiltonian has no explicit time dependence, the time evolution of the wavepacket is entirely described by the operator,

$$U(t_2, t_1) = e^{-iH(t_2-t_1)/\hbar}. \tag{2.19}$$

Now, we imagine a system which is entirely identical to the one above, except we have removed the coupling between the molecule and the leads, V. We shall refer to this system as *uncoupled*, since electrons experience each lead as free-standing, isolated systems. Starting out with the same wavepacket, $|\Psi\rangle$, the time evolution in this simplified system, is governed by H_0:

$$U_0(t_2, t_1) = e^{-iH_0(t_2-t_1)/\hbar}, \tag{2.20}$$

Because the coupling to the molecule is gone, as the electron runs up against the barrier to the molecule, it will be entirely reflected back into the first lead. However, since the wavepacket was prepared to be so far from the molecule that it could not initially feel its potential, we have the identity:

$$|\Psi(t)\rangle = |\Psi_0(t)\rangle\,, \quad \text{for } t \leq t_0, \tag{2.21}$$

where $|\Psi_0(t)\rangle$ is the wavepacket evolved using just H_0. That is, although the wave packets live in different systems, because they are prepared far away from the point which differentiates them, that is, the coupling to the molecule, the time evolution up until the point in time where the wave packet would feel this coupling is the same. Consequently, if we evolve the states described in the two systems back in time to t_0, they must coincide. Since this is true for all times prior to t_0 as well, it must hold that

$$U(t_0, t)\,|\Psi(t)\rangle = U_0(t_0, t)\,|\Psi_0(t)\rangle\,, \quad \text{for all } t, \tag{2.22}$$

and hence we obtain the identity:

$$|\Psi(t)\rangle = U(t, t_0)U_0(t_0, t)\,|\Psi_0(t)\rangle\,. \tag{2.23}$$

Since at any times prior to t_0, the wave packets are far away from the molecule, the identity in Eq. (2.23) holds for evolving the system back to all times $t' < t_0$. Thus, we are free to average over all such times with an arbitrary weight factor, $w(t)$:

$$|\Psi(t)\rangle = \frac{\int_{-\infty}^{t_0} dt' w(t') U(t, t') U_0(t', t)\,|\Psi_0(t)\rangle}{\int_{-\infty}^{t_0} dt' w(t')}. \tag{2.24}$$

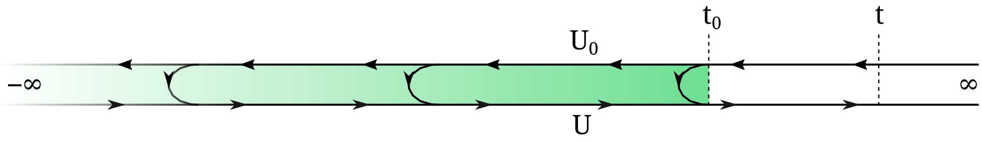

Figure 2.2: The Møller operator is constructed by evolving backwards from t along the uncoupled (upper) branch to any time prior to t_0 and then forward again along the full (lower) branch.

Here, we divide by the integral of the weight factor in order to ensure proper normalisation. Note that the statement that the wave packets are far away for all times prior to t_0 only strictly holds in the case of freely propagating electrons, if the leads are assumed infinitely long. For leads with a finite size—arguably, all realistic leads do have a finite size—we have to impose a lower cutoff. To allow a smooth cutoff, and because it is analytically easier to manipulate, we choose a weight function, $w(t) = e^{\eta t/\hbar}$, where $\hbar\eta^{-1}$ defines the timescale of the cutoff. For wavepackets in an infinitely long lead, they are allowed to come in from infinitely far away, and we are free to take the limit $\eta \to 0^+$. Such a choice recovers an average with equal weight assigned to each prior time. Plugging this weight factor in to the equation above, we obtain:

$$|\Psi(t)\rangle = \frac{\eta}{\hbar}\int_{-\infty}^{t_0} dt' e^{\eta(t'-t_0)/\hbar} U(t,t')U_0(t',t)\,|\Psi_0(t)\rangle \equiv \Omega_-(t)\,|\Psi_0(t)\rangle\,, \tag{2.25}$$

where in the last equality, we have defined the *Møller operator*,

$$\begin{aligned}\Omega_-(t_0,t) &= \frac{\eta}{\hbar}\int_{-\infty}^{t_0} dt' e^{\eta(t'-t_0)/\hbar} U(t,t')U_0(t',t)\\ &= \frac{\eta}{\hbar}\int_{-\infty}^{t_0} dt' e^{\eta(t'-t_0)/\hbar} e^{-iH(t-t')/\hbar} e^{-iH_0(t'-t)/\hbar},\end{aligned} \tag{2.26}$$

named after the Danish physicist, Christian Møller.

The next steps follows from realising that we are free to substitute $t_0 \to t$ for all finite t in the equation above. To see this, note that such a substitution is akin to introducing an error of:

$$\Delta\Omega_- = \frac{\eta}{\hbar} e^{\eta(t-t_0)/\hbar}\int_{t_0}^{t} dt' e^{\eta(t'-t)/\hbar} e^{-iH(t-t')/\hbar} e^{-iH_0(t'-t)/\hbar}. \tag{2.27}$$

In the limit $\eta \to 0^+$, this error vanishes. This limit is of course only strictly valid for infinite leads, but since the magnitude of the error scales as $(t - t_0)/\hbar\eta^{-1}$, it is still a good description provided t is sufficiently close to t_0. Performing the substitution and discarding the vanishing error term, we are thus left with:

$$\Omega_-(t) = \frac{\eta}{\hbar}\int_{-\infty}^{t} dt' e^{\eta(t'-t)/\hbar} e^{-iH(t-t')/\hbar} e^{-iH_0(t'-t)/\hbar}. \tag{2.28}$$

Inserting a complete basis of eigenstates for H_0, labelled by k, we obtain:

$$\begin{aligned}\Omega\_(t) &= \frac{\eta}{\hbar}\sum_k \int_{-\infty}^{t} dt' e^{-i(E_k - H + i\eta)(t'-t)/\hbar} \left|k\right\rangle \left\langle k\right| \\ &= \sum_k \frac{i\eta}{E_k - H + i\eta} \left|k\right\rangle \left\langle k\right| = \sum_k i\eta G(E_k) \left|k\right\rangle \left\langle k\right|,\end{aligned} \tag{2.29}$$

where we have defined the *propagator*,

$$G(E) = \frac{1}{E - H + i\eta}, \tag{2.30}$$

also known as the *resolvent*. Note that there is no time dependence on the right hand side of Eq. (2.29). Thus, the Møller operator is in fact independent of both t and t_0, and as such we do not have to worry about their values. Time dependence is not entirely lost, however, as it still resides in the states. Consequently, the full state can be written in terms of the uncoupled state as:

$$\left|\Psi(t)\right\rangle = \sum_k i\eta G(E_k) \left|k\right\rangle \underbrace{\left\langle k|\Psi_0(t)\right\rangle}_{\psi_k(t)}. \tag{2.31}$$

In order to calculate statistical quantities using these states, we must construct a density matrix. This is, fortunately, a straightforward prescription following the definition in Eq. (2.7):

$$\begin{aligned}\rho(t) &= \frac{1}{N}\sum_{\Psi} \langle n_\Psi\rangle \left|\Psi(t)\right\rangle \left\langle \Psi(t)\right| \\ &= \frac{\eta^2}{N} \sum_{\psi,k,k'} \langle n_\psi\rangle \psi_k(t)\psi^*_{k'}(t) G(E_k) \left|k\right\rangle \left\langle k'\right| G^\dagger(E_{k'}).\end{aligned} \tag{2.32}$$

Note that the uncoupled state referred to here, is the state one would get if there was no molecule, i. e. one that is reflected back entirely into the first lead, if the wave packet came from there.

2.2.1 *Time-averaged expectation values*

With the exception of a few experiments, most of them measure some sort of steady state quantity. That is, for a large number of the experiments we are not actually concerned with the transient behaviour of current, but rather the time-average of it over long time scales. Fortunately for us, the analysis is actually simplified in this case. In the scattering picture, a steady current means that we are considering a system in which we are continuously shooting electrons at the molecule. Because the incoming wave packets will have some variation between them, the density matrix we construct from such states is in general time-dependent. For a general operator, A, with no explicit time dependence, the statistical expectation value of it is simply, $\langle A(t)\rangle = \mathrm{tr}[\rho(t)A]$. Averaging the expectation value with respect to time thus amounts to replacing $\rho(t)$ with its time-average, $\bar{\rho}$. Using a normalised weight factor, $w(t)$, this time-averaged density matrix takes the form:

$$\begin{aligned}\bar{\rho} &= \frac{\eta^2}{N}\sum_{\psi,k,k'}\langle n_\psi\rangle G(E_k)\left|k\right\rangle\left\langle k'\right| G^\dagger(E_{k'})\int_{-\infty}^{\infty} dt\, w(t)\psi_k(t)\psi^*_{k'}(t) \\ &= \frac{\eta^2}{N}\sum_{\psi,k,k'}\langle n_\psi\rangle \psi_k\psi^*_{k'} G(E_k)\left|k\right\rangle\left\langle k'\right| G^\dagger(E_{k'}) \\ &\qquad\times\int_{-\infty}^{\infty} dt\, w(t)e^{-i(E_k-E_{k'})(t-t_0)/\hbar}.\end{aligned} \tag{2.33}$$

Here, we have used the fact that $\psi_k(t) = \psi_k e^{-iE_k(t-t_0)/\hbar}$. Using a weight factor of

$$w(t) = \frac{e^{-\zeta|t-t_0|/\hbar}}{\int_{-\infty}^{\infty} e^{-\zeta|t'-t_0|/\hbar}dt'} = \frac{\zeta}{2\hbar}e^{-\zeta|t-t_0|/\hbar}, \tag{2.34}$$

the final integral in Eq. (2.33) becomes:

$$\begin{aligned}&\frac{\zeta}{2\hbar}\int_{t_0}^{\infty} dt\left(e^{i(E_{k'}-E_k+i\zeta)(t-t_0)/\hbar} + e^{-i(E_{k'}-E_k-i\zeta)(t-t_0)/\hbar}\right) \\ &\quad= \frac{1}{2}\left(\frac{i\zeta}{E_{k'}-E_k+i\zeta} - \frac{i\zeta}{E_{k'}-E_k-i\zeta}\right) \underset{\zeta\to 0^+}{=} \delta_{E_k,E_{k'}}.\end{aligned} \tag{2.35}$$

Plugging this back in, and using the identity, $1 = \int \delta(E-E_k)dE$, the time-averaged density matrix becomes:

$$\bar{\rho} = \int dE\,\delta(E-E_k)\frac{\eta^2}{N}\sum_{\psi,k,k'}\langle n_\psi\rangle\psi_k\psi^*_{k'}\delta_{E_k,E_{k'}}G(E)\left|k\right\rangle\left\langle k'\right| G^\dagger(E). \tag{2.36}$$

This equation is a bit of a mouthful, so in order to simplify it, we define the *uncoupled energy-resolved average density matrix*

$$\bar{\rho}_0(E) \equiv \frac{1}{N}\sum_{\psi,k,k'}\langle n_\psi\rangle\psi_k\psi^*_{k'}\delta(E-E_k)\delta_{E_k,E_{k'}}\left|k\right\rangle\left\langle k'\right|. \tag{2.37}$$

The term uncoupled here refers to the fact that it is defined without the use of the propagators, and is thus to be interpreted as the average density matrix one would get without coupling to the molecule. In combination, we finally obtain the time-averaged single particle expectation value as

$$\langle \bar{A} \rangle = \mathrm{tr}[\bar{\rho} A] = \eta^2 \int_{-\infty}^{\infty} dE\, \mathrm{tr}[G(E) \bar{\rho}_0(E) G^\dagger(E) A]. \tag{2.38}$$

To proceed, it is instructive to consider the propagator $G(E)$. For brevity, we shall omit the energy dependence, and simply write

$$G = \frac{1}{E - H + i\eta} = \frac{1}{E - H_0 - V + i\eta} = G^0 + G^0 V G, \tag{2.39}$$

where $G^0 = (E - H_0 + i\eta)^{-1}$. This is the familiar *Dyson equation*. Note that Eq. (2.39) permits an equivalent solution with G and G^0 reversed in the final term, $G = G^0 + G V G^0$. Combining this with the identity:

$$i\eta G^0(E) \delta(E - E_k) |k\rangle = \delta(E - E_k) |k\rangle , \tag{2.40}$$

we get rid of the η's in front of the integral and the expectation value of Eq. (2.38) factors into four terms:

$$\langle \bar{A} \rangle = \int_{-\infty}^{\infty} dE\, \mathrm{tr}[\bar{\rho}_0 \left(A + AGV + VG^\dagger A + VG^\dagger AGV \right)]. \tag{2.41}$$

To advance further in our analytical exploration, we must insert a particular operator, A. We shall defer doing so for a little while, however. Instead, as we shall see in the next section, the mathematical result above is, in fact, applicable in more physical descriptions than just the scattering picture.

2.3 INITIAL STATE PICTURE

In this section, we take a different approach and assume that the density matrix is known at a given time, t_0. This approach is, as such, in some ways more general than the scattering picture, and may be either more or less intuitive to grasp. Our starting point is thus that we have a density matrix of the form

$$\rho(t_0) \equiv \frac{1}{N} \sum_{\psi,k,k'} \langle n_\psi \rangle \psi_{kk'} |k\rangle \langle k'| , \tag{2.42}$$

where k, k' are again eigenstates of the uncoupled Hamiltonian, H_0. Evolving this density matrix forward in time and considering the single particle expectation value of an operator A, we get:

$$\langle A(t) \rangle = \mathrm{tr}[\rho(t) A] = \mathrm{tr}[U(t, t_0) \rho(t_0) U(t_0, t) A], \tag{2.43}$$

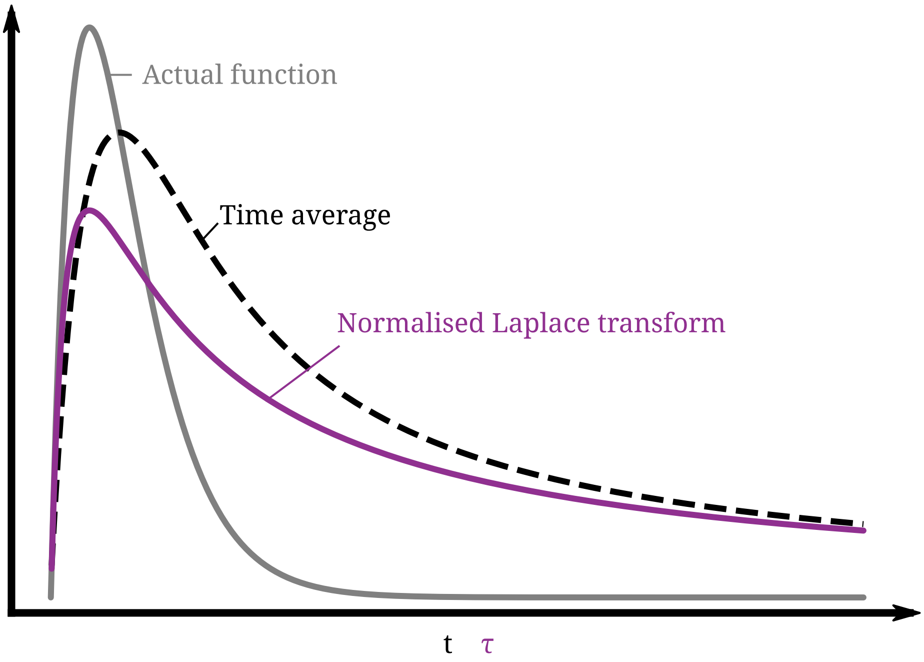

Figure 2.3: Plot of a function with an impulse-behaviour, $f(t)$ and its time-average $\bar{f}(t)$ versus t, superposed with its normalised Laplace transform, $\tilde{f}(\tau^{-1})$ versus τ. τ^{-1} would be the usual Laplace variable.

where $U(t, t')$ is the time evolution operator with the full Hamiltonian. The time average from t_0 onwards is then found as:

$$\langle\bar{A}\rangle = \int_{t_0}^{\infty} dt w(t) \langle A\rangle = \int_{t_0}^{\infty} dt w(t)\, \mathrm{tr}[U(t, t_0)\rho(t_0)U(t_0, t)A], \tag{2.44}$$

where $w(t)$ is a weight function. Unlike the scattering picture, we now want to be able to deal with averages over any time scale. However, using a box weight function, i. e. effectively truncating the integral above at a finite value and normalising it, is going to give expressions that are somewhat difficult to deal with analytically. To overcome this issue, we are going to introduce a weight function analogous to the one in the scattering picture, but instead of η, we shall use a finite "life-time" τ. That is, our weight function will take the form,

$$w(t) = \frac{e^{-t/\tau}}{\int_{t_0}^{\infty} dt' e^{-t'/\tau}} = \frac{1}{\tau} e^{-(t-t_0)/\tau}. \tag{2.45}$$

Using this weight function when calculating the average amounts to doing a Laplace transform in the Laplace variable τ^{-1}, normalised by the normalisation factor, τ. It is worth considering how well the average obtained from the normalised Laplace transform resembles the "actual" time-average using the box weight function.

To answer this, let us for simplicity consider functions which can be written as a power series:

$$f(t) = \sum_n a_n t^n. \tag{2.46}$$

The mean value of a function f on the interval 0 to t, versus its normalised Laplace transform, $\tilde{f}$, is then given as:

$$\bar{f}(t) = \frac{1}{t}\int_0^t f(t')dt' \qquad = \sum_n \frac{1}{n+1} a_n t^n, \tag{2.47}$$

$$\tilde{f}(\tau^{-1}) = \frac{1}{\tau}\int_0^\infty e^{-t'/\tau} f(t')dt' \qquad = \sum_n n! a_n \tau^n. \tag{2.48}$$

In the linear regime, $f(t) \sim t$, we thus find the equivalences,

$$f(t) \sim 2\bar{f}(t) \sim \tilde{f}(\tau^{-1}). \tag{2.49}$$

Therefore, the normalised Laplace transform resembles the actual function closer in the linear regime than the average. Now, the power series of $\tilde{f}(\tau^{-1})$ contains factorials which explode for high powers of n. We know that the integral should be well-behaved, however, so these must be regularised somehow. To illustrate this, we have plotted a simple impulse-like function (a polynomial with a suppressing exponential) and compared it to its time average and normalised Laplace transform in Figure 2.3. Here we indeed see that for such a function, the normalised Laplace transform is a good approximation of the rate at time $\tau \sim t$, and the higher order terms indeed do get regularised. In the long time limit, for a converging function, the normalised Laplace transform converges towards the box average.

Based on the analysis above, the normalised Laplace transform contains information about the time average on long time scales, and, on short time scales, matches the linear behaviour of the actual expectation value. With this in mind, we define the propagators or resolvents in the time domain as:

$$G(t, t_0) = -i\vartheta(t - t_0)U(t, t_0)e^{-(t-t_0)/2\tau}, \tag{2.50}$$

such that the Laplace transform of the expectation value takes the form:

$$\langle \tilde{A} \rangle = \frac{1}{\tau}\int_{-\infty}^{\infty} dt\, \mathrm{tr}[G(t, t_0)\rho(t_0)G^\dagger(t, t_0)A], \tag{2.51}$$

and the Laplace variable is thus contained in the propagators. Note that, in contrast to the scattering picture, the time dependence now also resides in the propagators. To advance, we use the fact that for a function or operator $f(t)$ and its Fourier transform, $f(E)$, it holds that:

$$\begin{aligned}\int_{-\infty}^{\infty} dt f(t) f^{\dagger}(t) &= \frac{1}{4\pi^2\hbar^2}\int dE \int dE' f(E) f^{\dagger}(E') \underbrace{\int_{-\infty}^{\infty} dt e^{i(E-E')t/\hbar}}_{2\pi\hbar\delta(E-E')} \\ &= \frac{1}{2\pi\hbar}\int dE f(E) f^{\dagger}(E).\end{aligned} \tag{2.52}$$

This relationship is also known as Plancherel's theorem. Fourier transforming the propagators, we get,

$$\int_{-\infty}^{\infty} dt e^{iEt/\hbar} G(t,t_0) = \frac{\hbar}{E - H + i\hbar/2\tau} = \hbar G(E), \tag{2.53}$$

where $G(E)$ is similar to the propagator that we introduced in the scattering picture, with $\eta \to \hbar/2\tau$. Consequently, by Plancherel's theorem, the weighted time-average of the expectation value of A is given by an integral over energies as:

$$\langle\tilde{A}\rangle = \frac{\hbar}{2\pi\tau}\int dE\, \mathrm{tr}[\rho(t_0) G^{\dagger}(E) A G(E)]. \tag{2.54}$$

To massage the expression above into one that resembles the one we got in the scattering picture, we now consider the long time limit, $\tau \to \hbar/2\eta$, where $\eta \to 0^+$ is an infinitesimal. To do so, we use the Dyson equation again and substitute $G = (1 + GV)G^0$ into the equation above,

$$\langle\bar{A}\rangle = \frac{\eta}{\pi}\int dE\, \mathrm{tr}[G^0(E)\rho(t_0)(G^0(E))^{\dagger}(1 + VG^{\dagger}(E))A(1 + G(E)V)]. \tag{2.55}$$

This equation is almost on the form we want, except we still have to deal with the term,

$$\frac{\eta}{\pi} G^0 \rho(t_0) (G^0)^{\dagger} = \frac{\eta}{\pi}\sum_{kk',\psi} \langle n_{\psi}\rangle \psi_{kk'} G^0 |k\rangle \langle k'| (G^0)^{\dagger}. \tag{2.56}$$

Fortunately, the sum contains terms of various orders of η^{-1}. Since η is small, the sum is dominated by terms with the highest negative power. To see this, consider the term:

$$\begin{aligned}\frac{\eta}{\pi} G^0 |k\rangle \langle k'| (G^0)^{\dagger} &= \frac{\eta}{\pi}\frac{1}{E - E_k + i\eta}\frac{1}{E - E_{k'} - i\eta} \\ &= \frac{1}{\eta\pi}\frac{1}{1 + i(E_k - E_{k'})/\eta + (E - E_k)(E - E_{k'})/\eta^2}.\end{aligned} \tag{2.57}$$

We can always pick an η that is smaller than the smallest energy spacing $E_k - E_{k'}$. In that case, the leading terms in the sum, are the ones for which $E = E_k = E_{k'}$, which results in a delta function, $\delta(E - E_k)$. The terms for which $E = E_k$ or $E = E_{k'}$ but for which $E_k \neq E_{k'}$ have two delta-function-like peaks at each energy, but the height of the peaks scale as η, and are thus vanishingly small. This is analogous to saying that, in the long time limit, the relative phases of two states cancel if they do not have the same energy. Thus, the only relevant terms are those for which $E_k = E_{k'}$, and we can therefore insert a Kronecker delta $\delta_{E_k,E_{k'}}$ under the sum in our expression for the density matrix:

$$\begin{aligned}\frac{\eta}{\pi}G^0\rho(t_0)(G^0)^\dagger &= \sum_{kk',\psi}\langle n_\psi\rangle\psi_{kk'}\delta_{E_k,E_{k'}}\,|k\rangle\,\frac{\eta/\pi}{(E-E_k)^2+\eta^2}\,\langle k'| \\ &= \sum_{kk',\psi}\langle n_\psi\rangle\psi_{kk'}\delta_{E_k,E_{k'}}\,|k\rangle\,\delta(E-E_k)\,\langle k'| \equiv \rho_0(E).\end{aligned} \tag{2.58}$$

Plugging this result back into Eq. (2.55), we find exactly the same formula as for the scattering picture,

$$\langle\bar{A}\rangle = \int dE\,\mathrm{tr}[\rho_0(E)(1+VG^\dagger(E))A(1+G(E)V)], \tag{2.59}$$

and thus expanding the parentheses under the integral on the right hand side, we obtain four similar terms:

$$\langle\bar{A}\rangle = \int dE\,\mathrm{tr}[\rho_0\,(A + AGV + VG^\dagger A + VG^\dagger AGV)]. \tag{2.60}$$

Note that although the resulting equations are identical, if one substitutes the initial density matrix for the time-averaged one in the scattering picture, the pictures which give rise to them are subtly different. In section 2.2, we considered a collection of incoming wave packets. These wave packets were allowed to take on any shape or form, with the one condition that there existed a time before which the wave packet was far away from the molecule. Doing a statistical and time average over all possible such wave packets as evolved using the uncoupled Hamiltonian, we got a time-averaged density matrix, $\bar{\rho}_0$, containing the information about the distribution of the incoming wave packets. In our treatment above, we instead considered a distribution, ρ, which we knew at time t_0 and let it evolve in time. This density matrix was not subject to any restrictions, but described the system at an exact point in time. In many ways, the initial state picture is more general, since it requires no assumptions about the system. However, the states in it are, in general, extended across the whole system whereas the states in the scattering picture are localised in each lead. The reason for that is that a wave packet starting out in one lead will, when evolved using the uncoupled Hamiltonian, remain in that lead. Importantly, the finite size of the molecule means that its

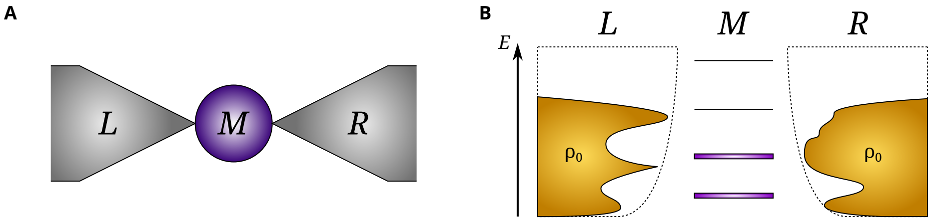

Figure 2.4: (A) Sketch of the two-lead system. (B) Illustration of the density matrix, ρ_0. The fact that the filled orange blobs do not fill out the entire band indicates that the initial state is not necessarily an equilibrium state, which would be a smooth distribution.

uncoupled Hamiltonian does not permit incoming wave packets, and thus the density matrix in the scattering picture will have no components there. Such a restriction does not exist for the initial state picture, which we shall use later. Thus, although the formal equations, Eqs. (2.41) and (2.60) are similar, the density matrices and physics involved are different.

Because of this, we can largely treat the two pictures in the same mathematical framework, but we will have to refer to the specific pictures, when discussing the terms that arise. In what follows, we shall use the notation ρ_0 to refer to the energy-resolved density matrices of the type that we find in the scattering picture and initial state picture. That is, calculations that happen in the long time limit, or steady state case. For quantities that relate to transient effects, where the $\eta \to 0^+$ limit correspondence is no longer valid, we shall use $\rho(t_0)$ and refer back to Eq. (2.54) in the description.

2.4 PARTICLE CURRENT

A large number of the experiments we are trying to describe measure an electron or charge current in steady state, and compare the measurements either using different polarisations of light, magnetic orientation or the chirality of the redox couple. Thus, a natural first operator to consider using the formalism above is the particle current. Since in all of the experiments, current effectively flows between two leads, to keep the mental model simple and concrete, we are going to assume that there are just two leads in our system in the following derivation. The extension to multiple leads is straightforward, however, and we shall do so later. Of course, not all of the experiments have actual leads in the sense of a wire. Instead, we use the term lead here to refer to any isolated medium connected to the molecule which allows an electronic current to flow.

For the sake of concreteness, we imagine that the molecule is aligned horisontally and connected to leads on the left and right, which we denote L and R respectively. This is illustrated in Figure 2.4A. To help us in our notation, let us introduce the projection operators, L, M, R as the full span over their respective regions, satisfying:

$$L + M + R = 1. \tag{2.61}$$

That is, the projection operator L is the full span of available states in the left lead,

$$L = \sum_{k \in \text{left lead}} |k\rangle \langle k| , \tag{2.62}$$

and similarly for M and R. It is easy to see that the expectation value of, for instance, the projection operator into the right lead,

$$\langle R \rangle = N\, \text{tr}[\rho R] = \sum_{\Psi, k \in \text{right lead}} \langle n_\Psi \rangle | \langle \Psi | k \rangle |^2, \tag{2.63}$$

gives the expectation value for the number of particles in the right lead. Thus, the net particle current into the right lead is*: $\langle \dot{R} \rangle = i \langle [H, R] \rangle / \hbar = i \langle H_{MR} - H_{RM} \rangle / \hbar$. Here the dot indicates the derivative of the operator w.r.t. time and H_{MR} is a shorthand notation for the product MHR. The last equality above follows from expanding the commutator and inserting unity,

$$\begin{aligned} [H, R] &= HR - RH = (L + M + R)HR - RH(L + M + R) \\ &= (L + M)HR - RH(L + M) = H_{MR} - H_{RM}, \end{aligned} \tag{2.64}$$

since the two leads are isolated from each other and thus, $LHR = 0$. This expression can in fact be simplified further by realising that $H_{MR} = H_{RM}^\dagger$, and thus the particle current into the right lead is twice the imaginary part of the expectation value of H_{RM}:

$$\langle \dot{R} \rangle = \frac{2}{\hbar} \text{Im}[\langle H_{RM} \rangle]. \tag{2.65}$$

Now, the coupling between the leads and the molecule can be written using a similar notation as:

$$V = (L + R)HM + MH(L + R) = H_{LM} + H_{RM} + H_{ML} + H_{MR}, \tag{2.66}$$

---

[*] The first equality can be shown by considering the time derivative of the expectation value of an arbitrary operator, A:

$$\begin{aligned} \partial_t \langle A \rangle &= \text{tr}[\partial_t \rho(t) A] = \text{tr}[\partial_t U(t, t_0) \rho(t_0) U(t_0, t) A] \\ &= \frac{i}{\hbar}\, \text{tr}[U(t, t_0) \rho(t_0) U(t_0, t)(HA - AH)] = \frac{i}{\hbar} \langle [H, A] \rangle, \end{aligned}$$

where we have used $U(t, t_0) = e^{-iH(t-t_0)/\hbar}$ and the cyclic property of the trace.

which now have to plug back into Eqs. (2.41) or (2.60) along with the time derivative of R in order to calculate the expectation value of the particle current. Doing so, we find all combinations of terms such as:

$$H_{RM}GH_{ML}, \quad H_{MR}GH_{LM}, \quad \text{etc.} \tag{2.67}$$

Before writing them out explicitly, there is a convenient way to deal with them, though. It involves defining the projections of the propagators in the same manner as we did for the Hamiltonian, i. e. through, $G_M = MGM$, $G_{RL} = RGL$, etc. Using the fact that the uncoupled propagators have no cross terms, i. e. $LG^0R = LG^0M = 0$, etc., the expansion of the projected propagator, G_M, using the Dyson equation allows us to conveniently collect terms related to the leads:

$$\begin{aligned} G_M &= G_M^0 + G_M^0 \underbrace{H_{ML}G_L^0H_{LM}}_{\Sigma_L} G_M + G_M^0 \underbrace{H_{MR}G_R^0H_{RM}}_{\Sigma_R} G_M \\ &= G_M^0 + G_M^0(\Sigma_L + \Sigma_R)G_M = \frac{1}{E - H_M - \Sigma_L - \Sigma_R + i\eta}, \end{aligned} \tag{2.68}$$

where Σ_L, Σ_R are the so-called *self-energies* of the left and right lead, respectively. In a similar way, we find for the other projections:

$$G_L = G_L^0 + G_L^0H_{LM}G_MH_{ML}G_L^0, \tag{2.69}$$

$$G_{LM} = G_L^0H_{LM}G_M, \tag{2.70}$$

$$G_{LR} = G_L^0H_{LM}G_MH_{MR}G_R^0. \tag{2.71}$$

The equations for G_R, G_{RM} and G_{RL} are obtained by substituting $L \leftrightarrow R$. Finally, the same logic applies to the density matrix, where we apply the notation $R\rho_0R = \rho_0^R$, $L\rho_0R = \rho_0^{LR}$, etc.

Equipped with the tools above, we are now ready to tackle the problem of calculating the particle current. The first term in Eq. (2.41), related to the intrinsic current embedded in the density matrix is

$$\langle \bar{H}_{RM} \rangle^{(1)} = \int dE \, \mathrm{tr}[\rho_0^{MR} H_{RM}]. \tag{2.72}$$

Now, to make the number of terms we have to deal with more manageable, we are going to assume that the electronic states entering the density matrix are localised in either lead or on the molecule. In the scattering picture, this assumption can be motivated on physical grounds quite easily, as discussed at the end of the last section. It amounts to assuming that the wave packets of the incoming electrons start out in a single lead. To see that, recall that ρ_0 in the scattering picture is the time-average of the density matrix evolved with the uncoupled Hamiltonian, and thus initially uncorrelated wave packets remain so. In the initial state picture, on the other hand, it is an assumption that the electrons are initially uncorrelated between regions. This will, in general, not be true for a system in equilibrium where the states are extended across both leads and the molecule. However, if we deal with an initial state that describes the excitation or addition of an electron to a system that is otherwise in equilibrium, we can split the initial density matrix into its equilibrium and non-equilibrium parts. The excited or added electron will, in general, be localised and thus its associated density matrix will be block-diagonal. For the equilibrium density we must still include all the cross-terms, but if the equilibrium state is one in which no current flows, then these terms can be ignored as they conspire to contribute zero current in total. For completeness, we derive the equations for the cross-terms in Appendix C.1.

As a consequence of the considerations above, the density matrix will be assumed diagonal in L, M, R, and therefore the term in Eq. (2.72) is zero. Before considering the other terms of Eq. (2.60), it turns out that the terms related to ρ_0^M are much easier to deal with, if we make use of Eq. (2.54) for the states in the molecular subspace first. This gives the expression:

$$\langle \bar{H}_{RM} \rangle_M = \frac{\eta}{\pi} \int dE \,\mathrm{tr}\left[\rho^M(t_0) G^\dagger_{MR} H_{RM} G_M\right] = \frac{\eta}{\pi} \int dE \,\mathrm{tr}\left[\rho^M(t_0) G^\dagger_M \Sigma^\dagger_R G_M\right]. \tag{2.73}$$

Consequently, the current into the right lead due to states starting out on the molecule is:

$$\langle \dot{\bar{R}} \rangle_M = \frac{\eta}{\pi} \int \frac{dE}{\hbar} 2\mathrm{Im}\,\mathrm{tr}\left[\rho^M(t_0) G^\dagger_M \Sigma^\dagger_R G_M\right]. \tag{2.74}$$

To simplify our analysis, we shall introduce the function, $\mathcal{A}$, to represent the anti-hermitian part of an operator, in analogy with Im for the imaginary part. That is, $2\mathcal{A}[A] = i(A^\dagger - A)$. Note that the imaginary part of a trace is $\mathrm{Im}[\mathrm{tr}[A]] = \mathrm{tr}[\mathcal{A}[A]]$, which follows from the invariance of the trace under transposition. Thus, we can pull the imaginary part under the trace, if we replace it by the anti-hermitian part. Using the fact that the product of operators, $G_M \rho G^\dagger_M$, is hermitian, the anti-hermitian part only acts on the self-energy. Defining, $\Gamma_R = 2\mathcal{A}[\Sigma^\dagger_R]$, we thus end up with:

$$\langle \dot{\bar{R}} \rangle_M = \frac{\eta}{\pi} \int \frac{dE}{\hbar} \,\mathrm{tr}\left[\rho^M(t_0) G^\dagger_M \Gamma_R G_M\right]. \tag{2.75}$$

The Γ-matrix has a physical interpretation. It is proportional to the strength of the coupling between the molecule and the leads and to the density of states in the lead at energy E. More formally, it is given as $\Gamma_R = 2\pi H_{MR} \delta(E - H_R) H_{RM}$. In the limit of an infinitely large lead, and thus a continuous spectrum of H_R, the fact that the coupling

H_{RM} only relates to the part of the lead connected to the molecule, and therefore scales as the square root of the inverse of the lead size, means that Γ_R is well approximated by a continuous, finite function. Being the anti-hermitian part of the self-energy, it gives rise to a non-unitary time evolution for states on the molecule, and thus describes leakage out of it. In steady state, we take the limit $\eta \to 0^+$, and since the molecule has a discrete spectrum and Γ_R has finite measure, the integral is finite and thus the suppression factor of η quenches the steady state current resulting from electrons initially on the molecule. This should make sense intuitively, since a steady state current from these electrons would require an infinite number of electrons initially on the molecule, to sustain a continuous current.

Such an infinite reservoir of electrons is found in the (comparatively) infinitely large leads, however. To calculate the current from electrons in them, we collect the second and third term from Eq. (2.41). Using the block diagonality of ρ_0 and the fact that we have already dealt with terms pertaining to ρ_0^M, we are left with just a single term:

$$\langle \bar{H}_{RM} \rangle^{(2,3)} = \int dE \, \mathrm{tr}[\rho_0 H_{RM} G H_{MR}]. \tag{2.76}$$

To simplify it, we now define the so-called γ-matrix, $\gamma_R \equiv H_{MR}\rho_0 H_{RM}$. The reason for doing so is that this operator only lives in the molecular subspace. In fact, we are going to end up with equations, in which all the operators are defined in the subspace M, which for computational purposes is convenient since M is, in general, of finite dimensionality. Consequently, the steady state current into the right lead from these terms is:

$$\langle \dot{\bar{R}} \rangle^{(2,3)} = \int \frac{dE}{\hbar} \, \mathrm{tr}[\gamma_R (2\mathcal{A}[G_M])], \tag{2.77}$$

and all we need to know is the anti-hermitian part of the propagator. It is given by:

$$\begin{aligned} 2\mathcal{A}[G_M] = i(G_M^\dagger - G_M) &= G_M i(G_M^{-1} - (G_M^\dagger)^{-1})G_M^\dagger \\ &= -G_M(\Gamma + 2\eta)G_M^\dagger. \end{aligned} \tag{2.78}$$

The last equality above contains an important relationship that we shall use in derivations later. It is known as the *Ward identity*, named after John Clive Ward, and in our single particle case it reads:

$$G_M^{-1} - (G_M^\dagger)^{-1} = i\Gamma + 2i\eta, \tag{2.79}$$

where in our current case, $\Gamma = \Gamma_L + \Gamma_R$. Plugging this result back in we finally obtain:

$$\langle \dot{\bar{R}} \rangle^{(2,3)} = -\int \frac{dE}{\hbar} \, \mathrm{tr}\Big[\gamma_R G_M (\Gamma_L + \Gamma_R + 2\eta) G_M^\dagger\Big], \tag{2.80}$$

Note that since we take the limit $\eta \to 0^+$ in steady state, we have greyed out the term 2η in Eq. (2.80), as it can be ignored as long as Γ is non-zero. Even in that limit, it is still required to ensure a mathematically well-defined behaviour in the limit $\Gamma \to 0$ as well, and thus it must be kept for consistency. For short times, it is replaced by $\hbar\tau^{-1}$, and thus contributes to the total current in that case. In what follows, we will keep these greyed out terms in the derivations, to the extent that they will turn out to prove useful in transient calculations, but otherwise we shall act as though they vanish.

The final piece to calculate the average particle current is to deal with the last term of Eq. (2.41). Ignoring cross-terms and terms related to M in ρ_0 again, we are left with:

$$\langle \bar{H}_{RM} \rangle^{(4)} = \int dE \,\mathrm{tr}[\rho_0(H_{LM} + H_{RM})G^\dagger H_{RM} G(H_{ML} + H_{MR})]. \tag{2.81}$$

Using the definitions and identities introduced above, it is straightforward to show that the particle current from this term becomes:

$$\langle \dot{\bar{R}} \rangle^{(4)} = \int \frac{dE}{\hbar} \,\mathrm{tr}\Big[(\gamma_L + \gamma_R) G_M^\dagger \Gamma_R G_M\Big]. \tag{2.82}$$

Combining all the terms, we thus find that the total particle current is given by:

$$\langle \dot{\bar{R}} \rangle = \int \frac{dE}{\hbar} \Big(\mathrm{tr}\Big[(\gamma_L + \gamma_R) G_M^\dagger \Gamma_R G_M\Big] - \mathrm{tr}\Big[(\Gamma_L + \Gamma_R + 2\eta) G_M^\dagger \gamma_R G_M\Big]\Big). \tag{2.83}$$

The result above can be simplified slightly by using the Ward identity, Eq. (2.79). Multiplying the identity by G_M and $G_M^\dagger$ from the left and right, we derive that we are free to interchange the propagators, G_M and $G_M^\dagger$ on either side of the Γ-matrix:

$$G_M(\Gamma + 2\eta) G_M^\dagger = G_M^\dagger (\Gamma + 2\eta) G_M. \tag{2.84}$$

Combining this derived property of the Ward identity with the cyclic property of the trace, we finally obtain:

$$\langle \dot{\bar{R}} \rangle = \int \frac{dE}{\hbar} \left(\underbrace{\mathrm{tr}\Big[\gamma_L G_M^\dagger \Gamma_R G_M\Big]}_{T_{L\to R}} - \underbrace{\mathrm{tr}\Big[\gamma_R G_M^\dagger \Gamma_L G_M\Big]}_{T_{R\to L}} - 2\eta \,\mathrm{tr}\Big[\gamma_R G_M^\dagger G_M\Big] \right). \tag{2.85}$$

This expression has a very intuitive interpretation, if we recognise that $T_{L\to R}$ describes the particle current from the left lead to the right lead, and $T_{R\to L}$ from right to left. Thus, the total particle current flowing into R is simply the difference between the amount flowing in and out.

EXAMPLE

SINGLE LEVEL LEAD As a consistency check, let us calculate the average current in the case where the left lead has just a single electronic level, closely coupled to the molecule, and the right lead is infinitely large but initially empty. Intuitively, in this case, one would assume that after a period of time, the electron has leaked out entirely from the left lead, and thus there should be no steady state current. Let the single level in the left lead have energy E_0, and its coupling to the molecule be given as, $H_{LM} = t\,|L\rangle\,\langle 1|$. Assuming that the electron starts in this single level in the left lead, the initial state is given by $\rho_0(E) = |L\rangle\,\delta(E - E_0)\,\langle L|$. The current, using Eq. (2.85) is thus:

$$\langle \dot{\bar{R}} \rangle = \int \frac{dE}{\hbar}\,\mathrm{tr}\left[\gamma_L G_M^\dagger \Gamma_R G_M\right] = \frac{|t|^2}{\hbar}\,\langle 1|\,G_M^\dagger(E_0)\Gamma_R(E_0)G_M(E_0)\,|1\rangle\,. \qquad (2.86)$$

Now, the uncoupled propagator in the left lead at this energy is $G_1^0(E_0) = -i\eta^{-1}$, and thus the self-energy from the left lead is $\Sigma_L = -i\eta^{-1}|t|^2$. In the limit, $\eta \to 0^+$, this term dominates entirely in the denominator of the propagator, $G_M(E_0)$, which is thus $\sim i\eta/|t|^2$. Plugging this back in, we thus find that the average current for this system is:

$$\langle \dot{\bar{R}} \rangle \propto \frac{\eta^2}{\hbar|t|^2}\Gamma_R(E_0) \underset{\eta\to 0^+}{=} 0. \qquad (2.87)$$

Note that the limit is still zero in the case where the right lead is also a single level with energy E_0. In this case, however, $\Gamma_R \sim \eta^{-1}$, and thus the scaling is to first order in η.

One may ask the question why this is not the case for *all* systems, since ρ_0 by definition always contains eigenstates of the uncoupled Hamiltonian in the leads. When the left lead becomes infinitely large, it is important to observe that there are two competing limits at play, one related to the $-i\eta^{-1}$ from the uncoupled propagator, and another to the normalisation of the wavefunctions in the lead. Consequently, $H_{ML} \propto N^{-1/2}$, where N is the size of the left lead, and thus $\Gamma \propto \eta^{-1}/N$. In other words, an infinitely sustained steady state leakage can only be sustained if the system from which it leaks is infinitely large. This observation is what lead us to claim that $\Gamma_R(E)$ as a function of energy has a finite value, despite consisting of a sum of delta-functions.

In section 2.4.3 we shall deal with the example above in more details for shorter time scales, where the limit $\eta \to 0^+$ is no longer valid.

2.4.1 *Generalisation to multiple leads*

In the calculations above, we have assumed the existence of only two leads, L and R. The extension to multiple leads, where we shall denote the projection into the $i$the lead by N_i is straightforward, however. Using the short-hand notation γ_i for the initial state in the ith lead, and similarly for Γ_i, we find that Eq. (2.83) generalizes to:

$$\langle \dot{N}_j \rangle = \int \frac{dE}{\hbar} \sum_i \left(T_{i\to j}(E) - T_{j\to i}(E) \right) - \frac{2\eta}{\hbar} \int dE \, \mathrm{tr}\left[\gamma_j G_M^\dagger G_M \right]. \tag{2.88}$$

That is, the current into j is simply the difference between the sum of all the currents flowing in and out of the lead. Note that summing over j, we find that the whole system retains net current conservation in steady state:

$$\sum_j \langle \dot{N}_j \rangle = \int \frac{dE}{\hbar} \sum_{ij} \left(T_{i\to j}(E) - T_{j\to i}(E) \right) = 0, \tag{2.89}$$

as one would expect. The relationship above also functions as a consistency check, which says that there is no net particle accumulation on the molecule. This follows from the fact that the particle current into M is given by:

$$\langle \dot{M} \rangle = \sum_i 2\mathrm{Im}[\langle H_{Mi} \rangle] = -\sum_i \langle \dot{N}_i \rangle = 0, \tag{2.90}$$

exactly as one's physical intuition would suggest.

2.4.2 *Thermal equilibrium*

Our next line of action is to show that in the limit where the initial state is in thermal equilibrium, we recover the standard Landauer formula for steady state transport. First, we have to define what we mean by the initial state being in thermal equilibrium. According to our brief discussion in section 2.1.2, it means that the electrons occupy the eigenstates of the Hamiltonian according to an energy-dependent distribution. There are two types of equilibria to consider. One is the whole system in equilibrium. In this case, by definition of it being in equilibrium, no current will flow. Another is one in which each of the leads are individually in thermal equilibrium with a reservoir with chemical potential μ. In this case, the initial state consists of eigenstates of the uncoupled Hamiltonian of each of the leads independently. Consequently, the density matrix must be block-diagonal in the leads. In the scattering picture, the density matrix is already block diagonal. Thus, we are simply requiring that the incoming wave packets follow a thermal distribution. In the initial state picture, the requirement is akin to preparing the system by thermalising the leads independently, and then at time t_0, inserting the molecule between the leads and letting time evolve.

Now, notice that the definition of Γ_R is:

$$\Gamma_R = iH_{MR}(G_R^0 - (G_R^0)^\dagger)H_{RM} = 2\pi H_{MR}\delta(E - H_R)H_{RM}. \tag{2.91}$$

From the definition of γ_R in the case of block-diagonal ρ_0, however:

$$\begin{aligned}\gamma_R &= H_{MR}\rho_0 H_{RM} = \frac{1}{N}\sum_{k\in R}\langle n_k\rangle_0 H_{MR}\left|k\right\rangle \delta(E-E_k)\left\langle k\right| H_{RM}\\ &\overset{\text{therm. eq.}}{=} \frac{1}{N}n(E-\mu_R)H_{MR}\delta(E-H_R)H_{RM} = \frac{n(E-\mu_R)}{2\pi N}\Gamma_R,\end{aligned} \tag{2.92}$$

and similarly for Γ_L and γ_L. Here, $n(E-\mu_R)$ is the Fermi-Dirac or Bose-Einstein distributions for fermions and bosons respectively, which we derived in section 2.1.2 or any other energy-dependent distribution, connected to a reservoir with chemical potential μ_R. Plugging these results back into Eq. (2.83), and multiplying by the number of particles in the system, N, to get the total particle current we find:

$$j_R = N\langle\dot{\hat{R}}\rangle = \int \frac{dE}{h}\left(n(E-\mu_L) - n(E-\mu_R)\right)\text{tr}\left[\Gamma_L G_M^\dagger \Gamma_R G_M\right], \tag{2.93}$$

which is exactly the Landauer formula. This holds not just in thermal equilibrium, but as long as the expectation values of the particle number operators, $\langle n_k\rangle$, only depend on energy. Note that in thermal equilibrium, the only difference between $T_{L\to R}$ and $T_{R\to L}$ is to which side the chemical potential, μ, in the distribution function belongs. Thus, the trace found in Eq. (2.93), $\text{tr}\left[\Gamma_L G_M^\dagger \Gamma_R G_M\right]$, is often referred to as the transmission function, which of course clashes with our definition of the transmission function in the more general case, $T_{L\to R}$. We shall denote this thermal transmission function, $T_{LR}(E)$, without the arrow, to distinguish it from the more general transmission function, as they have different properties.

It is important to emphasize that for the thermal transmission function, in the case of two leads, we have the important relationship $T_{LR} = T_{RL}$ in steady state. To see this, note that:

$$T_{LR} = \text{tr}\left[(\Gamma_L + \Gamma_R + 2\eta)G_M^\dagger \Gamma_R G_M\right] - \text{tr}\left[(\Gamma_R + 2\eta)G_M^\dagger \Gamma_R G_M\right]. \tag{2.94}$$

Using the Ward identity, Eq. (2.79), on the first term in the last equality and discarding the vanishing η-term, we obtain:

$$T_{LR} = \text{tr}\left[\Gamma_R G_M^\dagger(\Gamma_L + \Gamma_R)G_M\right] - \text{tr}\left[\Gamma_R G_M^\dagger \Gamma_R G_M\right] = T_{RL}, \tag{2.95}$$

which proves the relationship.

EXAMPLE

ELECTRIC CURRENT To relate the particle current to electric current in thermal equilibrium, we shall treat it in the case of fermions. In this case, the difference between the Fermi distributions is:

$$n_F(E-\mu_L) - n_F(E-\mu_R) = \frac{\sinh(\beta\Delta\mu/2)}{\cosh(\beta(E-E_F)) + \cosh(\beta\Delta\mu/2)}, \tag{2.96}$$

where $\Delta\mu = \mu_L - \mu_R$ and $E_F = (\mu_L + \mu_R)/2$. The detailed derivation of this expression can be found in Appendix A.2.1. For $\Delta\mu/2 \ll \beta^{-1}$, this reduces to:

$$n_F(E-\mu_L) - n_F(E-\mu_R) \approx \frac{\beta\Delta\mu/2}{\cosh(\beta(E-E_F))}, \tag{2.97}$$

which is exponentially suppressed as E deviates from E_F. Thus, integrating the transmission function with this factor will be dominated by its value around E_F:

$$j_R \approx \frac{1}{h} T_{LR}(E_F) \int_{-\infty}^{\infty} dE \left(n_F(E-\mu_L) - n_F(E-\mu_R)\right). \tag{2.98}$$

As shown in Appendix A.2.2, the integral above gives exactly $\mu_L - \mu_R$. Multiplying by the charge of the electron, we get Ohm's law:

$$\underbrace{-ej_R}_{I} = \underbrace{\frac{(\mu_R - \mu_L)}{e}}_{V} \underbrace{\frac{e^2}{h} T_{LR}(E_F)}_{G}, \tag{2.99}$$

where I, V, and G here refer to the electric current, voltage and conductance, respectively. Rewritten in terms of the quantum of conductance, $G_0 = 2e^2/h$, the electric current is given by:

$$I = V G_0 \frac{T_{LR}(E_F)}{2}. \tag{2.100}$$

Note that the factor $1/2$ above is due to the fact that the transmission function includes spin degrees of freedom. If the transmission was assumed independent of spin, the trace inside would yield a factor of two, cancelling it.

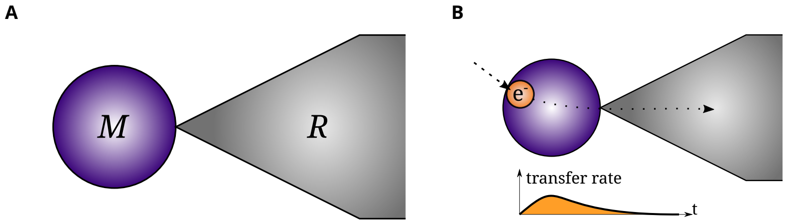

Figure 2.5: (A) Illustration of the molecule connected to a single lead. (B) An electron that is deposited on the molecule will after some time have left the molecule and have transferred to the lead.

2.4.3 *Transient effects*

In the analysis above, we wanted to calculate the particle current in the steady state case. This required either an endless flow of incoming electrons in the scattering picture, or an infinitely large bath in the initial state picture, such that a current would leak for an infinite amount of time. The steady state was reached in the limit $\eta \to 0^+$.

There are cases, however, where there is no steady state current. An example of this is illustrated in Figure 2.5, where the system consists of just a molecule coupled to a lead, which is analogous to the example of a single level lead studied earlier. If an electron is placed on the molecule, it will leak out into the lead, with a time-dependent rate. Because the electron's wavefunction is finite and the molecule has a finite size, eventually, all of the wavefunction will have leaked out, and thus the transfer rate must vanish for long times. On shorter time scales, however, this transfer rate or current is non-zero. This can be dealt with in the initial state picture, by substituting $\eta \to \hbar/2\tau$ back, as the time scale over which we average the current. As we have seen in section 2.3, this gives the linear behaviour of the current for short times.

There is one technicality with which we must deal, though, which is the issue that in thermal equilibrium, the result that the γ-matrices are proportional to the Γ-matrices no longer holds. I. e. the equilibrium distribution in the leads now looks like:

$$\gamma_j^{\text{eq.}} = \frac{2\pi}{N} \sum_{k \in j} n(E_k - \mu_j) \frac{\eta/\pi}{(E - E_k)^2 + \eta^2} H_{MR} \left| k \right\rangle \left\langle k \right| H_{RM}, \tag{2.101}$$

which is not trivially proportional to Γ_j anymore. However, we are not going to worry too much about this fact, since we know that in equilibrium, unless there are oscillating currents, the steady state current should be independent of the time scale and, typically, zero. Thus, if the density matrix consists of an equilibrium part and a non-equilibrium part, we simply split the density matrix into two and handle them separately, using the long time scale result for the equilibrium subspace.

Provided the initial state in the leads is diagonal in the basis of the eigenstates of the uncoupled Hamiltonian, the analysis from section 2.3 carries over to all values of η. Since we have in our derivations meticulously kept track of where it went, the greyed out terms now become physically relevant. Thus, all we have to do is to take the same equations and substitute $\eta \to \hbar/2\tau$, which yields a current of:

$$\begin{aligned}\langle \dot{\tilde{R}} \rangle_\tau = \frac{1}{\tau} \int dE \left(\frac{1}{2\pi} \operatorname{tr}\!\left[\rho^M(t_0) G_M^\dagger \Gamma_R G_M\right] - \operatorname{tr}\!\left[\gamma_R G_M^\dagger G_M\right] \right) \\ + \int \frac{dE}{\hbar} \left(T_{L\to R} - T_{R\to L}\right).\end{aligned} \tag{2.102}$$

If we now define $\gamma_\tau = \rho^M(t_0)\hbar/2\pi\tau$ and $\Gamma_\tau = \hbar/\tau$, the current at τ reduces to:

$$\langle \dot{\tilde{R}} \rangle_\tau = \int \frac{dE}{\hbar} \left(T_{\tau\to R} - T_{R\to\tau} + T_{L\to R} - T_{R\to L}\right), \tag{2.103}$$

where $T_{\tau\to R} = \operatorname{tr}\!\left[\gamma_\tau G_M^\dagger \Gamma_R G_M\right]$ are defined just as our usual transmission functions. Thus, comparing to the case with multiple leads discussed in section 2.4.1, the effect of including this time-dependence amounts to introducing an extra τ^{-1} "lead" which connects to every point in the system. We shall refer to it as the virtual τ-lead to distinguish it from the physical leads that we have discussed so far. However, in the multiple lead generalisation, it enters into the equations on equal footing. Since this virtual lead arises because of the greyed out terms from earlier, they should of course be ignored from now on. In fact, if we define a τ-self energy as:

$$\Sigma_\tau = -i\eta = -\frac{i\hbar}{2\tau}, \tag{2.104}$$

we can simply absorb it into the self-energy sum of the propagators, and thus we do not have to worry about keeping explicit track of it. Note, however, that there is no actual lead, but the total number of particles in the system must be conserved, since it is a closed system. Since we know that

$$\langle \dot{\tilde{M}} \rangle = - \sum_{i \in \text{physical leads}} \langle \dot{\tilde{N}}_i \rangle, \tag{2.105}$$

we can add and subtract the effect of the virtual τ-lead, to reduce the sum to zero by virtue of Eq. (2.89), and thus we identify:

$$\langle \dot{\tilde{M}} \rangle = \int \frac{dE}{\hbar} \sum_i (T_{i\to\tau} - T_{\tau\to i}). \tag{2.106}$$

This integral of course goes to zero in the long time limit, since all of the transmission functions are suppressed, and we recover the statement that there is no net particle accumulation on the molecule.

In the next section, we turn our attention to the formalism as it relates to spin currents. The reader interested in a perturbative treatment of the particle currents, and derivation of the no-polarisation theorem, can skip to chapter 3 and return to section 2.5 at a later stage for a derivation of the formalism related to the spin currents.

2.5 SPIN CURRENT

We have now established a solid foundation upon which to calculate particle currents. Before analysing them in the context of chiral molecules and thus relate them more concretely to the experiments, we must discuss spin currents, as these are in fact what the CISS effect is generally understood to cause. To get a measure for this, we again consider a system of two leads, L, R and a molecule, M. The spin along an axis $\hat{n}$ in the right lead is given by the operator,

$$S_{R\hat{n}} = R\vec{\sigma} \cdot \hat{n}R, \tag{2.107}$$

where we have used the vector notation for the Pauli matrices,

$$\vec{\sigma} = (\sigma_x, \sigma_y, \sigma_z). \tag{2.108}$$

As with the particle current being the time derivative of the projection into R, the spin current is analogously the rate of change of the spin polarisation operator:

$$\dot{S}_{R\hat{n}} = \frac{i}{\hbar}(HR\vec{\sigma} \cdot \hat{n}R - R\vec{\sigma} \cdot \hat{n}RH). \tag{2.109}$$

In general, we can decouple the Hamiltonian into terms proportional to the various Pauli matrices:

$$H = H^0\sigma_0 + H^x\sigma_x + H^y\sigma_y + H^z\sigma_z = H^0\sigma_0 + \vec{H} \cdot \vec{\sigma}, \tag{2.110}$$

where in the last equality, we have collapsed the x, y, z operators into their vector form. Plugging this result back into our equation for the spin current, Eq. (2.109), it reduces to the following terms:

$$\dot{S}_{R\hat{n}} = \frac{i}{\hbar}(H^0_{MR} - H^0_{RM})\vec{\sigma} \cdot \hat{n} + \frac{i}{\hbar}[\vec{H} \cdot \vec{\sigma}, R\vec{\sigma} \cdot \hat{n}R]. \tag{2.111}$$

To proceed, we must briefly review the commutation relations of operator products with the Pauli matrices. They are easily derived by considering the product of two such operators:

$$(\vec{a} \cdot \vec{\sigma})(\vec{b} \cdot \vec{\sigma}) = (\vec{a} \cdot \vec{b})\sigma_0 + i(\vec{a} \times \vec{b}) \cdot \vec{\sigma}. \tag{2.112}$$

Consequently, we derive the commutation relations:

$$[\vec{a}\cdot\vec{\sigma},\vec{b}\cdot\vec{\sigma}]_{\pm} = (\vec{a}\cdot\vec{b}\pm\vec{b}\cdot\vec{a})\sigma_0 + i(\vec{a}\times\vec{b}\pm\vec{b}\times\vec{a})\cdot\vec{\sigma}, \tag{2.113}$$

where ± is used for the anticommutator and commutator, respectively. With these relations in mind, the operator finally takes the vector form:

$$\begin{aligned}\dot{S}_{R\hat{n}} = {}& \frac{i}{\hbar}(H^0_{MR} - H^0_{RM})\vec{\sigma}\cdot\hat{n} + \frac{1}{\hbar}\hat{n}\times\left(2\vec{H}_R + \vec{H}_{MR} + \vec{H}_{RM}\right)\cdot\vec{\sigma}\\ &+ \frac{i}{\hbar}(\vec{H}_{MR} - \vec{H}_{RM})\cdot\hat{n}.\end{aligned} \tag{2.114}$$

For simplicity, for now we only deal with the case where the leads are independent of spin, that is, the leads are non-magnetic. In other words, $\vec{H}_R = \vec{H}_{RM} = \vec{H}_{MR} = 0$, and thus we are only left with the first term,

$$\dot{S}_{R\hat{n}} = \frac{i}{\hbar}(H_{MR} - H_{RM})\vec{\sigma}\cdot\hat{n} = \frac{2}{\hbar}\mathcal{A}[H_{RM}\vec{\sigma}\cdot\hat{n}]. \tag{2.115}$$

Carrying out an analysis similar to that of the particle current in section 2.4, we once again find that, if the density matrix has no cross-terms, the first term of Eq. (2.60) vanishes. The second and third terms, on the other hand, yield:

$$\langle\dot{S}_{R\hat{n}}\rangle^{(2,3)} = \int\frac{dE}{\hbar}\,\mathrm{tr}[\gamma_R(2\mathcal{A}[\vec{\sigma}\cdot\hat{n}G_M])]. \tag{2.116}$$

Here we have ignored the part related to the initial state on the molecule, which we shall deal with afterwards. Now, the anti-hermitian part of $G_M\vec{\sigma}\cdot\hat{n}$ is slightly more complicated than just that of G_M, but not impossible to deal with:

$$\begin{aligned}2\mathcal{A}[\vec{\sigma}\cdot\hat{n}G_M] &= i(G_M^{\dagger}\vec{\sigma}\cdot\hat{n} - \vec{\sigma}\cdot\hat{n}G_M)\\ &= iG_M^{\dagger}\left(\vec{\sigma}\cdot\hat{n}G_M^{-1} - (G_M^{\dagger})^{-1}\vec{\sigma}\cdot\hat{n}\right)G_M.\end{aligned} \tag{2.117}$$

The terms in the parentheses can be rewritten, by making use of the identity:

$$CA - BC = \left\{\frac{A-B}{2}, C\right\} - \left[\frac{A+B}{2}, C\right], \tag{2.118}$$

And thus we finally end up with:

$$2\mathcal{A}[G_M\vec{\sigma}\cdot\hat{n}] = -\frac{1}{2}G_M^{\dagger}\left(\{\Gamma,\vec{\sigma}\cdot\hat{n}\} + i\left[G_M^{-1} + (G_M^{\dagger})^{-1},\vec{\sigma}\cdot\hat{n}\right]\right)G_M. \tag{2.119}$$

Note that based on our analysis above, we have extended Γ to include also the virtual τ-lead, i. e. we are using $\Gamma = \Gamma_L + \Gamma_R + \Gamma_\tau$. Since we are dealing with normal leads, Γ is independent of spin and thus the anti-commutator (including the factor one-half) is simply $\Gamma\vec{\sigma}\cdot\hat{n}$, while the commutator becomes $-i[H_M, \vec{\sigma}\cdot\hat{n}] = 2\vec{H}_M \times \hat{n}\cdot\vec{\sigma}$, following the commutation relations derived earlier. Thus, the contribution from the second and third terms to the spin current is:

$$\langle \dot{\hat{S}}_{R\hat{n}} \rangle^{(2,3)} = -\int \frac{dE}{\hbar}\, \mathrm{tr}\Big[\gamma_R G_M^\dagger (\Gamma\hat{n} + 2\vec{H}_M \times \hat{n})\cdot\vec{\sigma} G_M\Big]. \tag{2.120}$$

Note that $\vec{H}_M$ encodes the spin-dependence of the molecule. It is, of course, the atomic spin-orbit coupling in the systems we are interested in, but for the sake of keeping the formula generic, we leave it simply as an unspecified vector quantity.

Now, the fourth term of Eq. (2.60) and the term related to the initial state on the molecule can be dealt with in one go, if we adopt the notation $\gamma = \gamma_L + \gamma_R + \gamma_\tau$. Doing so, we find after a bit of algebra:

$$\langle \dot{\hat{S}}_{R\hat{n}} \rangle^{(4)} = \int \frac{dE}{\hbar}\, \mathrm{tr}\Big[\gamma G_M^\dagger (2\mathcal{A}[\Sigma_R^\dagger \vec{\sigma}\cdot\hat{n}]) G_M\Big], \tag{2.121}$$

where the anti-hermitian part again reduces to simply $\Gamma_R\vec{\sigma}\cdot\hat{n}$, under the assumption that the right lead is independent of spin. Putting it all together, the total spin current in steady state into the right lead along an axis $\hat{n}$ is given by:

$$\begin{aligned} \langle \dot{\hat{S}}_{R\hat{n}} \rangle = \int \frac{dE}{\hbar} \Big(&\mathrm{tr}\Big[\gamma_L G_M^\dagger \Gamma_R (\hat{n}\cdot\vec{\sigma}) G_M\Big] - \mathrm{tr}\Big[\gamma_R G_M^\dagger \Gamma_L (\hat{n}\cdot\vec{\sigma}) G_M\Big] \\ &+ \mathrm{tr}\Big[\gamma_\tau G_M^\dagger \Gamma_R (\hat{n}\cdot\vec{\sigma}) G_M\Big] - \mathrm{tr}\Big[\gamma_R G_M^\dagger \Gamma_\tau (\hat{n}\cdot\vec{\sigma}) G_M\Big] \\ &+ 2\,\mathrm{tr}\Big[\gamma_R G_M^\dagger (\hat{n}\times\vec{H}_M)\cdot\vec{\sigma} G_M\Big] \Big). \end{aligned} \tag{2.122}$$

2.5.1 *Generalisation to multiple leads*

To generalise the results above to multiple leads, we must first consider the spin current in M. Similar to Eq. (2.114), it is given by:

$$\dot{S}_{M\hat{n}} = \frac{i}{\hbar}\sum_i (H_{Mi} - H_{iM})\vec{\sigma}\cdot\hat{n} + \frac{2}{\hbar}(n \times \vec{H}_M)\cdot\vec{\sigma}. \tag{2.123}$$

Plugging it in and going through the same algebra as above, it is a simple exercise to show that:

$$\begin{aligned} \langle \dot{\hat{S}}_{M\hat{n}} \rangle = \int \frac{dE}{\hbar} \Big(&\sum_i \Big(\mathrm{tr}\Big[\gamma_\tau G_M^\dagger \Gamma_i (\vec{\sigma}\cdot\hat{n}) G_M\Big] - \mathrm{tr}\Big[\gamma_i G_M^\dagger \Gamma_\tau (\vec{\sigma}\cdot\hat{n}) G_M\Big]\Big) \\ &+ 2\,\mathrm{tr}\Big[\gamma_\tau G_M^\dagger (\hat{n}\times\vec{H}_M)\cdot\vec{\sigma} G_M\Big] \Big). \end{aligned} \tag{2.124}$$

The generalisation to multiple leads is therefore straightforward and yields:

$$\begin{aligned}\langle \dot{S}_{j\hat{n}} \rangle = \int \frac{dE}{\hbar} \Big(\sum_i \mathrm{tr}\Big[\gamma_i G_M^\dagger \Gamma_j (\hat{n}\cdot\vec{\sigma}) G_M\Big] - \sum_i \mathrm{tr}\Big[\gamma_j G_M^\dagger \Gamma_i (\hat{n}\cdot\vec{\sigma}) G_M\Big] \\ + 2\,\mathrm{tr}\Big[\gamma_j G_M^\dagger (\hat{n}\times\vec{H}_M)\cdot\vec{\sigma} G_M\Big]\Big).\end{aligned} \tag{2.125}$$

Perhaps surprisingly, however, if we sum over all of the leads, even in the long time limit, the net spin is not conserved:

$$\sum_j \langle \dot{S}_{j\hat{n}} \rangle = \sum_j \int \frac{dE}{\hbar} 2\,\mathrm{tr}\Big[\gamma_j G_M^\dagger (\hat{n}\times\vec{H}_M)\cdot\vec{\sigma} G_M\Big]. \tag{2.126}$$

There is no spin accumulation on the molecule, though, which can be shown by a simple consistency check, derived by calculating the rate of change of total spin in the system, $\dot{S}_{\hat{n}} = i[H, \vec{\sigma}\cdot\hat{n}] = 2\hat{n}\times\vec{H}_M\cdot\vec{\sigma}$. Doing so, we find that it is exactly equal to the sum above in the long time limit, and thus:

$$\langle \dot{S}_{\hat{n}} \rangle = \langle \dot{S}_{M\hat{n}} \rangle + \sum_j \langle \dot{S}_{j\hat{n}} \rangle = \sum_j \langle \dot{S}_{j\hat{n}} \rangle \quad \Rightarrow \quad \langle \dot{S}_{M\hat{n}} \rangle = 0, \tag{2.127}$$

as anticipated. What this spin current really represents, however, is the precession of the spins, which can be seen by noting that if $\vec{H}_M$ is a magnetic field, there is no change in the spin along $\vec{H}_M$ by virtue of the cross product. This argument also extends to the case of the spin-orbit interaction, and in Appendix C.2, we present a proof that in equilibrium, these terms do indeed vanish. Out of equilibrium, however, the spins are allowed to precess and there will, in general, be a non-zero spin current due to precession.

2.5.2 *Magnetic leads*

We now consider the case of magnetic leads. As our model Hamiltonian for a magnet, we are going to use a kind of mean-field approach, in which electrons experience different Hamiltonians depending only on its spin along a single magnetisation axis, $\hat{m}$. Note that $\hat{m}$ is a unit vector. Thus, the Hamiltonian for the magnetic leads can be written as:

$$H_0 = \frac{1+\hat{m}\cdot\vec{\sigma}}{2} H_{0\uparrow} + \frac{1-\hat{m}\cdot\vec{\sigma}}{2} H_{0\downarrow} = \underbrace{\frac{H_{0\uparrow}+H_{0\downarrow}}{2}}_{\bar{H}_0} + (\hat{m}\cdot\vec{\sigma}) \underbrace{\frac{H_{0\uparrow}-H_{0\downarrow}}{2}}_{\Delta H_0}. \tag{2.128}$$

In this case, we have an extra term creeping into the equation for the spin current. From Eq. (2.114), it is given by:

$$\Delta \dot{S}_{R\hat{n}} = \frac{2}{\hbar}(\hat{n}\times\hat{m})\cdot\vec{\sigma}\Delta H_R. \tag{2.129}$$

As can be seen from the appearance of the cross product, this term describes precession due to the magnetic field. The second and third terms of Eq. (2.60) give, in this case:

$$\begin{aligned}\langle \Delta\dot{\hat{S}}_{R\hat{n}}\rangle^{(2,3)} = 2\int \frac{dE}{\hbar}\,\mathrm{tr}[\rho_0^R \Delta H_R(\hat{n}\times\hat{m})\cdot\vec{\sigma}G_R^0 H_{RM}G_M H_{MR}] \\ + 2\int \frac{dE}{\hbar}\,\mathrm{tr}\Big[\rho_0^R H_{RM}G_M^\dagger H_{MR}(G_R^0)^\dagger(\hat{n}\times\hat{m})\cdot\vec{\sigma}\Delta H_R\Big].\end{aligned} \tag{2.130}$$

Similarly, for the fourth term, we find:

$$\langle \Delta\dot{\hat{S}}_{R\hat{n}}\rangle^{(4)} = 2\int \frac{dE}{\hbar}\,\mathrm{tr}\Big[\gamma G_M^\dagger H_{MR}(G_R^0)^\dagger(\hat{n}\times\hat{m})\cdot\vec{\sigma}\Delta H_R G_R^0 H_{RM} G_M\Big]. \tag{2.131}$$

These terms can not immediately be reduced to a simpler form without further approximations. However, if we consider only the spin current along the magnetisation axis, i. e. setting $\hat{n}=\hat{m}$, the cross product vanishes, and we see that we do not have to deal with this correction at all. This is, of course, due to the fact that spins aligned with the axis of the magnet do not precess at all.

In the following, we are going to assume that all of the leads are magnetised along the same axis, but with, in general, different strengths. Thus, there will be a $\bar{H}_L$, $\bar{H}_R$, etc. that are not necessarily equal, and similarly for ΔH_L and ΔH_R. The reason for choosing the magnetisation along the same axis is such that we can ignore precession terms of the kind above. However, we still have to deal with other terms resulting from the magnetisation of the leads. The first is the anti-hermitian part from Eq. (2.119). To deal with it, we must first consider the self-energy of the magnetic leads, which for the right lead is given by $\Sigma_R = H_{MR}G_R^0 H_{RM}$. Since the uncoupled propagator is diagonal in the same basis as H_R, we can use the same magnetisation axis to write it as:

$$G_R^0 = \underbrace{\frac{G_{R\uparrow}^0 + G_{R\downarrow}^0}{2}}_{\bar{G}_R^0} + \hat{m}\cdot\vec{\sigma}\underbrace{\frac{G_{R\uparrow}^0 - G_{R\downarrow}^0}{2}}_{\Delta G_R^0}, \tag{2.132}$$

where $G_{R\uparrow}^0 = (E - H_{R\uparrow} + i\eta)^{-1}$, and similarly for $G_{R\downarrow}^0$. Thus, the self-energy can be decomposed in a similar manner as,

$$\Sigma = \bar{\Sigma} + \hat{m}\cdot\vec{\sigma}\Delta\Sigma. \tag{2.133}$$

Consequently, going back to Eq. (2.119), we have to consider the terms:

$$\left\{\bar{\Gamma} + (\vec{\sigma}\cdot\hat{m})\Delta\Gamma, \vec{\sigma}\cdot\hat{m}\right\} + i\left[\vec{\sigma}\cdot\hat{m}, \vec{H}_M + (\vec{\sigma}\cdot\hat{m})\Delta\Sigma\right]. \tag{2.134}$$

The first thing we notice is that the term involving $\bar{\Gamma}$ and $\vec{H}_M$ are similar to before. Because we are considering the case of spin aligned along $\hat{m}$, the term in the commutator has two parallel vectors and is therefore zero. Thus, the only new term is the one in the anti-commutator, which gives just $2\Delta\Gamma$, since $\hat{m}$ is a unit vector. We are therefore left with:

$$\langle \dot{S}_{R\hat{m}} \rangle^{(2,3)} = -\int \frac{dE}{\hbar} \,\mathrm{tr}\Big[\gamma_R G_M^\dagger \left((\bar{\Gamma}\hat{m} + 2\vec{H}_M \times \hat{m}) \cdot \vec{\sigma} + \Delta\Gamma \right) G_M \Big]. \tag{2.135}$$

The final terms we have to deal with are from Eq. (2.121). The only quantity that has changed has to do with $2\mathcal{A}[\Sigma_R^\dagger \vec{\sigma} \cdot \hat{m}]$, and thus calculating it, we find:

$$2\mathcal{A}[\Sigma_R^\dagger \vec{\sigma} \cdot \hat{m}] = \frac{1}{2}\left(\{\Gamma, \vec{\sigma} \cdot \hat{m}\} + i\left[\Sigma_R + \Sigma_R^\dagger, \vec{\sigma} \cdot \hat{m}\right] \right) = \bar{\Gamma}_R(\hat{m} \cdot \vec{\sigma}) + \Delta\Gamma_R, \tag{2.136}$$

as above. Thus, the fourth term is:

$$\langle \dot{S}_{R\hat{m}} \rangle^{(2,3)} = \int \frac{dE}{\hbar} \,\mathrm{tr}\Big[\gamma G_M^\dagger \left(\bar{\Gamma}_R(\hat{m} \cdot \vec{\sigma}) + \Delta\Gamma_R \right) G_M \Big]. \tag{2.137}$$

Putting it all together, the effect of magnetising the leads on the spin current along the magnetisation axis is:

$$\begin{aligned}
\langle \dot{S}_{j\hat{m}} \rangle = \int \frac{dE}{\hbar} \sum_i \Bigg(&\mathrm{tr}\Big[\gamma_i G_M^\dagger \bar{\Gamma}_j (\hat{m} \cdot \vec{\sigma}) G_M\Big] - \mathrm{tr}\Big[\gamma_j G_M^\dagger \bar{\Gamma}_i (\hat{m} \cdot \vec{\sigma}) G_M\Big] \\
&+ \mathrm{tr}\Big[\gamma_i G_M^\dagger \Delta\Gamma_j G_M\Big] - \mathrm{tr}\Big[\gamma_j G_M^\dagger \Delta\Gamma_i G_M\Big] \Bigg) \\
+ 2\int \frac{dE}{\hbar} \,&\mathrm{tr}\Big[\gamma_j G_M^\dagger (\hat{m} \times \vec{H}_M) \cdot \vec{\sigma} G_M\Big].
\end{aligned} \tag{2.138}$$

To round up, we note that the effect of including magnetisation in the case of the particle current is much simpler. Here, the derivation is unaffected by the possible magnetisation of the leads, and we simply have to substitute $\Gamma \to \bar{\Gamma} + (\vec{\sigma} \cdot \hat{m})\Delta\Gamma$. The result of this leads to the generalised formula:

$$\begin{aligned}
\langle \dot{N}_j \rangle = \int \frac{dE}{\hbar} \sum_i \Bigg(&\mathrm{tr}\Big[\gamma_i G_M^\dagger \bar{\Gamma}_j G_M\Big] - \mathrm{tr}\Big[\gamma_j G_M^\dagger \bar{\Gamma}_i G_M\Big] \\
&+ \mathrm{tr}\Big[\gamma_i G_M^\dagger \Delta\Gamma_j (\hat{m} \cdot \vec{\sigma}) G_M\Big] - \mathrm{tr}\Big[\gamma_j G_M^\dagger \Delta\Gamma_i (\hat{m} \cdot \vec{\sigma}) G_M\Big] \Bigg).
\end{aligned} \tag{2.139}$$

Besides the presence of the precession term in the spin current, the expressions for the particle and spin currents look identical under the interchange $\bar{\Gamma} \leftrightarrow \Delta\Gamma$ when measured along the magnetisation axis, $\hat{m}$, which makes them easier to memorise. One should be careful not to take the comparison too far, however, since there are also Γ's hidden inside the propagators.

2.6 SUMMARY

In this chapter, we set up the formalism for calculating particle and spin currents in the general case of non-interacting electrons propagating through a molecule, connected to any number of leads. The initial state of the electrons were described by the density matrix, ρ_0, which is either a time-averaged density matrix of scattering states, evolved using the uncoupled Hamiltonian, H_0, or a given initial state with no off-diagonal terms between the leads and the molecule. In this case, the initial density matrix could be represented in the molecule space through a set of operators γ_i, where i refers to the lead index. The coupling out of the molecule to the leads is represented by a set of operators Γ_i. In steady state, when the leads are in thermal equilibrium with an external reservoir, we find the equivalence $\gamma_i = n(E-\mu_i)\Gamma_i/2\pi$, where $n(E-\mu_i)$ is the equilibrium distribution at chemical potential, μ_i.

The general formula for the current into the jth lead, in the case of magnetic leads with magnetisation along a unit vector, $\hat{m}$, is given by the formula:

$$\langle \dot{N}_j \rangle = \int \frac{dE}{\hbar} \sum_i \Bigg(\mathrm{tr}\Big[\gamma_i G_M^\dagger \bar{\Gamma}_j G_M\Big] - \mathrm{tr}\Big[\gamma_j G_M^\dagger \bar{\Gamma}_i G_M\Big] + \mathrm{tr}\Big[\gamma_i G_M^\dagger \Delta\Gamma_j (\hat{m}\cdot\vec{\sigma}) G_M\Big] - \mathrm{tr}\Big[\gamma_j G_M^\dagger \Delta\Gamma_i (\hat{m}\cdot\vec{\sigma}) G_M\Big] \Bigg),$$

where $\bar{\Gamma}$ is the average coupling to the leads, and $\Delta\Gamma$ represents the difference in the coupling between spin aligned parallel and anti-parallel to the magnetisation directions. Thus, the non-magnetic limit is reached for $\Delta\Gamma \to 0$. This general formula is easily extended to handle transient effects by including an extra "virtual" lead, described by:

$$\gamma_\tau = \frac{1}{2\pi\tau}\rho^M(t_0), \quad \Sigma_\tau = \frac{-i}{2\tau},$$

where τ is effectively the time over which the current is averaged.

A similar analysis was done for the spin current, which gives an almost identical generalised formula for the spin current into the jth lead along the magnetisation axis:

$$\langle \dot{S}_{j\hat{m}} \rangle = \int \frac{dE}{\hbar} \sum_i \Bigg(\mathrm{tr}\Big[\gamma_i G_M^\dagger \bar{\Gamma}_j (\hat{m}\cdot\vec{\sigma}) G_M\Big] - \mathrm{tr}\Big[\gamma_j G_M^\dagger \bar{\Gamma}_i (\hat{m}\cdot\vec{\sigma}) G_M\Big] + \mathrm{tr}\Big[\gamma_i G_M^\dagger \Delta\Gamma_j G_M\Big] - \mathrm{tr}\Big[\gamma_j G_M^\dagger \Delta\Gamma_i G_M\Big] \Bigg) + 2\int \frac{dE}{\hbar} \mathrm{tr}\Big[\gamma_j G_M^\dagger (\hat{m}\times\vec{H}_M)\cdot\vec{\sigma} G_M\Big].$$

In the next chapter, we will treat the equations we have derived above pertubatively in the spin-orbit coupling, which allows us to make statements about the magnitude of particle and spin currents in various scenarios, and derive the no-polarisation theorem hinted at in the beginning of this chapter.

3

PERTURBATION THEORY

In this chapter, we start to use a bit more knowledge about the molecules being studied, and apply the formalism introduced in chapter 2. In particular, we shall derive the *no-polarisation theorem* that we mentioned in the beginning of the previous chapter. To do so, we make use of the fact that the only spin-dependent term in the Hamiltonian of the molecule, is the atomic spin-orbit interaction discussed in section 1.2 and given by Eq. (1.7). As a notational convenience, we define the Λ-operator, $\vec{\Lambda} \equiv \lambda \vec{L}/\hbar$ and use the definition of the electron spin operator, $\vec{S} = \hbar\vec{\sigma}/2$, where $\vec{\sigma} = (\sigma_x, \sigma_y, \sigma_z)$ is the vector of Pauli matrices, to write the atomic SOC as:

$$H_{\mathrm{SO}} = \vec{\Lambda} \cdot \vec{\sigma}. \tag{3.1}$$

For an atom with atomic number Z, the coupling constant, λ, scales roughly as Z^2 and thus the spin-orbit interaction is generally dominated by the heaviest elements in a molecule visited by an electron. For organic molecules, typical atoms (C, N, O) have a coupling constant of a few meV. In particular, for carbon atoms it is $\sim 6\,\mathrm{meV}$, as mentioned in chapter 1. Compared to other energy scales in the molecule, such as the energy spacing between molecular orbitals and the coupling to the leads, this energy is generally small. This smallness of the SOC allows us to treat it perturbatively in the propagators, which enables further manipulation of the equations derived earlier.

3.1 PARTICLE CURRENT

As a first study of the effect of the SOC and the techniques we shall use, we consider the particle current. To relate it to the experiments, we consider an initial state that has a spin polarisation, as is the case for the photoemission experiments using circularly polarised light, but in which the leads are considered independent of spin. For simplicity, we assume that all of the electrons in each lead have the same degree of polarisation, which allows us to write the density and γ matrices on the form:

$$\rho_0 \to \sum_i \frac{1 + \vec{a}_i \cdot \vec{\sigma}}{2} \rho_0^i, \quad \gamma_i \to \frac{1 + \vec{a}_i \cdot \vec{\sigma}}{2} \gamma_i, \tag{3.2}$$

where $\vec{a}_i$ is a vector describing the polarisation axis and amount in the ith lead. It is worth noting that this description does not generalise to all possible spin polarised states. For instance, consider a state in an atom where the spin and orbital degrees are entangled as:

$$|\psi\rangle = a\,|p_x, \uparrow\rangle + b\,|p_y, \downarrow\rangle\,. \tag{3.3}$$

Such a state cannot be written as a simple tensor product of the orbital and spin space, and hence its associated density matrix does not factorise as above. To keep our description simple and manageable, we are going to ignore entangled states such as the one above. The description does extend to the case where different states in the leads are polarised a different amount. In that case, the label i above can be extended to denote each channel in the leads, or orbitals on the molecule, and thus $\vec{a}_i$ describes the spin polarisation of electrons in that channel or orbital.

As we saw in section 2.4.1, all information regarding the particle current in the general case is encoded in the transmission function, $T_{i\to j}$. In our case, it is given by:

$$T_{i\to j}(\vec{a}_i) = \mathrm{tr}\left[\frac{1+\vec{a}_i\cdot\vec{\sigma}}{2}\gamma_i G_M^\dagger \Gamma_j G_M\right]. \tag{3.4}$$

To make use of the smallness of the SOC, we write the Hamiltonian as $H_M = h_M + \vec{\Lambda}\cdot\vec{\sigma}$. Thus, expanding G_M to first order in the SOC, we find

$$G_M \approx g_M + g_M(\vec{\Lambda}\cdot\vec{\sigma})g_M, \quad g_M = \frac{1}{E - h_M - \Sigma + i\eta}. \tag{3.5}$$

Here, g_M is the propagator of the molecule without the SO interaction. Plugging this result back in, we find, again to first order:

$$T_{i\to j}(\vec{a}_i) = \mathrm{tr}\left[\frac{1+\vec{a}_i\cdot\vec{\sigma}}{2}\gamma_i g_M^\dagger\left(\Gamma_j + \vec{\Lambda}\cdot\vec{\sigma} g_M^\dagger \Gamma_j + \Gamma_j g_M \vec{\Lambda}\cdot\vec{\sigma}\right) g_M\right] + \mathcal{O}[\lambda^2]. \tag{3.6}$$

For convenience, in all subsequent equations, the explicit notation that the equation contains terms of order λ^2 and higher is omitted, unless otherwise noted.

To advance, we must use the fact that the trace over the identity matrix in spin space is $\mathrm{tr}[\sigma_0] = 2$. The trace of all the Pauli matrices, though, are identical and equal to zero: $\mathrm{tr}[\sigma_x] = \mathrm{tr}\left[\sigma_y\right] = \mathrm{tr}[\sigma_z] = 0$. Thus, the trace over any Pauli matrix is zero,

$$\mathrm{tr}[\vec{a}\cdot\vec{\sigma}] = \vec{0}. \tag{3.7}$$

Using this result in conjuntion with Eq. (2.112), we conclude that for the trace of two products of Pauli matrices, we get:

$$\mathrm{tr}\left[(\vec{a}\cdot\vec{\sigma})(\vec{b}\cdot\vec{\sigma})\right] = 2\,\mathrm{tr}\left[\vec{a}\cdot\vec{b}\right]. \tag{3.8}$$

These two equations cover exactly the types of traces involved in Eq. (3.6). Using the fact that $\vec{a}_i$ is not an operator, and the operators γ_i, Γ_j, g_M are independent of spin, they commute and application of the two equations above is straight forward. The resulting transmission function becomes,

$$T_{i\to j}(\vec{a}_i) = \mathrm{tr}\Big[\gamma_i g_M^\dagger \Gamma_j g_M\Big] + \mathrm{tr}\Big[\gamma_i g_M^\dagger \left(\vec{\Lambda}\cdot\vec{a}_i g_M^\dagger \Gamma_j + \Gamma_j g_M \vec{\Lambda}\cdot\vec{a}_i\right) g_M\Big], \tag{3.9}$$

where we have now traced out the spin degrees of freedom to cancel the factor one-half.

The first thing we note about this expression is that if we define the propagator,

$$g_M(\vec{a}_i) = \frac{1}{E - h_M - \Sigma - \vec{a}_i\cdot\vec{\Lambda} + i\eta}, \tag{3.10}$$

it yields exactly the terms $g_M + g_M\vec{a}_i\cdot\vec{\Lambda}g_M$, when expanded to first order in $\vec{\Lambda}$. Thus, as long as we only care about terms up to linear order in $\vec{\Lambda}$, we can substitute it back into our equation for the transmission function, and we find the equivalence:

$$T_{i\to j}(\vec{a}_i) = \mathrm{tr}\Big[\gamma_i g_M^\dagger(\vec{a}_i)\Gamma_j g_M(\vec{a}_i)\Big]. \tag{3.11}$$

This equation is quite illuminating. First of all, the equation shows that the problem of an electron with spin travelling through a molecule with spin orbit coupling is analogous to a spinless electron travelling through a molecule with a magnetic field $\sim \lambda\vec{a}_i/\hbar$. That is, there is a Zeeman-like splitting of the energy of the electron, depending on the alignment of its orbital angular momentum with this effective magnetic field. Because it is proportional to $\vec{a}_i$, reversing the spin polarisation of the incoming electrons, in effect, reverses the effective magnetic field.

Since the trace is basis-invariant, we are free to choose any basis we want. It turns out that a convenient choice for a lot of calculations is a basis of real wave functions. In such a basis, as shown in Appendix B, time-reversal symmetry can be represented by complex conjugation. This ensures that the following identities hold for the matrices involved:

$$h_M = h_M^* = h_M^T, \quad \vec{\Lambda} = -\vec{\Lambda}^* = -\vec{\Lambda}^T,$$

where we have also used the hermitian nature of the Hamiltonian and angular momentum operators to relate them to their transpose. Similar equations also hold for the spin-independent uncoupled Hamiltonians of the leads, H_j. Consequently, the uncoupled propagator in the leads is invariant under transposition:

$$G_j^0 = (G_j^0)^T = \frac{1}{E - H_j + i\eta} \tag{3.12}$$

from which it follows that the self-energy is self-transposable, i. e.$\Sigma_j = \Sigma_j^T$, or $\Sigma_R^* = \Sigma_R^\dagger$. In combination, the propagator $g(\vec{a}_i)$ has a complex relationship with its adjoint. That is,

$$g_M^*(\vec{a}_i) = \frac{1}{E - h_M - \Sigma^\dagger + \vec{a}_i \cdot \vec{\Lambda} - i\eta} = g_M^\dagger(-\vec{a}_i). \tag{3.13}$$

We are going to make one additional assumption. This assumption is that the initial density matrix is also time-reversal invariant, which means that also $\gamma_i = \gamma_i^* = \gamma_i^T$. Using the fact that the trace is invariant under transposition of its argument, $\text{tr}[A] = \text{tr}[A^T]$, we therefore find that Eq. (3.11) can be rewritten as:

$$T_{i\to j}(\vec{a}_i) = \text{tr}\left[\Gamma_j g_M^*(\vec{a}_i)\gamma_i g_M^T(\vec{a}_i)\right] = \text{tr}\left[\gamma_i g_M(-\vec{a}_i)\Gamma_j g_M^\dagger(-\vec{a}_i)\right]. \tag{3.14}$$

This equation has the order of g_M and $g_M^\dagger$ reversed, when compared to our definition of the transmission functions. However, if we sum over j, we can use the Ward identity, Eq. (2.79), to flip them over across Γ, to restore their normal ordering. Doing so, we find the important identity:

$$\sum_j T_{i\to j}(\vec{a}_i) = \sum_j T_{i\to j}(-\vec{a}_i), \tag{3.15}$$

where the sum runs over both physical leads, and the time-dependent τ-lead in the short time limit. It is important to note that this equation *does not* say that $T_{i\to j}(\vec{a}_i) = T_{i\to j}(-\vec{a}_i)$, which would immediately get rid of any dependence of the transmission on the spin polarisation.

Now, for systems with more leads, it is more illuminating to consider the net particle current in and out of the jth lead, which we found in Eq. (2.88). It is given by:

$$\langle \dot{N}_j(\vec{a})\rangle = \int \frac{dE}{\hbar} \sum_i \left(T_{i\to j}(\vec{a}_i) - T_{j\to i}(\vec{a}_j)\right). \tag{3.16}$$

Using Eq. (3.15) on the last term, we find that the difference in the particle current between opposite initial polarisations is therefore:

$$\langle \dot{N}_j(\vec{a})\rangle - \langle \dot{N}_j(-\vec{a})\rangle = \int \frac{dE}{\hbar} \sum_i \left(T_{i\to j}(\vec{a}_i) - T_{i\to j}(-\vec{a}_i)\right). \tag{3.17}$$

Note that in contrast to Eq (3.15), the sum here runs over the initial state index, i, and not j.

3.1.1 *Thermal equilibrium*

We are now in a position to show a version of the no-polarisation theorem. It deals specifically with the steady state limit. In this limit, the first thing to realise is that in thermal equilibrium, where as we saw in the previous chapter, $\gamma_i = n(E-\mu_i)\Gamma_i/2\pi N$, Eq. (3.14) permits another identity, namely:

$$T_{i\to j}(\vec{a}) = n_F(E-\mu_i)T_{ij}(\vec{a}) = n_F(E-\mu_i)T_{ji}(-\vec{a}), \tag{3.18}$$

which follows by a permutation under the trace. Here, $T_{ij}(\vec{a}) = \mathrm{tr}\left[\Gamma_i g_M^\dagger(\vec{a})\Gamma_j g_M(\vec{a})\right]$ are the standard thermal transmission functions from Landauer transport that we discussed in section 2.4.2. This equation tells us that, $T_{ij}(\vec{a}) = T_{ji}(-\vec{a})$, which is a statement about time reversal symmetry and is a consequence of the *Onsager reciprocal relations*, named after the physicist Lars Onsager. I. e. moving from the ith to the jth lead with an effective magnetic field strength $\vec{a}$ has the same transmission probability as going in the opposite direction, with an opposite magnetic field. However, in the case of just two leads, L and R, we also derived using the Ward identity in Eq. (2.95) that, $T_{LR}(\vec{a}) = T_{RL}(\vec{a})$, i. e. equal transmission in both directions for the *same* effective magnetic field. Therefore, for a system with two leads in thermal equilibrium we arrive at the important result:

$$T_{LR}(\vec{a}) \overset{\text{therm. eq.}}{=} T_{LR}(-\vec{a}). \tag{3.19}$$

This relationship is quite profound and is exactly what was stated as the no-polarisation theorem. It tells us that to first order in the spin orbit coupling, no difference can be measured between the particle current of oppositely polarised initial states, for two leads in thermal equilibrium. It is in fact valid not just in thermal equilibrium, but for any thermal distribution, i. e. a density matrix for which states of equal energy have equal probability.

3.1.2 *Breaking the theorem*

The version of the theorem above, strictly speaking, only relates to experiments in which the transmission of oppositely polarised electrons is measured. This is realised in the photoemission experiments that use left- and right-handed polarised light to excite the electrons of opposite handedness and measure the intensity of the transmitted electrons. In those experiments, they *do* measure a difference between electrons polarised in opposite directions, however. It is therefore important to ask why the theorem does not hold in this case. The reason for that has to do with the fact that the initial state of the photoemitted electrons is not in general equally populated for states with the same energy. This is due to the fact that the transition elements of the interaction between an electron and an electromagnetic field between otherwise degenerate states is not the same, leading to so-called *selection rules*. These are indicated by a black dashed

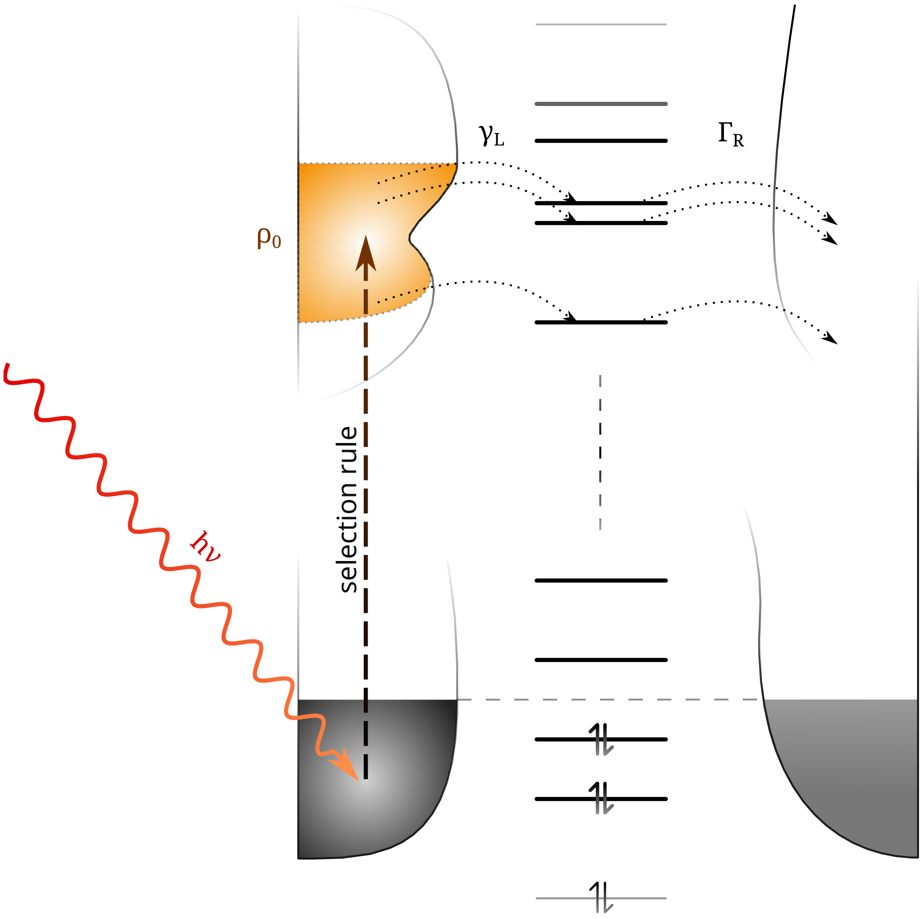

Figure 3.1: Illustration of the photoexcitation or photoemission process. Electrons from a band in the left lead are excited to higher-energy states. Because of the selection rules, otherwise degenerate excited states are not equally populated. The electrons transport through the molecule, primarily through resonant states and end up in the right lead where the current is measured. Adapted with permission from Ref. 1.

arrow in Figure 3.1, which illustrates the whole transport process. To see this, consider the matrix element in the Hamiltonian for an electron in an electric field, between two states, ψ_i and ψ_j:

$$V_{ij} = \int d\vec{r}\ \psi_i^*(\vec{r})\psi_j(\vec{r})\,\vec{r}\cdot\vec{E}(\vec{r}). \tag{3.20}$$

For simplicity, we consider the case where ψ_i is an s orbital and ψ_j is a p orbital. If the electric field is in the $\hat{x}$-direction, then $\vec{r}\cdot\vec{E}(\vec{r})$ is anti-symmetric along the $\hat{x}$-axis. Thus, the matrix element is only non-zero if ψ_j is also anti-symmetric along this axis. This is the case for the p_x orbital, but not for p_y and p_z. Thus, an electron in such an electric field will have a finite transition probability to the p_x state, but not p_y and p_z. However, for a free atom, the three p orbitals are degenerate, so in thermal equilibrium, they should be equally populated, leading to the excited electrons following a different distribution than the thermal one.

This argument also applies to larger systems, where the states are more complicated. The main message, however, is still the same, that is, the rate at which electrons are excited by photons into otherwise degenerate states depend on symmetry considerations related to the polarisation of the photon and the states. Therefore, the photoemitted electrons will, in general, not populate degenerate states with equal probability, thus breaking a fundamental assumption of the no-polarisation theorem. The theory we have derived so far is thus consistent with the fact that there is a non-zero difference in transmission in photoemission experiments.

3.1.3 *The $\vec{D}$-vector*

An alternative description of Eq. (3.9), which shall prove to be a powerful tool in describing spin polarisation comes from defining a vector quantity, which we shall refer to as the $\vec{D}$-vector,

$$\vec{D}_{i\to j}(E) = \frac{\mathrm{tr}\left[\gamma_i g_M^\dagger \left(\vec{\Lambda} g_M^\dagger \Gamma_j + \Gamma_j g_M \vec{\Lambda}\right) g_M\right]}{\mathrm{tr}\left[\gamma_i g_M^\dagger \Gamma_j g_M\right]}. \tag{3.21}$$

Note that the $\vec{D}$-vector is a dimensionless quantity that exists independent of the spin polarisation of the incoming electrons. It does, however, depend on the spin-independent part of the density matrix and so is not entirely independent of the initial conditions by which the electrons were prepared. With the definition of the $\vec{D}$-vector, the transmission function takes another form,

$$T_{i\to j}(\vec{a}_i) = T_{i\to j}(0)\left[1 + \vec{a}_i \cdot \vec{D}_{i\to j}(E)\right], \tag{3.22}$$

and thus we see that the $\vec{D}$-vector describes the polarisation direction along which transmission is maximised. Note that the transmission function is, by construction, linear in $\vec{a}_i$, and thus the transmission grows linearly with increasing polarisation.

Using Eq. (3.22), we can use it to write the difference in the particle current for opposite polarisations, Eq. (3.17), in terms of the $\vec{D}$-vector as:

$$\langle \dot{N}_j(\vec{a})\rangle - \langle \dot{N}_j(-\vec{a})\rangle = 2\int \frac{dE}{\hbar} \sum_i T_{i\to j}(0)\vec{a}_i \cdot \vec{D}_{i\to j}. \tag{3.23}$$

Since the bare transmission, $T_{i\to j}(0)$, is in general non-zero in thermal equilibrium, the no-polarisation theorem is thus a statement that the $\vec{D}$-vector vanishes in this case.

Note that the $\vec{D}$-vector is proportional to the angular momentum operator, $\vec{L}$, which is a so-called *axial vector*. Thus, the $\vec{D}$-vector is itself an axial vector. Axial vectors transform differently to polar vectors when looked at in a mirror. In particular, a mirror operation in the xy-plane, σ_{xy}, transforms the $\vec{D}$-vector as:

$$\sigma_{xy}(D_x, D_y, D_z) = (-D_x, -D_y, D_z).$$

Consequently, if a system has a mirror plane symmetry, the components of the $\vec{D}$-vector in the plane vanishes. It follows that if two such unique symmetry planes exist, the $\vec{D}$-vector vanishes entirely. These symmetry considerations must be extended to include both the coupling to the leads and the molecule, however. If we align the leads such that they are facing each other in the $\hat{z}$-direction, the fact that we distinguish between the leads in our setup breaks xy-plane symmetry, since it would interchange the two leads.

These symmetry considerations are important for understanding why the CISS effect is only seen in SAMs of chiral molecules. If the molecule is a flat, conjugated polymer like polyacetylene, the mirror symmetry in the plane prevents any polarisation in the transmission direction. The symmetry would of course still allow polarisation normal to the plane, but if the molecule is free to rotate along the axis, such a polarisation would cancel out.

Finally, with the definition of the $\vec{D}$-vector, we can begin to relate the asymmetry factors measured in the photoemission experiments in Table 1.1 back to it. Recall that the asymmetry factors were defined as $A = (I_+ - I_-)/(I_+ + I_-)$, where I_+ and I_- are the beam intensities for opposite orientations of the circular polarised light, which produce an electron beam with a polarisation of $|a| \approx 0.15$. These beam intensities are equivalent to the particle currents we have calculated, and thus the asymmetry factor is:

$$A = \frac{(1 + \vec{a}_i \cdot \vec{D}_+) - (1 - \vec{a}_i \cdot \vec{D}_-)}{(1 + \vec{a}_i \cdot \vec{D}_+) + (1 - \vec{a}_i \cdot \vec{D}_-)} = \frac{\vec{a}_i \cdot (\vec{D}_+ + \vec{D}_-)}{2 + \vec{a}_i \cdot (\vec{D}_+ - \vec{D}_-)}. \tag{3.24}$$

Here we distinguish between $\vec{D}_+$ and $\vec{D}_-$, since induced chirality of the wave functions of the substrate near the surface would, in principle, lead to two inequivalent initial states being produced for the two directions of circular polarisation. In the limiting case where the two are equal, the asymmetry factor reduces to $\vec{a}_i \cdot \vec{D}$, and is thus a direct way to probe the $\vec{D}$-vector. In section 3.2, however, we shall see that the second generation of photoemission experiments, which measured the spin polarisation of the outgoing electrons directly, allow for an even better determination.

3.1.4 *Transient effects*

We now turn our attention to transient effects. As we saw earlier, in the long time limit, the transmission function in the case of just a single lead was the same for opposite directions of polarisation. This means that an electron with spin up has escaped with equal certainty as an electron with spin down after enough time has passed. The statement was not that they escaped at the same rate, though. On shorter time scales, though, we have to include the transmission functions, $T_{\tau\to R}$ and $T_{R\to\tau}$. Assuming that only the initial state on the molecule is spin polarised, the difference between the transfer rates for opposite polarisations is again given by:

$$\begin{aligned}\langle \dot{R}(\vec{a})\rangle_\tau - \langle \dot{R}(-\vec{a})\rangle_\tau &= \int \frac{dE}{\hbar}\left(T_{\tau\to R}(\vec{a}) - T_{\tau\to R}(-\vec{a})\right) \\ &= 2\int \frac{dE}{\hbar} T_{\tau\to R}(0)\vec{a}\cdot\vec{D}_{\tau\to R}.\end{aligned} \tag{3.25}$$

Here we again see the appearance of a $\vec{D}$-vector quantity. The equation tells us that two electrons put on the molecule with opposite spin, but in otherwise identical states will, as time evolves, escape the molecule at different rates. They will both eventually escape, but there is a difference in how long they will stay on the molecule. This difference is relevant for all of the experiments that rely on transient effects. For instance, in the experiment where molecules were adsorbed on a surface, if equilibrium is established after only a single electron has left the molecule, this electron will preferentially have one spin over the other. It is also relevant for photoexcitation experiments, where recombination is measured, since one spin species will stay longer on the molecule, thus giving it more time to recombine. In these experiments, the working hypothesis was that one spin species would be preferentially transported to the substrate. To test this, they put the molecules on a magnetic substrate and claimed that by changing the orientation of the magnet, one spin species would preferentially escape. It is not immediately clear, however, that the magnet does not have an additional influence on the experiment. Thus, in order to fully understand the mechanism, we must treat the case of magnetic leads explicitly.

3.1.5 *Transient effects with magnetic leads*

We saw at the end of chapter 2 that the inclusion of magnetic leads lead to a substitution of $\Sigma \to \bar{\Sigma} + (\hat{m}\cdot\vec{\sigma})\Delta\Sigma$, where $\hat{m}$ is a unit vector pointing along the magnetisation direction. This substitution must be done not only in the numerator of the transmission functions, but also in denominators of the propagators. Fortunately, we can use the fact

Table 3.1: Result of performing the partial trace over products of Pauli matrices.

Rank	Formula
0	2
1	0
2	$2\vec{a}\cdot\vec{b}$
3	$2i(\vec{a}\times\vec{b})\cdot\vec{c}$
4	$2\left[(\vec{a}\cdot\vec{b})(\vec{c}\cdot\vec{d})-(\vec{a}\times\vec{b})\cdot(\vec{c}\times\vec{d})\right]$
5	$2i[((\vec{a}\cdot\vec{b})(\vec{c}\times\vec{d})+(\vec{a}\times\vec{b})(\vec{c}\cdot\vec{d})-(\vec{a}\times\vec{b})\times(\vec{c}\times\vec{d}))\cdot\vec{e}]$

that the only spin dependence of the propagators comes from this self energy, which is diagonal for spin pointing along $\hat{m}$. Thus, we can identify:

$$g_M = \underbrace{\frac{g_{M\uparrow}+g_{M\downarrow}}{2}}_{\bar{g}_M} + (\hat{m}\cdot\vec{\sigma})\underbrace{\frac{g_{M\uparrow}-g_{M\downarrow}}{2}}_{\Delta g_M}, \quad \text{where} \quad g_{M\sigma} = \frac{1}{E-h_M-\Sigma_\sigma}. \tag{3.26}$$

In fact, we can make an additional simplification by realising that to first order in $\Delta\Sigma$:

$$\bar{g}_M = \frac{1}{E-h_M-\bar{\Sigma}}, \quad \Delta g_M = \bar{g}_M\Delta\Sigma\bar{g}_M. \tag{3.27}$$

If we substitute this back into our equations for the bare transmission and the $\vec{D}$-vector, we are going to get a rich number of terms, containing up to six products of Pauli matrices. To keep things manageable, we are going to assume that the initial states are unpolarised. In that case, we only have to include up to five. Thus, our first line of action must be to extend our trace rules to higher number of products, so we can deal with the terms efficiently. They can be derived from Eq. (2.112), and the result of performing the partial trace over spin for traces of various ranks is shown in Table 3.1.

After using the formulas, only terms of rank 0, 2 and 4 survive and we end up with a total of twenty non-zero terms, involving different permutations of the various barred and Δ'd operators. All twenty terms are listed in Appendix D.1 for completeness. In order to get a handle of the terms, we assume that the magnetisation is weak, so that $\Delta\Sigma$ is small compared to $\bar{\Sigma}$. In this case, only nine of the twenty terms are left to first order in $\Delta\Sigma$. The first term is the bare transmission:

$$T^0_{i\to j} = \mathrm{tr}\left[\gamma_i\bar{g}_M^\dagger\bar{\Gamma}_j\bar{g}_M\right], \tag{3.28}$$

while the second and third looks reminiscent of the numerator in the $\vec{D}$-vector, but with $\Delta\Gamma_j$ instead of Γ_j:

$$T^1_{i\to j} = \hat{m}\cdot\mathrm{tr}\left[\gamma_i\bar{g}_M^\dagger\left(\vec{\Lambda}\bar{g}_M^\dagger\Delta\Gamma_j+\Delta\Gamma_j\bar{g}_M\vec{\Lambda}\right)\bar{g}_M\right]. \tag{3.29}$$

The final six terms are a bit more involved and can be reduced to:

$$2\hat{m} \cdot \mathrm{Re}\,\mathrm{tr}\left[\gamma_i \bar{g}_M^\dagger \left(\vec{\Lambda}\bar{g}_M^\dagger \bar{\Gamma}_j \bar{g}_M \Delta\Sigma + \vec{\Lambda}\bar{g}_M \Delta\Sigma^\dagger \bar{g}_M^\dagger \bar{\Gamma}_j + \bar{g}_M^\dagger \Delta\Sigma^\dagger \vec{\Lambda}\bar{g}_M^\dagger \bar{\Gamma}_j\right) \bar{g}_M\right]. \tag{3.30}$$

They represent a correction to the $\vec{D}$-vector, arising from the induced magnetisation of the electron from going in and out of the lead. Near molecular resonances, g_M is in general comparable to Γ_j, and thus they will be of the same order as the term in Eq. (3.29). Away from resonances, however, the extra factor of g_M causes them to be suppressed. Note, on short time scales, Γ_τ is large and thus the resonances of g_M are smeared out, which means that the term in Eq. (3.29) dominates. Another way to view this is by considering the fact that on short time scales, the electron does not have time to become magnetised by proximity to the lead.

In either case, in the case of the photoexcitation experiments, we find that we can formulate the problem of finding the difference in the escape rates for two different orientations using the same construct, namely the $\vec{D}$-vector. The existence of a $\vec{D}$-vector for this problem means that the rate at which electrons escape the molecule, does indeed depend on the orientation of the magnet in relation to this vector, specific to the molecule. Thus, our theory at least qualitatively predicts the experimental observations that the quenching of the emission spectrum depends on the orientation of the magnet. To actually calculate the emission spectrum, we can consider recombination in the chromophore as a kind of lead, in the sense that once an electron emits a photon, and it is detected, the system has relaxed back to its ground state.

To join the results of the no-polarisation theorem and the result above, we can interpret them as saying that there is a difference in the speed with which an electron traverses the molecule, depending on its spin. It does not say that there is a difference in the conductance, though, since we saw that there is no difference in the current for two oppositely polarised electron beams in equilibrium. To get a better understanding of this observation, we now turn our attention to the spin current.

3.2 SPIN CURRENT

Armed with the tools from the previous section, we now tackle the problem of calculating the spin current. To keep things simple, we are still going to assume that the leads are independent of spin, and thus this description does not apply to magnetised leads. Furthermore, to avoid unnecessary complications, we are going to consider an initial state that is entirely in one lead, while calculating the spin current into another. From Eq. (2.138), the spin current from i into j is thus given by a single term:

$$\langle \dot{S}_{j\hat{n}} \rangle = \int \frac{dE}{\hbar} \operatorname{tr}\left[\gamma_i G_M^\dagger \Gamma_j (\hat{n} \cdot \vec{\sigma}) G_M\right]. \tag{3.31}$$

To deal with the expansion of the propagators and the introduction of a polarised initial state, we must consider traces over products of up to three Pauli matrices. Using the fact that both $\vec{a}_i$ and $\vec{n}$ are not operators, we can move them freely about under the trace. By counting the number of Pauli matrices and applying the appropriate formulas for the traces, from Table 3.1, it is straightforward to show that the surviving terms are:

$$\langle \dot{S}_{j\hat{n}} \rangle = \int \frac{dE}{\hbar} T^0_{i\to j} \left(\vec{a}_i + \vec{D}_{i\to j} + \vec{C}_{i\to j} \times \vec{a}_i\right) \cdot \vec{n}, \tag{3.32}$$

where the $\vec{D}$-vector is the same $\vec{D}$-vector that we encountered when calculating the particle current. There is a new vector showing up, though, which we call the $\vec{C}$-vector. It is defined through the relation:

$$T^0_{i\to j} \vec{C}_{i\to j} = i \left(\operatorname{tr}\left[\gamma_i g_M^\dagger \Gamma_j g_M \vec{\Lambda} g_M\right] - \operatorname{tr}\left[\gamma_i g_M^\dagger \vec{\Lambda} g_M^\dagger \Gamma_j g_M\right] \right), \tag{3.33}$$

and, as evidenced by its cross-product with $\vec{a}_i$, describes a kind of precession of the polarisation in the measured spin current. Like the $\vec{D}$-vector, the $\vec{C}$-vector is also constructed from the angular momentum operator, and so it is also an axial vector and share similar symmetry properties. The two vectors are in fact very closely connected through a complex vector construct that we shall refer to as the $\vec{A}$-vector:

$$\vec{A}_{i\to j} = \frac{\operatorname{tr}\left[\gamma_i g_M^\dagger \vec{\Lambda} g_M^\dagger \Gamma_j g_M\right]}{\operatorname{tr}\left[\gamma_i g_M^\dagger \Gamma_j g_M\right]} = \frac{\vec{D}_{i\to j} + i\vec{C}_{i\to j}}{2}. \tag{3.34}$$

That is, the $\vec{D}$- and $\vec{C}$-vectors are twice the real and imaginary parts of the $\vec{A}$-vector, respectively.

To help interpret these two vector quantities, it is instructive to consider the polarisation of the current, which we define as the ratio between the spin current and the particle current. In the case studied above, where the initial state is entirely in the ith lead and we measure the currents in another, jth lead, the total polarisation of the current along the axis $\hat{n}$ can be written as:

$$P_{j\hat{n}} = \frac{\langle \dot{S}_{j\hat{n}} \rangle}{\langle \dot{N}_j \rangle} = \frac{\vec{a}_i + \overline{\vec{D}_{i\to j}} + \overline{\vec{C}_{i\to j}} \times \vec{a}_i}{1 + \overline{\vec{D}_{i\to j}} \cdot \vec{a}_i} \cdot \vec{n}. \tag{3.35}$$

Here we have introduced the "barred" vectors, $\overline{\vec{D}}, \overline{\vec{C}}$, which are defined through the integrals over their energy-resolved counterparts, and weighted by the bare transmission at that energy. They are therefore again related to an analogous barred $\overline{\vec{A}}$-vector as twice its real and imaginary parts,

$$\overline{\vec{A}_{i\to j}} = \frac{\int dE\, T^0_{i\to j}(E)\vec{A}_{i\to j}(E)}{\int dE\, T^0_{i\to j}(E)} = \frac{\overline{\vec{D}_{i\to j}} + i\overline{\vec{C}_{i\to j}}}{2}. \tag{3.36}$$

Before delving into the meaning of these equations, let us put Eq. (3.35) on a slightly different form by loosening the notation. That is, we get rid of the subscripts and the bars and replace $\vec{a}_i$ by $\vec{P}_{\text{in}}$:

$$\vec{P}_{\text{out}} = \frac{\vec{P}_{\text{in}} + \vec{D} + \vec{C} \times \vec{P}_{\text{in}}}{1 + \vec{D} \cdot \vec{P}_{\text{in}}}. \tag{3.37}$$

This equation is probably easiest to interpret using the scattering picture. It gives us a way to calculate the polarisation of the outgoing wave packets, given the polarisation of the incoming wave packets, along with some vectors that are specific to the molecule and the distribution of the electrons. The most striking feature of the equation is that for an unpolarised electron beam, $\vec{P}_{\text{in}} = 0$, the outgoing electrons will become polarised with polarisation $\vec{D}$. If the electrons are already polarised, they will gain an additional polarisation along $\vec{D}$, which is renormalised by the factor $1 + \vec{D} \cdot \vec{a}$ in the denominator, and rotated around the axis, $\vec{C}$. It is important to remember that this equation is the result of a perturbation to first order in a weak spin-orbit interaction, and thus the cross product must be rescaled appropriately by higher order terms in λ, which allows us to interpret it as a rotation. Importantly, the fact that the net polarisation is a result of the quantities being integrated up and weighted with the bare transmission functions means that the effect is dominated by the $\vec{D}$-vectors near molecular resonances. We shall return to this point in the next chapter. For now, we shall try relate the values for the photoemission experiments found in Table 1.2 to the $\vec{D}$- and $\vec{C}$-vectors above.

To do so, we first realise that taking the dot product with $\vec{P}_{\text{in}}$ on both sides of Eq. (3.37) allows us to isolate $\vec{D} \cdot \vec{P}_{\text{in}}$ as:

$$\vec{D} \cdot \vec{P}_{\text{in}} = \frac{\vec{P}_{\text{in}} \cdot \vec{P}_{\text{in}} - \vec{P}_{\text{out}} \cdot \vec{P}_{\text{in}}}{\vec{P}_{\text{out}} \cdot \vec{P}_{\text{in}} - 1}. \tag{3.38}$$

Thus, unlike the first generation of photoemission experiments, where the spin polarisation was determined using an asymmetry factor, we can extract the component of the $\vec{D}$-vector along $\vec{P}_{\text{in}}$ directly using the polarisation measurements before and after.

Substituting this result back into Eq. (3.37) yields, after some algebra, an expression for the $\vec{D}$ vector directly:

$$\vec{D} = \frac{1 - \vec{P}_{\text{in}} \cdot \vec{P}_{\text{in}}}{1 - \vec{P}_{\text{out}} \cdot \vec{P}_{\text{in}}} \vec{P}_{\text{out}} - \vec{P}_{\text{in}} - \vec{C} \times \vec{P}_{\text{in}}. \tag{3.39}$$

Note that if the experiments produce excitations for different polarisations of light which only affects the spin polarisation, $\vec{P}_{\text{in}}$, but otherwise leave the distribution untouched, we can add the $\vec{D}$-vectors together from two experiments with $\pm\vec{P}_{\text{in}}$, and divide by two which then yields:

$$\vec{D} = \frac{1 - \vec{P}_{\text{in}} \cdot \vec{P}_{\text{in}}}{2} \left(\frac{\vec{P}^{+}_{\text{out}}}{1 - \vec{P}^{+}_{\text{out}} \cdot \vec{P}_{\text{in}}} + \frac{\vec{P}^{-}_{\text{out}}}{1 + \vec{P}^{-}_{\text{out}} \cdot \vec{P}_{\text{in}}} \right), \tag{3.40}$$

where the superscripts $\pm$ on $\vec{P}_{\text{out}}$ refer to the measured outgoing polarisation for the corresponding incoming spin polarisations of $\pm\vec{P}_{\text{in}}$, respectively.

It is worth pointing out that the whole analysis above is also valid for transient effects through the virtual τ-lead. Thus, just as we found earlier, there are also $\vec{D}$- and $\vec{C}$-vectors associated with the spin current on short time scales.

3.2.1 *Analysis of photoemission experiments*

To fully understand the photoemission experiments, we must discuss the physics involved in creating the initial state or density matrix. To this end, it is helpful to think of a single electron in a bath of photons. The electron is initially in a non-excited state, but as time evolves, it may interact with one of the photons and become excited. We are interested *only* in what happens to the excited electrons. Thus, we are going to introduce the projection operators, P and N that project into the excited and ground state electronic subspaces, respectively. Following our brief discussion in section 3.1.1, the absorption of a photon leading to the excitation is dependent on its polarisation. We are going to consider photons that can be polarised either along the x- or the y-axis, i. e. they are incident along the z-axis.

We consider states in the scattering picture. For simplicity, let us assume that the system contains n photons initially. Projecting into the P space, we find:

$$P \left|\Psi\right\rangle = i\eta \sum_{k \in N} \psi_k P G(E_k + \hbar\omega n) \left|k, n\right\rangle, \tag{3.41}$$

where the sum runs over ground state states. Consequently, inserting a complete set $P + N$, and using $P\left|k, n\right\rangle = 0$, we end up with

$$P \left|\Psi\right\rangle = i\eta \sum_{k \in N} \psi_k G^0_P H_{PN} G_N \left|k, n\right\rangle, \tag{3.42}$$

where we have omitted the energy dependence for brevity and H_{PN} are the transition matrix elements of the interaction of the electron with the electromagnetic field, that was given in Eq. (3.20). The superscripted zero on G_P^0 indicates that it is the propagator in the P subspace without this transition matrix, but still evolved using the full pure electronic Hamiltonian. Consequently, the derivation is exactly identical to before, with $|k\rangle$ substituted by $H_{PN}G_N\,|k\rangle$.

Importantly, as we have seen, the transition elements depend on the polarisation of the incoming light. Therefore, for linearly polarised light, the associated density matrix will look like:

$$\rho_P^{x/y} = H_{PN}^{x/y} G_N^{x/y} \rho_0 (G_N^{x/y})^\dagger H_{NP}^{x/y}. \tag{3.43}$$

Now, in the experiments they use either clockwise $(+)$ or counter-clockwise$(-)$ polarised light, which have transition matrices given by:

$$H_{PN}^{\pm} = \frac{1}{\sqrt{2}}\left(H_{PN}^x \pm iH_{PN}^y\right), \quad H_{NP}^{\pm} = \frac{1}{\sqrt{2}}\left(H_{NP}^x \mp iH_{NP}^y\right). \tag{3.44}$$

The full propagators, $G_N^{x/y}$ are going to contain self-energies of the type:

$$\Sigma_P^{x/y} = H_{NP}^{x/y} G_0^P H_{PN}^{x/y}. \tag{3.45}$$

Consequently, the corresponding self-energies for circularly polarised light are given by:

$$\Sigma_P^{\pm} = \frac{1}{2}\left(H_{NP}^x \mp iH_{NP}^y\right) G_0^P \left(H_{PN}^x \pm iH_{PN}^y\right) = \underbrace{\frac{\Sigma_P^x + \Sigma_P^y}{2}}_{\bar{\Sigma}_P} \mp \underbrace{\frac{\Sigma_P^{xy} - \Sigma_P^{yx}}{2i}}_{\Delta\Sigma_P}, \tag{3.46}$$

and we find

$$G_N^{\pm} = \frac{1}{E - H_N - \bar{\Sigma}_P \pm \Delta\Sigma_P + i\eta}. \tag{3.47}$$

Here, $\bar{\Sigma}_P$ represents the self-energy one would get for randomly polarised/unpolarised light, and $\Delta\Sigma_P$ represents the deviation from this.

If the coupling is weak, such that H_{NP} is small, we can treat it pertubatively. Since the density matrix already contains two factors of H_{NP}, terms involving the self-energy would be to fourth order, and assuming that $\Delta\Sigma_P$ is smaller than $\bar{\Sigma}_P$, we can approximate $G_N \approx \bar{G}_N$. In this case, we can write the density matrix as:

$$\rho_P^{\pm} = \frac{1}{2}\left(H_{PN}^x \pm iH_{PN}^y\right) \bar{G}_N \rho_0 \bar{G}_N^\dagger \left(H_{NP}^x \mp iH_{NP}^y\right) = \underbrace{\frac{\rho_P^x + \rho_P^y}{2}}_{\bar{\rho}_P} \pm \underbrace{\frac{\rho_P^{xy} - \rho_P^{yx}}{2i}}_{\Delta\rho_P}, \tag{3.48}$$

where $\bar{\rho}_P$ is the density matrix of randomly polarised light, and $\Delta\rho_P$ is the deviation. Note that the notation $\Delta\rho_P$ might be a bit misleading, since $\Delta\rho_P$ does not satisfy the usual requirements of a density matrix, i. e. it is not positive semi-definite. It is, however, still hermitian and when added or subtracted from $\bar{\rho}_P$ it must form a proper density matrix, since $\rho_P^{\pm}$ is. Assuming that the substrate is achiral, symmetry would dictate that the number of electrons excited by the incoming light is independent of its handedness. Thus, it must be the case that $\mathrm{tr}[\rho_P^+] = \mathrm{tr}[\rho_P^-]$. Consequently,

$$\mathrm{tr}[\rho_P^{\pm}] = \mathrm{tr}[\bar{\rho}_P] \pm \mathrm{tr}[\Delta\rho_P] \quad \Rightarrow \quad \mathrm{tr}[\Delta\rho_P] = 0. \tag{3.49}$$

This is trivially satisfied if $\Delta\rho_P = \sum_i (\vec{a}_i \cdot \vec{\sigma})\bar{\rho}_{P,i}$, i. e. if the correction is only related to changing the distribution of spin of the excited electrons. Note that the right hand side must contain the blocks of $\bar{\rho}$, since an unpaired $\vec{\sigma}$ would result in negative probabilities, which is unphysical. $\Delta\rho_P$ may, however, also contain terms that are unrelated to spin, but modulate the distribution of the orbitals into which the electrons are excited. Pulling out the spin-dependence of $\Delta\rho_P$, we thus find:

$$\rho_P^{\pm} = \sum_i \frac{1 \pm \vec{a}_i \cdot \vec{\sigma}}{2}\bar{\rho}_{P,i} \pm \frac{1}{2}\Delta\rho_P. \tag{3.50}$$

Note that the factors of a half is to ensure that a fully polarised state does not contain two electrons. The analysis now carries on as before, except we are now going to consider the possibility of multiple channels for the $\bar{\rho}_P$ terms. Summing over all of the channels, we get that the spin current is given by:

$$\langle \dot{S}_{j\hat{n}} \rangle = \int \frac{dE}{\hbar} \left(\sum_i T^0_{i\to j}(\pm\vec{a}_i + \vec{D}_{i\to j} \pm \Delta\vec{D} \pm \vec{C}_{i\to j} \times \vec{a}_i) \cdot \hat{n} \right), \tag{3.51}$$

where, the bare transmission is defined as that relating only to $\bar{\rho}_P$, i. e.

$$T^0_{i\to j} = \mathrm{tr}\left[\bar{\gamma}_i g_M^\dagger \Gamma_j g_M\right]. \tag{3.52}$$

Eq. (3.51) is a kind of average over the different initial polarisations and $\vec{D}$-vectors from each channel, weighted by the transmission through that channel and multiplied by the bare transmission. To see this, if we divide and multiply the integrand by the sum over bare transmissions,

$$\left(\sum_i T^0_{i\to j} \right) \left[\frac{\sum_i T^0_{i\to j}(\vec{a}_i + \vec{D}_{i\to j} + \vec{C}_{i\to j} \times \vec{a}_i) \cdot \hat{n}}{\sum_i T^0_{i\to j}} \right], \tag{3.53}$$

the object inside square brackets is the weighted average of each of the terms. The term related to the $\vec{C}$-vector, however, becomes the weighted average of the whole precession term, $\vec{C}_i \times \vec{a}_i$. There is also a new vector in the problem, the $\Delta\vec{D}$-vector, which we have defined as:

$$\Delta\vec{D} = \frac{2\mathrm{Re}\,\mathrm{tr}\left[\Delta\gamma g_M^\dagger \vec{\Lambda} g_M^\dagger \Gamma_j g_M\right]}{\sum_i T^0_{i\to j}}, \tag{3.54}$$

and thus relates to the difference in the orbital distribution of the excited electrons.

To get the polarisation, we have to consider the particle current as well. It is given by:

$$\langle \dot{N}_j \rangle = \int \frac{dE}{\hbar} \sum_i T^0_{i\to j}(1 \pm \vec{a}_i \cdot \vec{D}_{i\to j} \pm \Delta T), \tag{3.55}$$

where, analogous to the $\Delta\vec{D}$-vector, ΔT is defined as:

$$\Delta T = \frac{\mathrm{tr}\left[\Delta\gamma g_M^\dagger \Gamma_j g_M\right]}{\sum_i T^0_{i\to j}}. \tag{3.56}$$

Introducing bars as before, to indicate the weighted average now over both energies and channels, we thus find that the total polarisation of the outgoing electrons is given by:

$$\vec{P}^\pm = \frac{\pm\overline{\vec{a}} + \overline{\vec{D}} \pm \overline{\Delta\vec{D}} + \overline{\vec{C}\times\vec{a}}}{1 \pm \overline{\vec{D}\cdot\vec{a}} \pm \overline{\Delta T}}. \tag{3.57}$$

Now, if $\vec{a}_i$ and $\vec{D}_{i\to j}$ and $\vec{a}_i$ and $\vec{C}_{i\to j}$ are uncorrelated, then we can split up the average into the product of the average of the two vectors independently. To attempt to justify this, we must consider the origin of the two quantities. $\vec{a}_i$ is related to the polarisation of the light, while $\vec{D}_i$ and $\vec{C}_i$ are related to the initial state for random light polarisation, and should therefore be independent. Consequently, the vectors must be uncorrelated and we may write $\overline{\vec{D}\cdot\vec{a}} = \overline{\vec{D}}\cdot\overline{\vec{a}}$.

We can thus lose the bars and replace $\overline{\vec{a}}$ by the incoming polarisation:

$$\vec{P}^\pm_{\text{out}} = \frac{\vec{P}^\pm_{\text{in}} + \vec{D} \pm \Delta\vec{D} + \vec{C}\times\vec{P}^\pm_{\text{in}}}{1 + \vec{D}\cdot\vec{P}^\pm_{\text{in}} \pm \Delta T}. \tag{3.58}$$

Similar to how we did at the end of the previous section, we can now take the inner product with $\vec{P}^\pm_{\text{in}}$ to isolate the $\vec{D}$-vector. After a bit of algebra, this yields:

$$\vec{D} = \frac{1 \pm \Delta T - |P^\pm_{\text{in}}|^2}{1 - \vec{P}^\pm_{\text{in}}\cdot\vec{P}^\pm_{\text{out}}}\vec{P}^\pm_{\text{out}} - \vec{P}^\pm_{\text{in}} - \vec{C}\times\vec{P}^\pm_{\text{in}} \pm \left(\frac{(\vec{P}^\pm_{\text{in}}\cdot\Delta\vec{D})\vec{P}^\pm_{\text{out}}}{\vec{P}^\pm_{\text{in}}\cdot\vec{P}^\pm_{\text{out}} - 1} - \Delta\vec{D}\right). \tag{3.59}$$

This equation is similar to what we got before, except for the terms involving $\Delta\vec{D}$ and ΔT. Unfortunately, this equation contains four unknowns, $\vec{D}$, $\vec{C}$, $\Delta\vec{D}$ and ΔT, but in all of the photoemission experiments, only three polarisations were measured: linear and the two circular polarisations. This leaves us unable to determine all four quantities.

We can make some progress, however, by noting that the experiments all measure the spin polarisation only along the $\hat{z}$-axis. Projecting along this axis, assuming that the photoemitted electrons are initially polarised in the $\hat{z}$-direction, the cross product with the $\vec{C}$-vector vanishes. We are thus left with the simpler equations:

$$P_{\text{out}}^{\pm} = \frac{P_{\text{in}}^{\pm} + D \pm \Delta D}{1 + DP_{\text{in}}^{\pm} \pm \Delta T} \quad \Rightarrow \quad D = \frac{P_{\text{out}}^{\pm} - P_{\text{in}}^{\pm} \pm (\Delta T P_{\text{out}}^{\pm} - \Delta D)}{1 - P_{\text{in}}^{\pm} P_{\text{out}}^{\pm}}. \tag{3.60}$$

Using the fact that ΔD and ΔT are only present for circularly polarised light, and givesthe projection of $\vec{D}$-vector can easily be calculated for unpolarised photons, and gives:

$$D = \frac{P_{\text{out}}^{u} - P_{\text{in}}^{u}}{1 - P_{\text{in}}^{u} P_{\text{out}}^{u}}, \tag{3.61}$$

where the superscript, u, refers to unpolarised light. Note that we retain the possibility of the unpolarised light to still generate spin polarised electrons. The reason for keeping this is due to the fact that such a non-zero polarisation for linearly polarised light is found in experiments on polycrystalline gold substrates. Plugging this into the equation for circularly polarised light, we can define a factor relating the quantities ΔT and ΔD, to the measured polarisations:

$$A^{\pm} \equiv (1 - P_{\text{in}}^{\pm} P_{\text{out}}^{\pm}) \frac{P_{\text{out}}^{u} - P_{\text{in}}^{u}}{1 - P_{\text{in}}^{u} P_{\text{out}}^{u}} - (P_{\text{out}}^{\pm} - P_{\text{in}}^{\pm}) = \pm(\Delta T P_{\text{out}}^{\pm} - \Delta D). \tag{3.62}$$

From this definition, a bit of algebra lets us extract ΔT and ΔD as:

$$\Delta T = \frac{A^{+} + A^{-}}{P_{\text{out}}^{+} - P_{\text{out}}^{-}}, \quad \Delta D = \Delta T \frac{P_{\text{out}}^{+} + P_{\text{out}}^{-}}{2} - \frac{A^{+} - A^{-}}{2}. \tag{3.63}$$

Now, there is one technicality that we have not dealt with. It is related to the fact that in our derivation, we have spoken of unpolarised light, whereas in the experiments, they use a linearly polarising filter, such that the incoming light is in fact not randomly polarised, as we had assumed. However, we are going to blindly ignore this fact and assume that the distribution of excited electrons for linearly polarised and randomly polarised light is, for our purpose, the same. In Table 3.2 we list the calculated values of the projection of the D- and ΔD-vectors, as well as ΔT, for the different experiments using the reported data. The errors on the experimental data have been estimated from the data to be around $\pm 5\%$ for all experiments. Although there are slight variations, the 5% error has been choosen as a reasonable lower bound. In some of the columns, a dash is printed instead of a value. This has been done in the cases where the calculation yielded an error of more than 10^3. For the experiments, on polycrystalline gold using bacteriorhodopsin and oligopeptides, the polarisation of the bare gold profiles were not reported and the values from the dsDNA studies was used instead as the incoming polarisations. The polarisation from the bare surfaces are shown in Table D.1.

Table 3.2: Polarisation quantities for photoemission experiments calculated from experimental data.

Molecule	Substrate	D (%)	ΔD (%)	ΔT (%)	δ (%)
50-bp dsDNA	Au(111)	-31 ± 7	30 ± 90	-40 ± 280	0.0 ± 8
40-bp dsDNA	Au(poly.)	-40 ± 7	20 ± 120	-50 ± 330	1.3 ± 8
50-bp dsDNA		-38 ± 7	12 ± 82	-40 ± 230	1.3 ± 8
78-bp dsDNA		-58 ± 6	-10 ± 140	10 ± 240	-0.4 ± 7
Bacteriorhodopsin	Au(poly.)	12 ± 7	1 ± 24	10 ± 190	-0.5 ± 9
Bacteriorhodopsin	Al(poly.)	15 ± 7	–	–	0.0 ± 9
AL5 oligopeptide	Au(poly.)	-13 ± 7	2 ± 18	-10 ± 160	0.4 ± 8
AL6 oligopeptide		-16 ± 7	0 ± 26	0 ± 170	-0.1 ± 9
AL7 oligopeptide		-20 ± 7	3 ± 38	-20 ± 210	0.9 ± 9
M-helicene	Cu(332)	-7 ± 7	20 ± 630	–	0.6 ± 9
P-helicene		12 ± 7	10 ± 210	–	-0.5 ± 9
M-helicene	Ag(110)	-9 ± 7	2 ± 34	-20 ± 350	-0.5 ± 9
P-helicene		7 ± 7	–	–	-0.9 ± 9
M-helicene	Au(111)	-8 ± 7	-3 ± 5	-2 ± 29	0.7 ± 9
P-helicene		8 ± 7	0 ± 6	0 ± 33	0.0 ± 9
L-CuO film (20 nm)	Au(111)	-12 ± 7	–	–	–
D-CuO film (20 nm)		4 ± 7	–	–	–

The last column of the table contains a value, δ, which we have defined as:

$$\delta = \frac{D^+ + D^-}{2} - \vec{D}^u, \tag{3.64}$$

where $D^\pm$ are the $\vec{D}$-vectors calculated assuming ΔD and ΔT are zero. I. e. the difference between the $\vec{D}$-vector for unpolarised light and the $\vec{D}$-vector as calculated using Eq. (3.40). If this assumption was true, we should find $\delta = 0$. In our analysis above, we assumed that the emitted electrons had their spin aligned exactly parallel to the $\hat{z}$-axis. If this was not the case, Eq. (3.40) would still hold assuming ΔD and ΔT were zero. Thus, δ is a measure of how consistent the experiments are with ΔD and ΔT being zero.

Unfortunately, as evidenced by the table, the errors on the experiments are too large to really say anything meaningful about ΔD and ΔT, except for the fact that they are consistent with being zero. This is also reflected in δ, which, despite the large errors, is generally vanishing. Thus, the data is consistent with the simpler model, i. e. the assumption that the part of $\Delta\rho_P$ pertaining to the orbital degrees of the excitation can be ignored.

3.2.2 *No-polarisation theorem*

Having studied the particle and spin currents and how they relate to the experiments, we are now ready to derive a more general form of the no-polarisation theorem. It takes its outset in traces of the type $\mathrm{tr}\left[\gamma_L g_M^\dagger \vec{\Lambda} g_M^\dagger \Gamma_R g_M\right]$, which we have seen in the numerator of the $\vec{A}$-vector. The proof is about showing that if γ_L is proportional to Γ_L, and the system has only two leads, the $\vec{A}$-vector is a purely imaginary quantity, i. e. the $\vec{D}$-vector vanishes. Our starting point is to consider the trace

$$\mathrm{tr}\left[\Gamma_L g_M^\dagger \vec{\Lambda} g_M^\dagger \Gamma_R g_M\right] = i\,\mathrm{tr}\left[\Gamma_L g_M^\dagger \vec{\Lambda}(g_M - g_M^\dagger)\right] - \mathrm{tr}\left[\Gamma_L g_M^\dagger \vec{\Lambda} g_M^\dagger (\Gamma - \Gamma_R) g_M\right], \quad (3.65)$$

where in the last equality, we have used $\Gamma = \Gamma_L + \Gamma_R$ and the relationship, $i(g_M - g_M^\dagger) = g_M^\dagger \Gamma g_M$ that we have seen several times already. Using the fact that in a real basis, $\vec{\Lambda} = -\vec{\Lambda}^T$, $\Gamma_L = \Gamma_L^T$ and $g_M = g_M^T$, the real part of the first term is identically zero. To see this, note that from transposition and cyclic permutations of the argument inside the trace, we find that

$$\mathrm{tr}\left[\Gamma_L g_M^\dagger \vec{\Lambda} g_M^\dagger\right] = -\,\mathrm{tr}\left[\Gamma_L g_M^\dagger \vec{\Lambda} g_M^\dagger\right] = 0, \quad (3.66)$$

and,

$$\mathrm{tr}\left[\Gamma_L g_M^\dagger \vec{\Lambda} g_M\right] = -\,\mathrm{tr}\left[\Gamma_L g_M \vec{\Lambda} g_M^\dagger\right] = -\,\mathrm{tr}\left[\Gamma_L g_M^\dagger \vec{\Lambda} g_M\right]^*. \quad (3.67)$$

Since the first equation is zero and the last equation tells us that it is purely imaginary, we find that the real part of this term vanishes.

For the second term in Eq. (3.65), we again use the invariance of the trace under transposition and cyclic permutations, to end up with:

$$\mathrm{tr}\left[\vec{\Lambda} g_M^\dagger \Gamma_L g_M \Gamma_L g_M^\dagger\right] = -\,\mathrm{tr}\left[\vec{\Lambda} g_M^\dagger \Gamma_L g_M \Gamma_L g_M^\dagger\right] = 0. \quad (3.68)$$

Consequently, the $\vec{A}$-vector is purely imaginary and given by:

$$\vec{A}_{L\to R} = i\frac{\mathrm{tr}\left[\Gamma_L g_M^\dagger \vec{\Lambda} g_M\right]}{\mathrm{tr}\left[\Gamma_L g_M^\dagger \Gamma_R g_M\right]}. \quad (3.69)$$

The fact that the real part of the $\vec{A}$-vector vanishes, means that only the $\vec{C}$-vector survives. Thus, the spin of the incoming electrons may precess, but they will not become additionally polarised. Crucially, the theorem depends on the requirement that $\Gamma = \Gamma_L + \Gamma_R$. If we add an extra lead to the system, which contributes a term to the self-energy, Γ_Y, we would have found instead: $\Gamma - \Gamma_R = \Gamma_L + \Gamma_Y$. The Γ_L term would still vanish, but now there would be a new non-zero real part,

$$\operatorname{Re}\operatorname{tr}\left[\Gamma_L g_M^\dagger \vec{\Lambda} g_M^\dagger \Gamma_R g_M\right] = -\operatorname{Re}\operatorname{tr}\left[\Gamma_L g_M^\dagger \vec{\Lambda} g_M^\dagger \Gamma_Y g_M\right]. \tag{3.70}$$

This is consistent with previous theoretical works, which found that in the Landauer transport regime, significant spin polarisation could only be achieved if a third lead or other dephasing terms, resulting in an anti-hermitian self-energy, were added to the system.

In fact, we see that the total spin is conserved. The addition of an extra lead simply means that a spin current into the right lead results in an opposite spin current into the extra Y-lead. Therefore, to make an argument for dephasing terms, somehow spin has to be lost to the environment.

As mentioned, dephasing due to coupling to vibrations or other bosonic degrees of the system does not permit breaking of the no-polarisation theorem. This can be realised by the following analysis: Let the full Hamiltonian of the electronic and bosonic system be written in second quantisation as:

$$H_{\text{full}} = \underbrace{H_e \otimes H_b}_{H} + V_{\text{int}}, \quad V_{\text{int}} = \sum_{kk',q} V_{kk',q} c_k^\dagger c_{k'} (b_q + b_q^\dagger). \tag{3.71}$$

If there is a total of N bosonic modes, the full state can be written using $N+1$ quantum numbers: the electron state and the occupation of the N bosonic modes:

$$|\Psi\rangle = |k, n_1, \dots n_N\rangle . \tag{3.72}$$

Now, the claim is that the self-energy from the coupling to bosons leads to an extra "dephasing lead". If we look at the propagator for the full state, and only consider terms which leave the bosonic part unchanged, we do indeed get out an effective electronic propagator, with an effective self-energy from the coupling to the bosons. To see this, we can write the full propagator using the Dyson equation as:

$$G_{\text{full}} = G + GV_{\text{int}}G + GV_{\text{int}}GV_{\text{int}}G_{\text{full}}. \tag{3.73}$$

Because of the fact that V_{int} contains only products involving one bosonic creation or annihilation operator, we must have an even number of interactions to leave the bosonic degrees unchanged. Thus, the self-energy from the bosons in this case becomes:

$$\Sigma_b = \operatorname{tr}_b[V_{\text{int}} G V_{\text{int}}], \tag{3.74}$$

where the trace only runs over the bosonic degrees, and it has been introduced to ensure that only diagonal terms are included. We therefore get an effective electron propagator,

$$G_e = \frac{1}{E - H_e - \Sigma_b + i\eta}, \tag{3.75}$$

which would indeed appear to allow us to break the no-polarisation theorem. However, if we are calculating the current, the transmission function, $\mathrm{tr}\left[\gamma_L G_M^\dagger \Gamma_R G_M\right]$, contains *two* full propagators. Thus, from the Dyson expansion above, there is an extra term related to taking one power of V_{int} from each propagator. This term is known as a *vertex correction*, and turns out to be a crucial ingredient to a correct analysis. To see this, no additional calculations actually need to be done, since at no point in our derivations have we assumed that the states we were dealing with did not include extra bosonic degrees of the type above. Thus, we can simply use the full Hamiltonian given above which includes both the electronic and bosonic degrees and do the analysis using the full states. Consequently, if the combined electron and bosonic system is in thermal equilibrium, the no-polarisation theorem will still hold. It does mean, however, that if the electronic system is in thermal equilibrium, but the bosonic system is not, the theorem will be broken. An example of coupling to a bosonic system out of equilibrium are the experiments which involve laser irradiation, since the laser beam comes from a particular direction, often with a specific polarisation. In this case, otherwise degenerate photonic states are unequally populated. In general, though, in the case of phonons or vibrations, it is fair to assume that the bosonic system is thermalised. Therefore, such a coupling to the environment does not provide a means to break the no-polarisation theorem.

3.2.3 *Electrochemistry experiments and the sudden approximation*

We now turn our attention towards the electrochemistry experiments in which a gate voltage is applied. In these experiments, we have a molecule connected to a single lead. The system is initially in equilibrium, and thus no current flows between the molecule and the lead. When the gate voltage is applied, the Hamiltonian of the molecule is altered by adding a constant electric field across, and thus a linear potential, U, depending on the z coordinate:

$$H_M = H_{M,0} + eU(z). \tag{3.76}$$

To describe this, we can attempt to use a very simple model, the *sudden approximation*. This approximation says that the density matrix before and after the field is applied

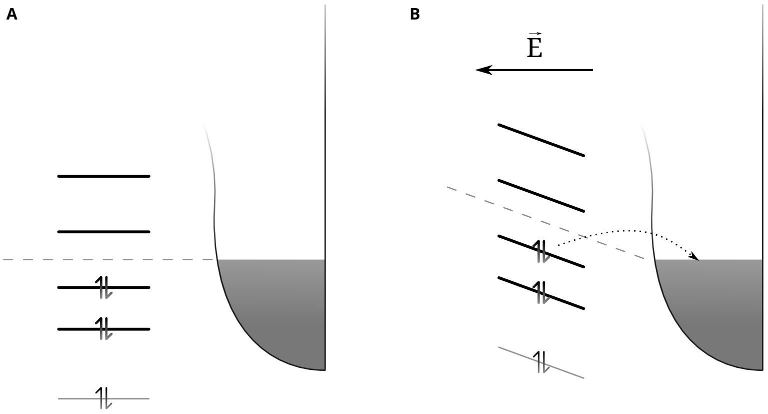

Figure 3.2: (A) Illustration of a molecule in equilibrium with a lead. (B) The application of an electric field shifts the molecular levels and causes electrons to flow from the molecule to the lead.

is the same. In other words, the field is applied so suddenly that the electrons do not have time to react. Of course, the application of the voltage does not happen so fast in reality, but we shall use it for illustrative purposes. Now, we know that the initial state was in equilibrium for the system without the gate. We denote the associated density matrix ρ_i. We also assume that as time evolves, the density matrix with the gate will evolve into an equilibrium configuration, that we denote ρ_U. In this configuration, by assumption of it being an equilibrium state, no net current will flow on any time scale. The interesting physics happens in the transition between the two configurations. Thus, we are interested in the difference,

$$\Delta\rho = \rho_i - \rho_U, \tag{3.77}$$

which is the density matrix we are going to plug into our equations, to find the response of the system on short time scales.

Now, we assume that the gate is grounded to the lead, such that the equilibrium state projected into the lead is the same with and without it. The cross-terms between the lead and the molecule, are a little harder to do away with, and should in principle be treated in full. However, for simplicity, we are going to argue that the important physics can be understood from the fact that the molecular orbitals are shifted above the chemical potential of the leads, thus resulting in the transfer of electrons away from the molecules. The information about the number of electrons on the molecule resides in the block of the density matrix belonging to the molecule, i. e. the diagonal ρ_M block. To see this, note that the number of electrons on the molecule is exactly the trace, $\mathrm{tr}[\rho M] = \mathrm{tr}[\rho_M]$. Thus, the change in the occupation numbers can be understood from the diagonal part, and we therefore ignore the cross-terms of $\Delta\rho$ between the lead and the molecule. The spin current is therefore given by the usual equation:

$$\langle \dot{\hat{S}}_{R\hat{n}} \rangle_\tau = \int \frac{dE}{\hbar} \operatorname{tr}\left[\Delta\gamma_\tau G_M^\dagger \Gamma_R (\vec{\sigma} \cdot \hat{n}) G_M\right], \tag{3.78}$$

where $\Delta\gamma_\tau = \Delta\rho\hbar/2\pi\tau$. Importantly, this equation is not covered by the no-polarisation theorem. To see this, note that $\Delta\gamma_\tau$ is, in general, not proportional to Γ_τ, which is proportional to the identity matrix. Only in the specific case where $\Delta\gamma_\tau$ spans the entire molecular subspace are they proportional, and the no-polarisation theorem causes the effect to vanish. As a consequence, applying a sudden gate voltage leads to charge reorganisation. Because of the charging of the molecule, it is likely that only one electron will have to be transferred to the substrate. Since we have already seen that for such transient effects, one spin escapes faster than the other, there will be a preferential transfer of that spin species. We can find associated time-dependent $\vec{D}$- and $\vec{C}$-vectors to describe the polarisation. The time scale over which this happens is undoubtedly shorter than the experimental relaxations observed in the Hall response of devices measuring this effect. However, as discussed in section 1.3.4, the anomalous Hall effect is also much stronger than can be explained by just an interaction with the magnetic moments of the injected spins. Thus, further work needs to be done in order to explain the details of the response of the Hall device to this transient polarisation.

3.2.4 *Magnetic equilibrium*

We end this chapter with a discussion of the transport experiments involving a magnet, as covered in section 1.3.3 and the analogous cyclic voltammetry electrochemistry experiments. These are the only types of experiments that we have not yet discussed in the context of the theory. In these experiments, they measure a difference in the steady state current, depending on the direction of the magnetic field for a finite applied bias. To describe the current when the leads are in thermal equilibrium, we are going to use the scattering picture. In this case, the cross-terms in the density matrix vanish, so we do not have to worry about them at all, and the case of thermal equilibrium is described exactly by the γ-matrices, $\gamma_i \to n(E-\mu_i)\Gamma_i/2\pi N$.

Now, in the experiments, they use two leads, one of which is magnetic. As usual, we denote the leads L and R, and let R be the magnetic lead. It turns out that we have to be extremely careful with applying our perturbation to describe this problem. If we considered only the first-order terms, we would find that there is an effect. However, a full numerical calculation shows that the transmission is symmetric in under a reversal of the direction of the magnetisation of the lead. This can also be shown from the symmetry arguments that we present below. The full propagator of the molecule is given by:

$$G_M(\hat{m}) = \frac{1}{E - H_M - \Sigma(\hat{m})}, \tag{3.79}$$

where the dependence on the magnetisation direction, $\hat{m}$, is only present in the self-energy, $\Sigma(\hat{m})$. The only term in the self-energy that depends on the magnetisation, is the self-energy from the right lead, which is given by:

$$\Sigma_R(\hat{m}) = H_{MR} \frac{1}{E - \bar{H}_R - \Delta H_R(\hat{m} \cdot \vec{\sigma}) + i\eta} H_{RM}. \tag{3.80}$$

In thermal equilibrium, as we have seen in section 2.4.2, transport is governed by the thermal transmission functions,

$$T_{LR}(\hat{m}) = \mathrm{tr}[\Gamma_L G^\dagger(\hat{m}) \Gamma_R(\hat{m}) G(\hat{m})]. \tag{3.81}$$

For these, it holds that if the full self-energy is given by $\Sigma = \Sigma_L + \Sigma_R$, then the Ward identity guarantees that, $T_{LR}(\hat{m}) = T_{RL}(\hat{m})$. However, from the identities following from time reversal of the Hamiltonian, we also find that:

$$T_{LR}(\hat{m}) = \mathrm{tr}[G(-\hat{m}) \Gamma_R(-\hat{m}) G^\dagger(-\hat{m}) \Gamma_L] = T_{RL}(-\hat{m}), \tag{3.82}$$

the derivation of which is found in Appendix B. Consequently, $T_{LR}(\hat{m}) = T_{LR}(-\hat{m})$. This result is analogous to the first version of the no-polarisation theorem we presented in section 3.1.1, except this is valid to *all* orders of the spin-orbit coupling, i. e. it is an exact result. It is not a result that says that there is no-polarisation of the electrons, however. The spin current is non-zero and dependent on the direction of the magnetisation, but the total current is the same for opposite magnetisations, which simply states that the magnet works as a spin injector into the other lead. Thus, it seems like we have proven that there can be no difference in the measured current, when the magnet is flipped. The experiments *do* show an effect though, so there must be something wrong with our assumptions somehow. In these transport experiments, we would be hard pressed to argue that the initial state is non-thermal. Thus, there either *has* to be another term in the self-energy in order to break the Ward identity, or some alternative explanation altogether that helps us in this regard. There is no third lead in the problem, and as we have mentioned already, even coupling to phonons or another bosonic bath does not permit breaking of the no-polarisation theorem.

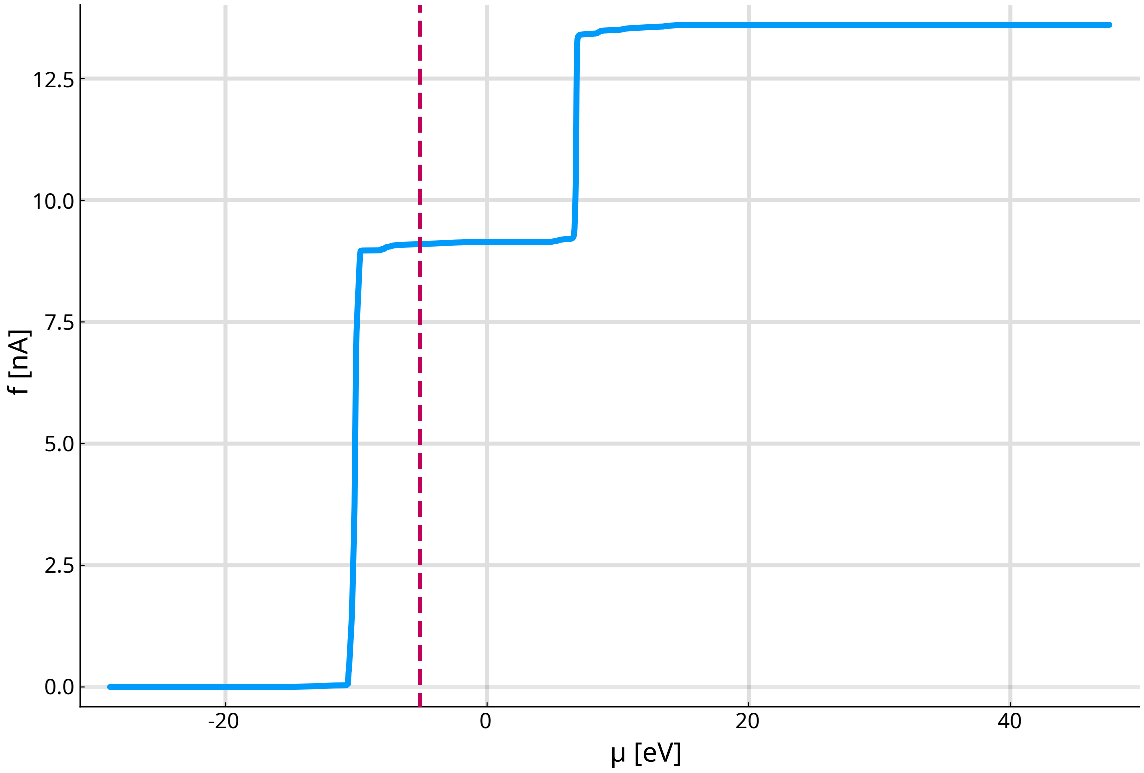

Figure 3.3: Integrated asymmetry in the induced magnetisation of the left lead, as a function of the chemical potential for a model of twisted polyacetylene, to be described in detail in section 4.1. The dashed line indicates the position of the chemical potential of the molecule in its ground state.

To explore the possibility of another explanation, it is worth considering the efficiency of the spin-injection. From Eq. (2.138) the total spin current (i. e. multiplied by the total number of particles, N) into the left lead is given by:

$$\begin{aligned}\langle \dot{\vec{S}}_{L\hat{m}} \rangle = \int \frac{dE}{h} \Big(& n(E-\mu_R)\,\mathrm{tr}\big[(\bar{\Gamma}_R + \Delta\Gamma_R(\hat{m}\cdot\vec{\sigma}))G_M^\dagger(\hat{m})\Gamma_L(\hat{m}\cdot\vec{\sigma})G_M(\hat{m})\big] \\ & - n(E-\mu_L)\,\mathrm{tr}\big[\Gamma_L G_M^\dagger(\hat{m})(\Delta\Gamma_R + \bar{\Gamma}_R(\hat{m}\cdot\vec{\sigma}))G_M(\hat{m})\big]\Big).\end{aligned} \tag{3.83}$$

In this case, the fact that the roles of $\Delta\Gamma_R$ and $\bar{\Gamma}_R$ has been interchanged in the first term, as compared to their order in the self-energy, and that Γ_L is attached to a $(\hat{m}\cdot\vec{\sigma})$ in the second term means that we can not use the Ward identity to interchange the order of the propagators. In fact, the two terms do not even translate into each other using the time reversal identities. That they are different is also confirmed by numerical calculations for a model system, the details of which we shall get into in the next chapter. In Figure 3.3, we show a plot of the sum of the spin current into the left lead as a function of the chemical potential, μ, when the two leads are assumed in equilibrium,

i. e. their chemical potentials are equal $\mu = \mu_L = \mu_R$. For simplicity, we have assumed $n(E-\mu) = \vartheta(\mu - E)$, i. e. the low temperature limit such that:

$$f(\mu) = \frac{e}{h}\int_{-\infty}^{\mu} dE\left(S_{L,\hat{m}}(E) + S_{L,-\hat{m}}(E)\right), \tag{3.84}$$

where:

$$\begin{aligned} S_{L,\hat{m}}(E) = \mathrm{tr}\Big[&(\bar{\Gamma}_R + \Delta\Gamma_R(\hat{m}\cdot\vec{\sigma}))G_M^{\dagger}(\hat{m})\Gamma_L(\hat{m}\cdot\vec{\sigma})G_M(\hat{m})\Big] \\ &- \mathrm{tr}\Big[\Gamma_L G_M^{\dagger}(\hat{m})(\Delta\Gamma_R + \bar{\Gamma}_R(\hat{m}\cdot\vec{\sigma}))G_M(\hat{m})\Big]. \end{aligned} \tag{3.85}$$

The reason for plotting this quantity is that one would expect that reversing the magnetisation would simply lead to a sign change in the spin current, in which case $f(\mu)$ should be zero for all values. However, Figure 3.3 clearly shows that this is not the case. In fact, there are some noticable steps in the spin current, as if there are some *hotspots* or specific states in the molecular spectrum that carries the spin current. We will get into more details about this in the next chapter.

To move forward, there are two important things to notice in the analysis above. First, there is a finite spin current when a magnetic lead is put into contact with a normal lead. This result is hardly surprising, as the electrons in the normal lead feels the effect of the magnetisation in the magnetic lead through the self-energy. Here we have ignored the effect of the paramagnetic response of the normal lead, but focus purely on the effects due to electrons hybridising near the interface. Consequently, we know that the real equilibrium state of the system is one in which the normal lead is magnetised slightly, at least locally close to the magnetic lead. Typically, however, we would assume that this effect is anti-symmetric when the magnetisation is changed. I. e. the induced magnetisation simply changes sign. However, when the two leads are connected through a chiral molecule with spin orbit coupling, this is not the case. In other words, the induced magnetisation in the normal lead is *not* anti-symmetric under reversal of the magnetic field, as evidenced by the non-zero values found in Figure 3.3. The result of this effect is that there is a kind of magnetoresistance effect, due to fact that the magnitude of the induced magnetisation is not equal when the magnetic lead is flipped.

Let us denote this induced magnetisation $\vec{a}_+$ and $\vec{a}_-$ for magnetisations of the lead $\pm\hat{m}$, respectively. That is, our new equilibrium state in the left lead is now

$$\Gamma_L^{\pm} = \bar{\Gamma}_L + \Delta\Gamma_L(\vec{a}_{\pm}\cdot\vec{\sigma}), \tag{3.86}$$

where ± stands for the magnetisation of the right lead. Here we have assumed, for simplicity, that only the magnitude of the magnetisation is different, and thus $\bar{\Gamma}_L$ and $\Delta\Gamma_L$ are independent of $\hat{m}$. For the current, the Ward identity still holds for the transmission functions, i. e. $T_{LR}(\pm\hat{m}) = T_{RL}(\pm\hat{m})$, but the new equilibrium state means that time reversal no longer takes us from one to the other, i. e. $\vec{a}_+ \neq -\vec{a}_-$ and thus $T_{LR}(+\hat{m}) \neq T_{LR}(-\hat{m})$. We can now go back and calculate the difference between the electric current of the two magnetisations.

$$I_+ - I_- = \frac{e}{h}\int dE\,(n(E-\mu_L) - n(E-\mu_R))\,(T_{LR}(+\hat{m}) - T_{LR}(-\hat{m}))\,. \tag{3.87}$$

To proceed, we have to consider the explicit form of the thermal transmission functions:

$$T_{LR}(\pm\hat{m}) = \mathrm{tr}\Big[(\bar{\Gamma}_L + \Delta\Gamma_L(\vec{a}_\pm\cdot\vec{\sigma}))G^\dagger_M(\pm\hat{m})(\bar{\Gamma}_R \pm \Delta\Gamma_R(\hat{m}\cdot\vec{\sigma}))G_M(\pm\hat{m})\Big]. \tag{3.88}$$

Since we have established that there is an induced magnetisation and non-zero difference in the current, we are going to ignore the spin dependence of the propagators for simplicity. In this case we find:

$$T_{LR}(\pm\hat{m}) = 2\,\mathrm{tr}\Big[\bar{\Gamma}_L g^\dagger_M \bar{\Gamma}_R g_M\Big] \pm 2(\vec{a}_\pm\cdot\hat{m})\,\mathrm{tr}\Big[\Delta\Gamma_L g^\dagger_M \Delta\Gamma_R g_M\Big], \tag{3.89}$$

where the factor of two comes from tracing out the spin degrees. Defining,

$$A \equiv \frac{\mathrm{tr}\Big[\Delta\Gamma_L g^\dagger_M \Delta\Gamma_R g_M\Big]}{\mathrm{tr}\Big[\bar{\Gamma}_L g^\dagger_M \bar{\Gamma}_R g_M\Big]}, \quad T^0_{LR} = \mathrm{tr}\Big[\bar{\Gamma}_L g^\dagger_M \bar{\Gamma}_R g_M\Big], \tag{3.90}$$

the difference between the currents for opposite magnetisations, Eq. (3.87), becomes:

$$I_+ - I_- = \frac{2e}{h}\int_{-\infty}^{\infty} T^0_{LR} A\,\hat{m}\cdot(\vec{a}_+ + \vec{a}_-)(n_F(E-\mu_L) - n_F(E-\mu_R))\,dE. \tag{3.91}$$

Since $\vec{a}_+ \neq \vec{a}_-$, this is finite even for small bias voltages. In fact, for small bias voltages, assuming $T^0_{LR}A\,\hat{m}\cdot(\vec{a}_+ + \vec{a}_-)$ is slowly varying as a function of energy, we can follow the example in section 2.4.2, and find a kind of Ohmic relationship:

$$I_+ - I_- = VG_0T^0_{LR}(E_F)A(E_F)\,\hat{m}\cdot(\vec{a}_+ + \vec{a}_-). \tag{3.92}$$

Consequently, in the linear regime the ratio of the difference over the sum of the currents is

$$\frac{I_+ - I_-}{I_+ + I_-} = \frac{VG_0T^0_{LR}(E_F)A(E_F)\,\hat{m}\cdot(\vec{a}_+ + \vec{a}_-)}{2VG_0T^0_{LR}(E_F)} = A\frac{\vec{a}_+ + \vec{a}_-}{2}\cdot\hat{m}. \tag{3.93}$$

The experimental values listed in Table 1.6 is for values where the I-V curves clearly show, that it is not linear around zero bias anymore. In that case, we would still have to retain the integrals, but the simplicity of the formula above can be used as an effective picture, where $A(E_F)$ has to be replaced by a "weighted average" over the energy window,

$$A = \frac{\int_{\mu_L}^{\mu_R} T^0_{LR}(E)\,A(E)\,dE}{\int_{\mu_L}^{\mu_R} T^0_{LR}(E)\,dE}. \tag{3.94}$$

3.3 SUMMARY

In this chapter we developed on the formalism introduced in chapter 2 by assuming a weak spin-orbit coupling on the molecule and expanding the equations to first order in the strength. We found that the problem of finding the particle current with an initially spin polarised distribution was, to first order, equivalent to the problem of spinless electrons moving in a magnetic field coupling to their angular momenta, i. e.the transmission functions could be written as

$$\operatorname{tr}\left[\frac{(1+\vec{a}\cdot\vec{\sigma})}{2}\gamma_L G_M^\dagger \Gamma_R G_M\right] \approx \operatorname{tr}\left[\gamma_L g_M^\dagger(\vec{a})\Gamma_R g_M(\vec{a})\right], \quad g_M(\vec{a}) = \frac{1}{E - h_M - \lambda\vec{a}\cdot\vec{\Lambda} - \Sigma}.$$

In the case where the leads were in thermal equilibrium, $\gamma_L \to n_F(E-\mu_L)\Gamma_L/2\pi$, a combination of time reversal and the Ward identity, Eq. (2.79), gave us the no-polarisation theorem. It states that there can be no difference in the transmission to first order in the spin-orbit coupling of two electron beams prepared with opposite spin. If the initial state is not thermal, a difference in the transmission can arise, and a complex vector quantity for the transport can be defined, $\vec{A}$, which allows one to calculate the polarisation of the outgoing electrons. Its real and imaginary parts are referred to as the $\vec{D}$- and $\vec{C}$-vectors, which relate to the incoming and outgoing polarisation of the electrons through the non-linear relation:

$$\vec{P}_{\text{out}} = \frac{\vec{P}_{\text{in}} + \vec{D} + \vec{C}\times\vec{P}_{\text{in}}}{1 + \vec{D}\cdot\vec{P}_{\text{in}}}.$$

This model can be used to understand most of the photoemission and photoexcitation experiments, due to the fact that the excitations created by the light due to selection rules that populates otherwise degenerate states with unequal probabilities. When extended to include short times, similar time-dependent $\vec{D}$- and $\vec{C}$-vectors describe the polarisation of electrons escaping a molecule. The fact that the $\vec{D}$-vector is non-zero, but an electron will eventually escape independent of its spin, shows that an electron effectively propagates with a spin-dependent velocity through a chiral molecule.

We also saw that for transport experiments, where the current through the molecule is measured for two opposite directions of magnetisation of one of the leads, a naïve assumption about the equilibrium distribution does not yield any difference. Instead, if we include the effect of the injected spin into the other lead, we find that it is not simply anti-symmetric, when the magnetisation is flipped. As a consequence, the experiments do not measure a difference in a spin-dependent resistance through the molecule, but rather a difference in the magnetoresistance of the two different equilibrium distributions induced by the chirality of the molecule.

4

NUMERICAL MODELS

We now take the theory developed in the preceding two chapters, and apply them to models of some simple, but realistic molecules for numerical evaluation. It is therefore relevant to discuss how to construct the relevant molecular Hamiltonian. Since we are concerned with the properties of electrons in molecules of finite size and odd shapes, we cannot in general assume any spatial symmetries. An adequate level of description for such a problem is generally to use a linear combination of atomic orbitals (LCAO) for each atom in the molecule. Let us label all the atomic orbitals of the molecule by ϕ_n, where n is an index that refers both to its position and orbital index. Then the matrix elements of the single-particle Hamiltonian take the form:

$$H_{nn'} = \langle \phi_n | \, H \, | \phi_{n'} \rangle = \int \phi_n^*(\vec{r}) \left(-\frac{\hbar \nabla^2}{2m} + V(\vec{r}) \right) \phi_{n'}(\vec{r}) \, d\vec{r}, \tag{4.1}$$

where $V(\vec{r})$ is the effective self-consistent potential at position $\vec{r}$ due to the other electrons and nuclei of the atoms.

For practical purposes when modelling, it is convenient to assume spherically symmetric potentials centered around each atom. To simplify further, we also only include potentials of the nuclei associated with the two labels, n, n', an approximation known as the *two-center approximation*. It is a simple exercise to show that for real s and p orbitals, with the centres separated by $\vec{d}$, the matrix elements in the two-center approximation take the form:

$$\begin{aligned} H_{s,s} &= V_{ss\sigma}(d), & H_{s,p_i} &= d_i V_{sp\sigma}(d), \\ H_{p_i,p_i} &= d_i^2 V_{pp\sigma}(d) + (1 - d_i^2) V_{pp\pi}(d), & H_{p_i,p_j} &= d_i d_j (V_{pp\sigma}(d) - V_{pp\pi}(d)), \quad \text{for } i \neq j, \end{aligned}$$

where the Vs are functions which depend only on the magnitude of the distance between them, and i, j are indices which run over the three spatial components, x, y, z. This was first realised by Slater and Koster in 1954[75], and thus this parameterisation is generally referred to as the Slater-Koster scheme. In this rewriting, we have of course not actually performed the integral in Eq. (4.1), but simply reduced it to a form in which the directionality of the separation of the orbitals have been extracted explicitly. That is, the Vs are still integrals that include the positions of the two atoms involved.

Now, since these atomic orbitals have exponential tails that extend outwards, two states $\phi_n, \phi_{n'}$ are in general not orthogonal,

$$\langle \phi_n | \phi_{n'} \rangle = \int d\vec{r} \phi_n^*(\vec{r}) \phi_{n'}(\vec{r}) \neq 0, \tag{4.2}$$

unless symmetry dictates it. We demand, however, that the states are normalised to unity such that $\langle \phi_n | \phi_n \rangle = 1$. If we insist on using the Hamiltonian matrix elements, $H_{nn'}$ as given above, this non-orthogonality has important implications for our mathematical description. To see this, let us denote the Hilbert space in which the atomic orbitals, ϕ_n, reside by $\mathcal{H}$. Next, we define a new Hilbert space, $\mathcal{C}$, and for each orbital, we associate a unique orthonormal state, $c_n \in \mathcal{C}$. Since the states, c_n, are orthonormal, we can define the linear map, $x : \mathcal{C} \mapsto \mathcal{H}$ in the usual bra-ket notation:

$$x = \sum_n |\phi_n\rangle \langle c_n| \,. \tag{4.3}$$

In other words, x is an operator that takes an orthonormal ket in $\mathcal{C}$-space, $|c_n\rangle$ from the right and yields the corresponding orbital, $|\phi_n\rangle$ in the atomic orbital space, $\mathcal{H}$, $|\phi_n\rangle = x\,|c_n\rangle$. To find the time evolution of the states in $\mathcal{C}$-space, we simply plug the relationship above into the time-dependent Schrödinger equation:

$$i\partial_t \, |\phi_n(t)\rangle = ix\partial_t \, |c_n(t)\rangle = \hat{H}x \, |c_n(t)\rangle \,. \tag{4.4}$$

Multiplying by $x^\dagger$ from the left we get

$$iS\partial_t \, |c_n\rangle = H \, |c_n\rangle \,, \tag{4.5}$$

where we have omitted the time-dependence for brevity and defined the Hamiltonian and so-called overlap matrix, S, in $\mathcal{C}$-space as:

$$H \equiv x^\dagger \hat{H} x = \sum_{jj'} |c_j\rangle \, H_{jj'} \, \langle c_{j'}| \,, \quad S \equiv x^\dagger x = \sum_{nn'} |c_n\rangle \, \langle \phi_n | \phi_{n'} \rangle \, \langle c_{n'}| \,. \tag{4.6}$$

Consequently, for a time-independent Hamiltonian, the time-evolution operator in $\mathcal{C}$-space becomes

$$U(t) = e^{-iS^{-1}Ht}. \tag{4.7}$$

Note that the energy of an eigenstate, c_ψ, obtained by diagonalising the matrix $S^{-1}H$ is the same as its counterpart, ψ, which is an eigenstate of $\hat{H}$. To see this, we use the fact that the atomic orbitals is a complete basis. Thus, we can express any vector in terms of coefficients in this basis, including eigenstates:

$$|\psi\rangle = \sum_n \psi_n \, |\phi_n\rangle = \sum_n \psi_n x \, |c_n\rangle = x \, |c_\psi\rangle \,. \tag{4.8}$$

Note that in the last equality above, we have defined the state vector, c_ψ residing in the Hilbert space $\mathcal{C}$ through the relationship $c_\psi \equiv \sum_n \psi_n |c_n\rangle$. It is important to stress, however, that such an eigenstate is in general not normalised to unity due to the non-orthogonality of the basis. As a concrete example, consider the non-orthogonal basis vectors $a_1 = (1,0)$, $a_2 = (1/\sqrt{2}, 1/\sqrt{2})$. To construct the vector $(0,1)$ we need a linear combination, $\sqrt{2}a2 - a1$. In the corresponding $\mathcal{C}$-space, in which a_1, a_2 are assumed orthogonal, this vector would have a norm of $\sqrt{3}$. Thus, in the non-orthogonal representation of the states, properly normalised states such as the eigenstates of the system will appear incorrectly normalised. Although there are generally numerical routines to deal with this, it is an issue conceptually, so we shall seek to put it the problem on a form in which we are dealing with properly normalised and orthogonal states.

Now, the time-independent Schrödinger equation reads:

$$\hat{H} |\psi\rangle = \hat{H} x |c_\psi\rangle = E_\psi x |c_\psi\rangle . \tag{4.9}$$

Multiplying again from the left by $x^\dagger$, we find:

$$H |c_\psi\rangle = E_\psi S |c_\psi\rangle , \tag{4.10}$$

which shows that $|c_\psi\rangle$ is a right eigenvector of $S^{-1}H$ with eigenvalue E_ψ. As noted above, there are some issues with this formulation. Because the matrix $S^{-1}H$ is non-hermitian, the eigenstates c_ψ are not related to the c_n's through a unitary transformation, and thus they are not properly normalised. Secondly, the non-hermiticity also means that the left and right eigenvectors are not simply the adjoint of each other, which is an annoyance to keep track of.

To overcome this, we first note that the overlap matrix is a Grammian matrix, named after the Danish mathematician, Jørgen Pedersen Gram, which endows it with a number of desirable properties. The first property serves as a sanity check and simply is that if the atomic orbitals were orthonormal, S becomes the identity operator, and we restore our usual equations. The second property is that the overlap matrix is positive definite. This ensures that both the inverse and principal square root of the matrix exists, and thus we can, in a well-defined manner, substitute:

$$|C_n\rangle \equiv S^{1/2} |c_n\rangle , \quad H' \equiv S^{-1/2} H S^{-1/2}, \tag{4.11}$$

into Eq. (4.10), which after some basic algebra brings it on the familiar form:

$$H' |C_\psi\rangle = E_\psi |C_\psi\rangle . \tag{4.12}$$

This form of the problem was first discovered by Per-Olov Löwdin in 1950[76]. On this form, H' is hermitian, and thus diagonalisation of the matrix yields eigenvectors, $|C_\psi\rangle$

which behave as usual, i. e. the left eigenvectors are simply the corresponding adjoint bra, $\langle C_\psi|$. The eigenstates are therefore also related to the C_n's by a unitary transformation, and are thus normalised by definition. To see this, note that the diagonal of S is 1, and thus $\langle C_n|C_n\rangle = \langle c_n| S |c_n\rangle = 1$. Using the definitions in Eq. (4.11) on the time-dependent Schrödinger equation, we also get a more familiar time-evolution operator,

$$i\partial_t |C_n\rangle = S^{-1/2} H S^{-1/2} |C_n\rangle \quad \Rightarrow \quad U(t) = e^{-iH't}, \tag{4.13}$$

in the space of C_n-vectors. Finally, for a general operator A written in the non-orthogonal basis, we find that

$$A = \sum_{ij} A_{ij} |\phi_i\rangle \langle\phi_j| = \sum_{ij} A_{ij} x S^{-1/2} |C_i\rangle \langle C_j| S^{-1/2} x^\dagger, \tag{4.14}$$

and as a consequence, traces over operators are unaffected by changing to an orthogonal basis:

$$\begin{aligned} \text{tr}[\rho A] &= \text{tr}\left[\sum_{ijkl} x S^{-1/2} |C_i\rangle \rho_{ij} \langle C_j| S^{-1/2} x^\dagger x S^{-1/2} |C_k\rangle A_{kl} \langle C_l| S^{-1/2} x^\dagger\right] \\ &= \text{tr}\left[\sum_{ijkl} |C_i\rangle \rho_{ij} \langle C_j|C_k\rangle A_{kl} \langle C_l|\right] = \sum_{ij} \rho_{ij} A_{ji}. \end{aligned} \tag{4.15}$$

Thus, after the dust has settled, the effect of describing the problem using non-orthogonal atomic orbitals for our formalism is that the Hamiltonian has to be adjusted using the overlap matrix as prescribed in Eq. (4.11).

Of course, we still need to know the Hamiltonian and overlap matrix elements. For the purpose of this thesis, we use parameter sets that have been extracted from *ab initio* studies and fitted to a number of organic molecules[77]. The energy spectra obtained with the given parameter sets for our model systems were compared to density functional calculations of the same structure, and found to be in good agreement. To facilitate the calculation and modelling of the molecules, a small package suite for the Julia scientific programming language was developed and is available from public repositories at:

- Main repository: `https://github.com/dalum/TheoryOfCISS.jl`
- Modelling toolkit: `https://github.com/dalum/Molecules.jl`
- SKF-file importing: `https://github.com/dalum/SlaterKoster.jl`

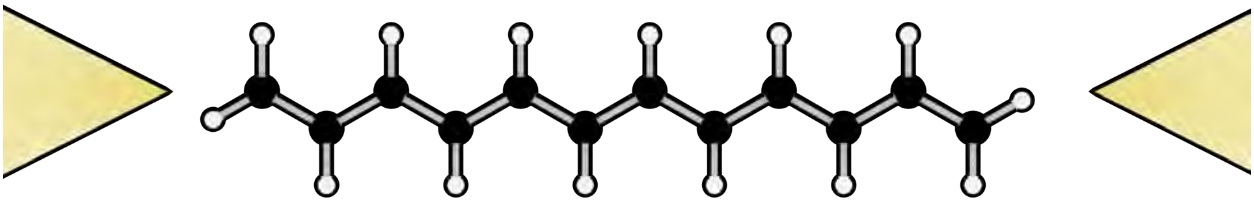

Figure 4.1: Illustration of flat polyacetylene placed between two leads. In the model, the leads connect to the outermost carbon atoms and the coupling must obey the flat symmetry of the molecule for the whole system to be achiral.

4.1 POLYACETYLENE

With the modelling details out of the way, we can start to explore the theory derived in the previous chapters in the context of semi-realistic molecules. In particular, we want to calculate the $\vec{D}$- and $\vec{C}$-vectors given some generic non-thermal initial state and leads. To better be able to understand the ingredients that lead to finite $\vec{D}$-vectors, we start by considering polyacetylene, i. e. a flat chain of conjugated carbon atoms. The setup is illustrated in Figure 4.1. We know that in such molecules transport occurs mainly through the π-band of p_z orbitals, orthogonal to the plane of the molecule. Here, we consider the molecule when aligned such that the leads are connected to the far ends of the molecule along the x-direction. By virtue of being flat in the xy-plane, and hence achiral, the symmetry of the molecule also demands that the $\vec{D}$-vector does not have any components in the x-direction. Therefore, if the model does not reproduce this result, we know there is something wrong with it.

Now, to introduce chirality into the system, we apply a “twist” to each of the bonds, which we denote θ. We do this in such a way that the angles and distance between neighbouring bonds is preserved, which retains the general sp_2-hybridisation of the orbitals. This allows us to smoothly vary the geometry of the molecule from an achiral configuration to a chiral one, to observe the effect of breaking the mirror symmetry of the system. It also allows us to change the chirality from one handedness to the other, by twisting the bonds either way. The twist angle denotes the relative angle between adjacent p_z orbitals, where we have chosen $\theta = \pi$ to correspond to flat polyacetylene, and $\theta = 0$ to correspond to a flat benzene-like helix. Figure 4.2 shows a stereoscopic cross-eyed view of a twisted polyacetylene molecule with $\theta = \pi/2$.

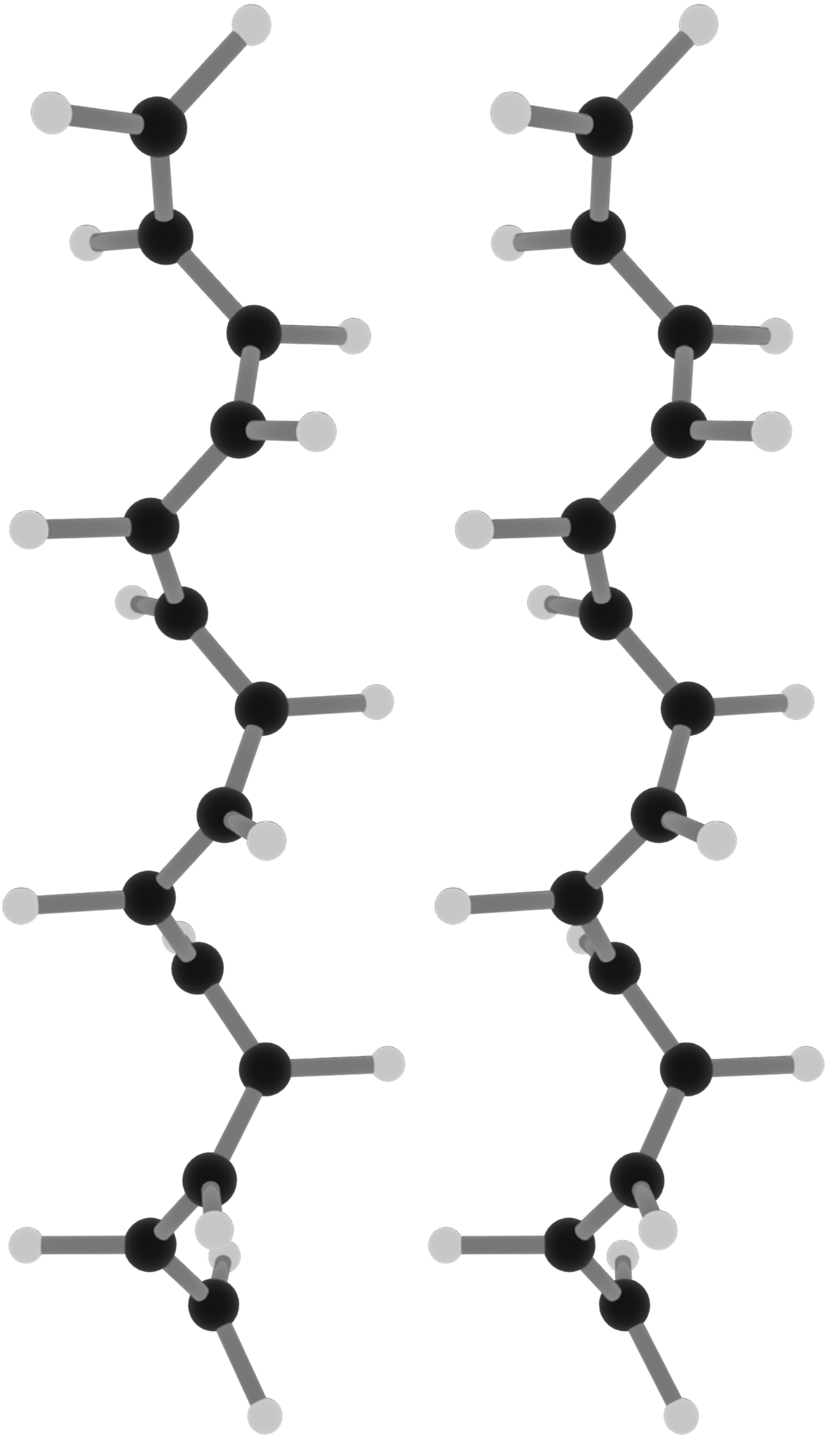

Figure 4.2: Stereoscopic cross-eyed model of twisted polyacetylene with $N = 14$ carbon atoms. *To get a stereoscopic view, the left eye should focus on the image on the right, while the right eye should focus on the image on the left.*

For simplicity, in the numerical calculation, we are going to assume that the leads only connect to the outermost carbon atoms in the chain. The carbon atoms are modelled using the four $n = 2$ real orbitals, $2s$, $2p_x$, $2p_y$, and $2p_z$, such that the spinless couplings, Γ, and initial state γ, are positive-semidefinite 4-by-4 matrices. Additionally, we are going to ignore the hermitian part of the self-energies, Σ. The reason for this is the fact that the only effect of the hermitian part is to change the effective molecular Hamiltonian, and thus the molecular spectrum. The key to the polarisation effects that we are after, though, relate to the anti-hermitian part, as we have seen in the previous chapters. Therefore, inclusion of the hermitian part of the self-energy will lead to a correction of the eigenstates and energies of the Hamiltonian, but is not expected to change the overall picture.

To ensure that we are measuring the effect of the chirality of the molecule and not an effect related to a chiral coupling of the leads to the molecule, it is worth considering how the Γ-matrices transform under symmetry operations. For instance, let us consider the achiral polyacetylene in Figure 4.1, where the molecule is invariant under a mirror operation in the xy-plane. If one or both of the leads are positioned out of plane, the full system lacks this symmetry and therefore it is still chiral. For the whole system to be achiral, we must require that the leads are coupled to the molecule in such a way that the symmetry of the molecule is still a symmetry of the full system. If the leads is diagonal in states of p-orbital-like symmetries, the symmetric placement means that the coupling elements between the molecule and the lead, for instance H_{LM}, only couples p_z orbitals on the molecule to p_z orbitals in the lead. Therefore, if we demand that the coupling to the leads should not introduce chirality into the system, the Γ-matrices must have no off-diagonal elements coupling the outermost p_z orbitals to the rest of the orbital subspace of the molecule.

With this in mind, we now want to investigate the effect of twisting. Because the molecule changes orientation as the bonds are twisted, we fix the $\hat{z}$-direction to always point along the helix axis of the molecule. In Figure 4.3, we plot the molecular spectrum of twisted polyacetylene for $N = 14$ as a function of the twist angle, and show a representative molecule with $N = 6$ below for reference. The most notable feature of the plot is the fact that as the molecule is twisted, some of the molecular levels cross leading to degeneracies in the spectrum. This is particularly pronounced around $\theta = \pi/2$. The inset shows the levels in the lower band overlaid ontop of a heatmap of the energy-resolved $\vec{D}$-vector component in the $\hat{z}$ direction, i. e. along the molecular axis. In this plot, following our discussion above, to ensure that there is no chirality in the coupling to the leads, the Γ-matrices are diagonal in the orbitals of the outermost carbon atoms. Additionally, in order to perform the calculation, we are considering the so-called wide-

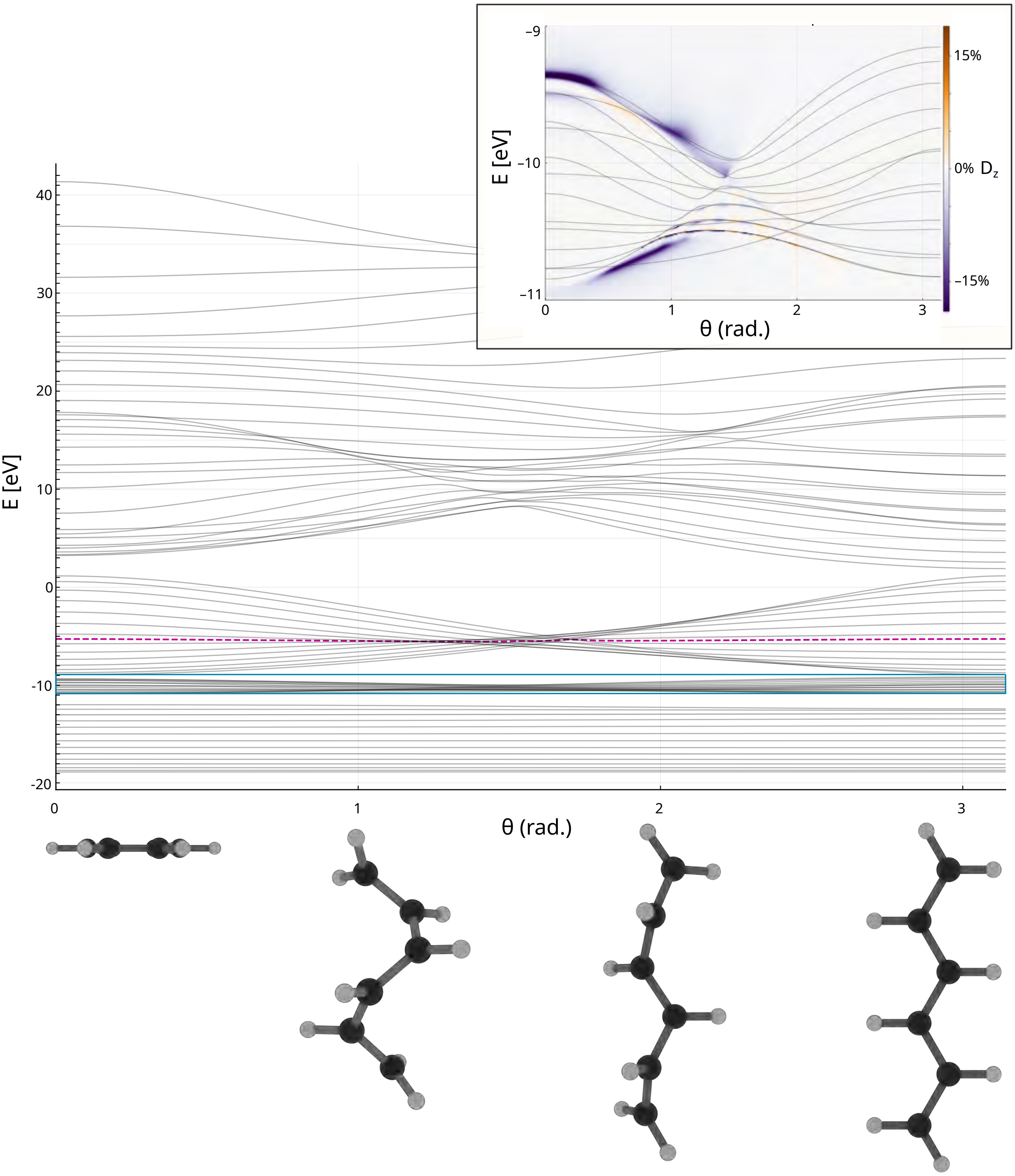

Figure 4.3: Energy levels of twisted polyacetylene as a function of the twist angle. The levels form bands that interweave as the molecule is deformed and becomes more helical. The inset shows the lower bands indicated by a blue square, overlaid on a heatmap of the $\hat{z}$-component of the $\vec{D}$-vector.

band limit in which the Γ and γ-matrices are finite and constant as a function of energy. To ensure that the SOC is small in comparison to the coupling to the leads, the diagonal components are set to 100λ, i. e. a hundred times the atomic SOC of carbon of $\lambda = 6\,\text{meV}$. The γ-matrix is chosen to couple only to the p_y-orbital of the carbon atom near the left lead. From the inset we see that the $\hat{z}$-component of the $\vec{D}$-vector indeed vanishes for $\theta = \pi$, as the symmetry dictates. In the limit $\theta = 0$, the molecule becomes highly unphysical, since the atoms have been mashed ontop of eachother. The reason that the polarisation does not vanish in the limit $\theta = 0$, is due to the fact that the tight-binding model of the molecule in this configuration is in fact still chiral, and therefore does not have the necessary mirror symmetry for the $\hat{z}$-component to vanish.

Upon closer inspection, the inset in Figure 4.3 also shows us that the $\vec{D}$-vector is largest near level crossings or around the edges of the band. The large polarisation near the band edges, however, generally happens for surface states that carry vanishingly little current. Thus, since the total spin polarisation is the integral over energy of the $\vec{D}$-vector weighed by the transmission, the spin polarisation due to these states have a negligible contribution. The main contribution to the spin polarisation therefore comes from the level crossings. This is more visible, when the length of the molecule is increased, which is shown in in Figure 4.4, where we have zoomed further in around the centre of the band for a length of $N = 30$. In Figure 4.4b, we show a heatmap of the transmission. This observation allows us to understand the sudden jump in the asymmetry of the induced magnetisation we saw in the previous section in Figure 3.3, which happened exactly around $-10\,\text{eV}$, and was done using twisted polyacetylene with $\theta = \pi/2$. The jump is due to the fact that the $\vec{D}$-vector, and therefore the polarisation of the current due to the chirality of the molecule, is largest near degeneracies in the spectrum.

We saw another jump around $8\,\text{eV}$, which matches the upper bands in Figure 4.3. This is caused by similar features. To show that the form of the polarisation is robust against changes in the coupling and Hamiltonian matrix elements, Figure 4.5a shows a plot of the upper band when the overlap matrix is not taken into account, and where the coupling to the leads is randomly generated, for $N = 38$. In this case we still see that the polarisation is generally largest near the web-like level crossings of the spectrum. Figure 4.5b shows the weighted integral over the energies indicated by the orange box in Figure 4.5a, where we indeed see spikes in the polarisation when level crossings enter the integration window. To investigate the length dependence of the polarisation, the $\hat{z}$-component of the $\vec{D}$-vector is plotted in Figure 4.5c as a function of the length of the molecule at a level crossing near the blue circle in Figure 4.3a. Because the degeneracies shift when the length changes, we have employed an optimisation routine to find the

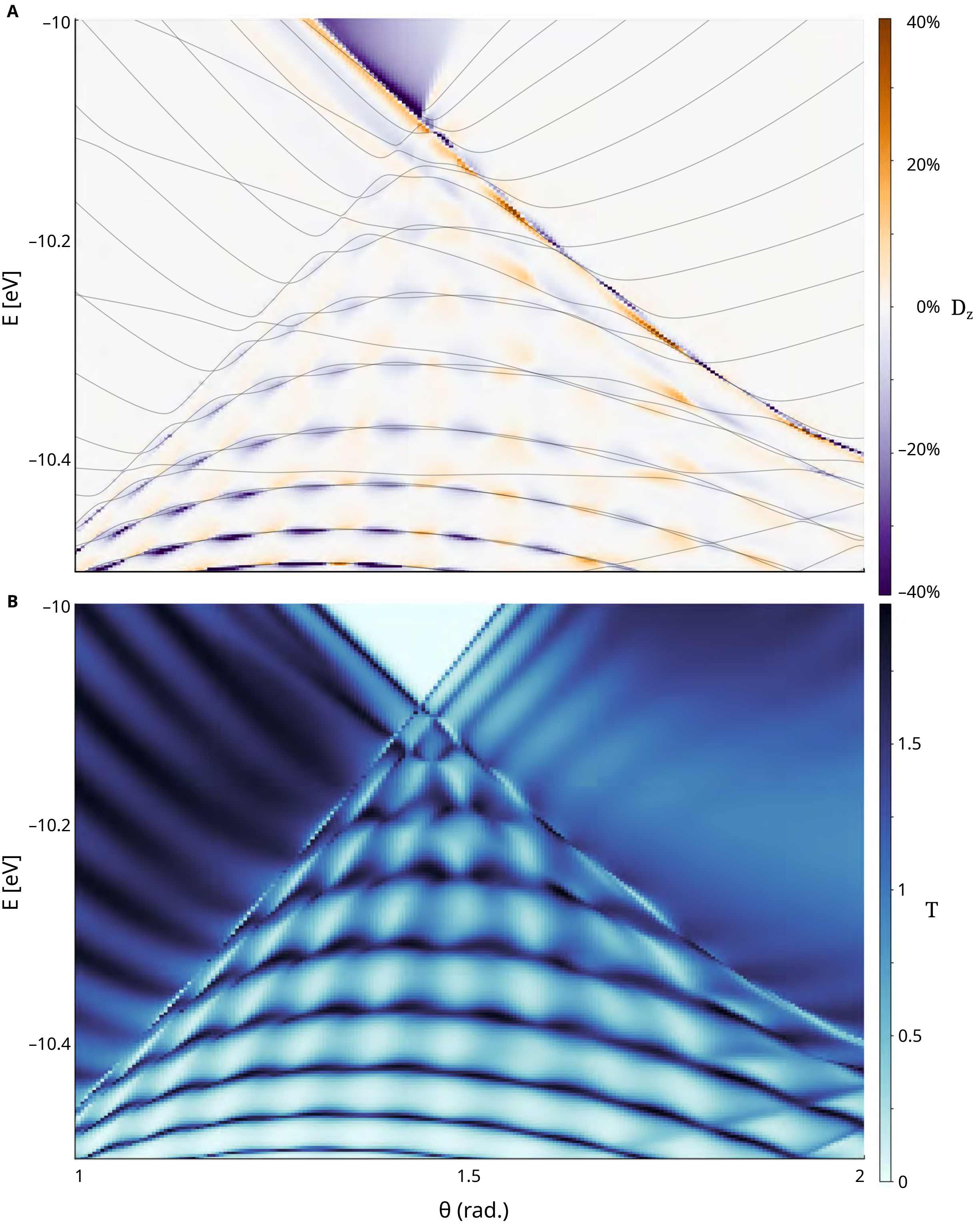

Figure 4.4: (A) Zoom-in of the region shown in the inset of Figure 4.3 for twisted polyacetylene of a length of $N = 30$. Except for the region near the band edge at the top, the polarisation is largest near level crossings. (B) The corresponding transmission function that must be used when integrating over energies to get a weighted $\vec{D}$-vector.

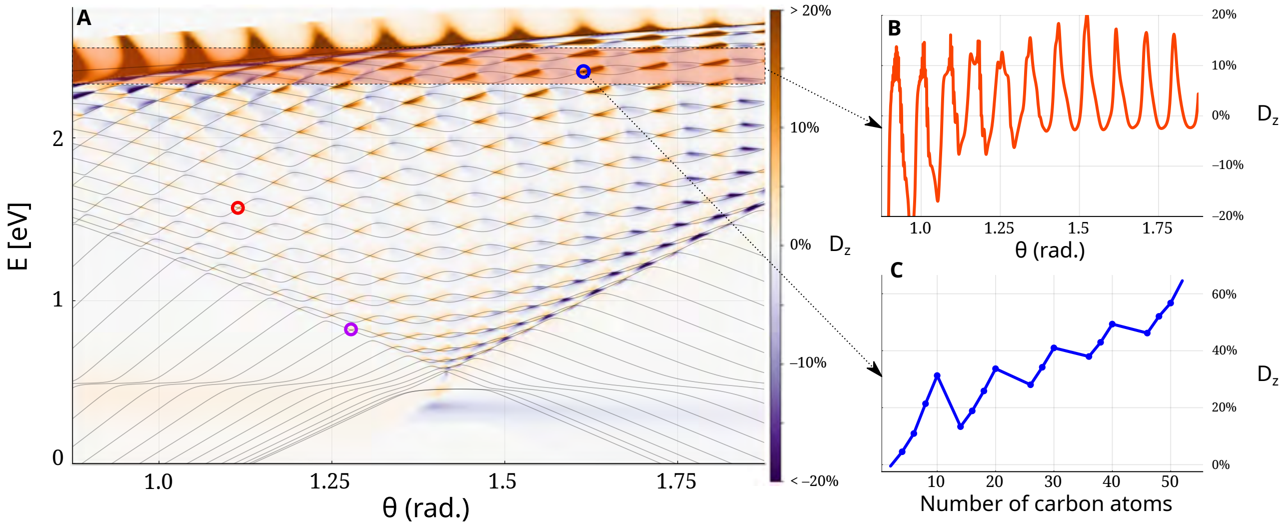

Figure 4.5: (A) Heatmap of the magnitude of the $\vec{D}$-vector in a band for a model of polyacetylene with $N = 38$. (B) Integrated polarisation over the energy window indicated by the orange box in A, weighted by the transmission for each energy. (C) Length dependence of the peak of the polarisation near the blue circle in A. As the length is varied, the exact energy and twist angle of the peak changes, resulting in the sawtooth-like shape of the length dependence. Adapted with permission from Ref. 1.

nearest level crossing, by varying both energy and bond twist. This fact is responsible for the sawtooth-like shape of the length dependence. However, we clearly see a linear dependence emerging below the oscillations.

To understand these results, it is helpful to consider the fact that near resonances, the propagators are dominated by terms involving the resonant states. Thus, near a level crossing, two states enter the picture, which we shall denote $|1\rangle$ and $|2\rangle$. Note that $|1\rangle$ and $|2\rangle$ are eigenstates of the uncoupled, spinless molecular Hamiltonian. Because the eigenstates of the molecule are real, the matrix elements of the operator $\vec{\Lambda}$ are purely imaginary, i. e. $\vec{\Lambda}_{12} = -\vec{\Lambda}_{21}$. Because $\vec{\Lambda}$ is hermitian, this fact also tells us that the diagonal matrix elements are zero, $\vec{\Lambda}_{11} = 0$, etc. Thus, the $\vec{D}$-vector can only be non-zero when more than one state is involved, which is why we observe peaks near degeneracies. If a large value is found away from degeneracies, it must generally be due to quenching of the transmission, which allows contributions from off-resonant states. From this observation, we can calculate the $\vec{D}$-vector more easily at the degeneracy point, by inserting projection operators into the subspace of the states $|1\rangle$ and $|2\rangle$ around each propagator. To see this, consider the $\vec{A}$-vector, defined as:

$$\vec{A} = \frac{\mathrm{tr}_{12}[\vec{\Lambda} g_M^\dagger \Gamma_R g_M \gamma_L g_M^\dagger]}{\mathrm{tr}_{12}[\gamma_L g_M^\dagger \Gamma_R g_M]}. \tag{4.16}$$

Table 4.1: Polarisation factors for three selected level crossings in polyacetylene.

Circle	$\mathrm{Im}[\Lambda^z_{12}]$ [meV]	$\mathrm{Re}[f_{21}]$ [meV^{-1}]	D_z (%)
Blue	0.62	0.69	43
Purple	0.08	1.3	10
Red	0.22	0.31	7

Expanding the trace in the numerator in a real basis, and using the fact that $\vec{\Lambda}$ only contains off-diagonal elements, the trace reduces to:

$$\vec{\Lambda}_{12} \langle 2| g_M^\dagger \Gamma_R g_M \gamma_L g_M^\dagger |1\rangle + \vec{\Lambda}_{21} \langle 1| g_M^\dagger \Gamma_R g_M \gamma_L g_M^\dagger |2\rangle , \tag{4.17}$$

where the matrices are all projected into the subspace of degenerate states. Using the fact that we are dealing with a real basis, $\vec{\Lambda}_{21} = -\vec{\Lambda}_{12}$, and assuming that the initial state is time-reversal invariant, we end up with:

$$\vec{\Lambda}_{12} \langle 2| g_M^\dagger (\Gamma_R g_M \gamma_L - \gamma_L g_M \Gamma_R) g_M^\dagger |1\rangle . \tag{4.18}$$

At resonance, in the degenerate subspace, $g_M = -2i\Gamma^{-1}$, and consequently we find that the $\vec{D}$-vector at the crossing point is given by:

$$\vec{D} = \mathrm{Im}[\vec{\Lambda}_{12}]\mathrm{Re}[f_{21}], \quad \text{where} \quad f_{21} = 4\frac{\langle 2| \Gamma^{-1}(\gamma_L \Gamma^{-1}\Gamma_R - \Gamma_R \Gamma^{-1}\gamma_L)\Gamma^{-1} |1\rangle}{\mathrm{tr}_{12}[\gamma_L \Gamma^{-1}\Gamma_R \Gamma^{-1}]}, \tag{4.19}$$

where the trace again runs over the two degenerate states, and the matrices are all 2-by-2 matrices in the degenerate subspace. Evaluation of the factors, $\mathrm{Im}[\vec{\Lambda}_{12}]$ and $\mathrm{Re}[f_{21}]$ at the level crossings marked by a blue, purple and red circle in Figure 4.5, are summarised in Table 4.1. Here we see that the magnitude of the polarisation is not dominated by either $\vec{\Lambda}_{12}$ or f_{21}, but can be due to either factor. I. e. the purple circle has a large f_{21} as compared to the blue circle, but $\vec{\Lambda}_{12}$ is comparatively much smaller which leads to a net reduced $\vec{D}$-vector. At the red circle, on the other hand, both factors are slightly smaller, leading to a reduction.

Now, we have only commented on the component of the $\vec{D}$-vector in polyacetylene parallel to its helical axis. This is due to two factors. First, in experiments, if the molecule has some freedom to rotate around the molecular axis, the perpendicular components will on average cancel. Second, and more importantly the perpendicular components are in fact much smaller than the parallel ones. This is illustrated in Figure 4.6, where the direction of the $\vec{D}$- and $\vec{C}$-vectors of the molecule are plotted, in relation to the orientation of the molecule. Additionally, the red arrows on the molecule indicate the relative magnitude and direction of the $\vec{D}$-vector, when the SOC is included only for

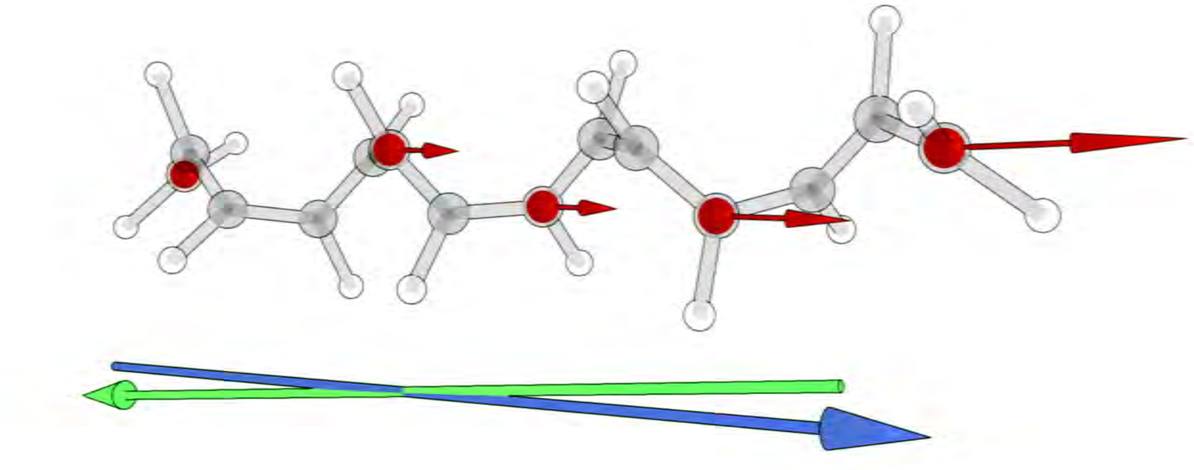

Figure 4.6: Illustration of the direction of the $\vec{D}$-vector (blue) and $\vec{C}$-vector (green) in relation to the molecule near a level crossing. The red arrows indicate the relative magnitude of the polarisation if the SOC is only included for atoms left of each of the respective red balls. The magnitude of the $\vec{C}$-vector has been multiplied by a factor of 10, relative to the $\vec{D}$-vector.

carbon atoms to the left of the marked site. We see that, as we include more atoms in the calculation, the magnitude of the polarisation increases. This shows that the resultant spin polarisation is a cumulative effect of the electron interacting with all of the carbon atoms in the molecule.

Finally, to understand the linear increase with the length of the molecule seen in Figure 4.5c, we can study the length dependence of the $\vec{D}$-vector from Eq. (4.19). Assume that the molecule contains N atoms. In that case, the amplitude of a normalised wave function on each atom scales approximately as $1/\sqrt{N}$. Because the Γ- and γ-matrices are located at the end of the molecule, this leads to a scaling behaviour of $1/N$ for the matrix elements between the two degenerate states. However, since $\vec{\Lambda}$ consists of a contribution from each atom, we expect it to be independent of the length of the molecule. Consequently, because the denominator in f_{21} contains two terms that scale as N and two that scale as $1/N$, the denominator has no scaling behaviour. The numerator, on the other hand, contains three terms that scale as N, but only two that scale as $1/N$, and thus the net scaling of the $\vec{D}$-vector is $\vec{D} \sim N$, as we see in Figure 4.5c. This behaviour is also consistent with the experiments, which generally found a linear increase in the measured polarisation with the length of the molecule.

4.2 BAND TWISTING

In Figure 4.3, we saw a general trend where, as we twisted the bonds, degeneracies started to appear in the spectrum. We thus dedicate this section to studying whether this is a general feature of twisted linear molecules. We do this by considering a class of parameterised Hamiltonians, $H(\theta)$, where θ is a cyclic parameter, that is, $H(0) = H(2\pi n)$ for all $n \in \mathbb{Z}$. We shall refer to θ as the helicity parameter. The cyclicity of θ allows us to write the Hamiltonian in its diagonal form as a Fourier series:

$$\begin{aligned} H(\theta) &= \sum_i E_i(\theta) \left| i(\theta) \right\rangle \left\langle i(\theta) \right| \\ &= \sum_i \left| i(\theta) \right\rangle \left\langle i(\theta) \right| \sum_n \left(a_{n,i} \cos n\theta + b_{n,i} \sin n\theta \right), \end{aligned} \tag{4.20}$$

where $a_{n,i}, b_{n,i}$ are Fourier components. Degeneracies in the spectrum are found when, for two states, i, j,

$$E_i(\theta) - E_j(\theta) = \sum_n \left[(a_{n,i} - a_{n,j}) \cos n\theta + (b_{n,i} - b_{n,j}) \sin n\theta \right] = 0, \tag{4.21}$$

which is itself a Fourier series. The important thing to note about this equation is the fact that if the constant, direct component $a_{0,i} - a_{0,j}$ is sufficiently small, the two states will, at least twice during one cycle, become degenerate. To see this, note that the average energy gap over one cycle is given by:

$$\frac{1}{2\pi} \int_0^{2\pi} d\theta (E_i(\theta) - E_j(\theta)) = a_{0,i} - a_{0,j}. \tag{4.22}$$

Thus, if the fluctuations exceed this threshold, they will cross an even number of times during one cycle.

Let us illustrate this concept by considering a simple model of an infinitely long chain of sites with up to next-nearest neighbour hopping. For the sake of simplicity, we imagine that at each site, we have a single p-orbital sticking out perpendicular to the axis of the chain. This is can be seen as an effective model of the π-band of polyacetylene, but generalises to other molecules with a similar structure. Mathematically, such a model is described by the Hamiltonian:

$$\begin{aligned} H = -t_1 \sum_n \left(|n\rangle \langle n+1| + |n+1\rangle \langle n| \right) \\ - t_2 \sum_n \left(|n\rangle \langle n+2| + |n+2\rangle \langle n| \right), \end{aligned} \tag{4.23}$$

where t_1 and t_2 are the coupling between nearest and next-nearest neighbours respectively. The model is readily diagonalised in the basis of Bloch states, $\{k\}$,

$$|k\rangle = \frac{1}{\sqrt{N}} \sum_n e^{ink} |n\rangle , \quad |n\rangle = \frac{1}{\sqrt{N}} \sum_k e^{-ink} |k\rangle , \tag{4.24}$$

as:

$$H = -2 \sum_k |k\rangle \langle k| \left(t_1 \cos k + t_2 \cos 2k \right). \tag{4.25}$$

We now introduce a helicity parameter, θ, describing the relative angle of rotation around the helicity axis between adjacent sites. Since we are dealing with p-orbitals, this angular dependence enters through a cosine relationship, such that

$$t_1(\theta) = t_1 \cos \theta, \quad t_2(\theta) = t_2 \cos 2\theta. \tag{4.26}$$

Degeneracies in this spectrum are thus found by looking for solutions to the equation:

$$E_k = 2t_1 \cos k \cos \theta + 2t_2 \cos 2k \cos 2\theta, \tag{4.27}$$

for different k. From our analysis above, we note that the direct component is zero and thus there must exist at least two values on the interval $\theta \in [0, 2\pi)$ for which we find a degeneracy. The values of θ for which this happens for any given pair of momenta, k, k', are found by solving the equation:

$$t_1(\cos k' - \cos k) \cos \theta + t_2(\cos 2k' - \cos 2k) \cos 2\theta = 0, \tag{4.28}$$

which can be re-arranged as the requirement:

$$\frac{t_1}{t_2} \frac{\cos k' - \cos k}{\cos 2k' - \cos 2k} = -\frac{\cos 2\theta}{\cos \theta} = \frac{1 - 2\cos^2 \theta}{\cos \theta}. \tag{4.29}$$

Before solving this equation, let us first simplify the left hand side:

$$\frac{t_1}{t_2} \frac{\cos k' - \cos k}{\cos 2k' - \cos 2k} \equiv 4y. \tag{4.30}$$

Here, we have defined it as $4y$, in anticipation of a later simplification step. Using the three trigonometric identities,

$$2\sin a \sin b = \cos(a-b) - \cos(a+b), \tag{4.31}$$

$$2\cos a \cos b = \cos(a-b) + \cos(a+b), \quad \text{and} \tag{4.32}$$

$$\sin 2a = 2\sin a \cos a, \tag{4.33}$$

on the numerator and denominator, we find:

$$y = \frac{1}{8}\frac{t_1/t_2}{\cos k + \cos k'}. \tag{4.34}$$

Returning now to Eq. (4.29), it reads:

$$2\cos^2\theta + 4y\cos\theta - 1 = 0. \quad \Rightarrow \quad \cos\theta = \pm\sqrt{y^2 + 1/2} - y. \tag{4.35}$$

Because $\cos\theta$ is bounded between ± 1, we find the solutions for θ as:

$$\theta = \begin{cases} \arccos\left[-\sqrt{y^2+1/2} - y\right] & \text{for } y < -\frac{1}{4}, \\ \arccos\left[\pm\sqrt{y^2+1/2} - y\right] & \text{for } -\frac{1}{4} \le y \le \frac{1}{4}, \\ \arccos\left[\sqrt{y^2+1/2} - y\right] & \text{for } \frac{1}{4} < y. \end{cases} \tag{4.36}$$

This result is quite remarkable. First of all, it confirms the theorem that for any two pairs of momenta, k, k', there exists an angle, $\theta \in [0, \pi]$, for which the two states are degenerate. Second, if the two momenta satisfy:

$$|\cos k + \cos k'| \ge \frac{1}{2}\left|\frac{t_1}{t_2}\right|, \tag{4.37}$$

two angles exist on the interval, for which the momenta are degenerate. Note that the left hand side of Eq. (4.37) is bounded on the interval $[0, 2]$, and can thus only be satisfied if $|t_2| \ge |t_1|/4$. This exercise thus shows that in twisted chains of p-orbitals, it is a general feature that accidental degeneracies appear as the twisting is increased. Of course, in actual molecules and even the twisted polyacetylene molecule we studied above, the eigenstates share characteristics of different orbitals. Therefore, the symmetry properties of an individual eigenstate may change as the bonds are twisted, resulting in avoided crossings and deviations from the general principle that all levels will cross. However, since we know from our study of polyacetylene that we do have level crossings, this simple model can help understand why. Note that the hydrogen atoms in twisted polyacetylene are crucial in order to establish an sp_2-hybridisation, which separates the π-band from the rest.

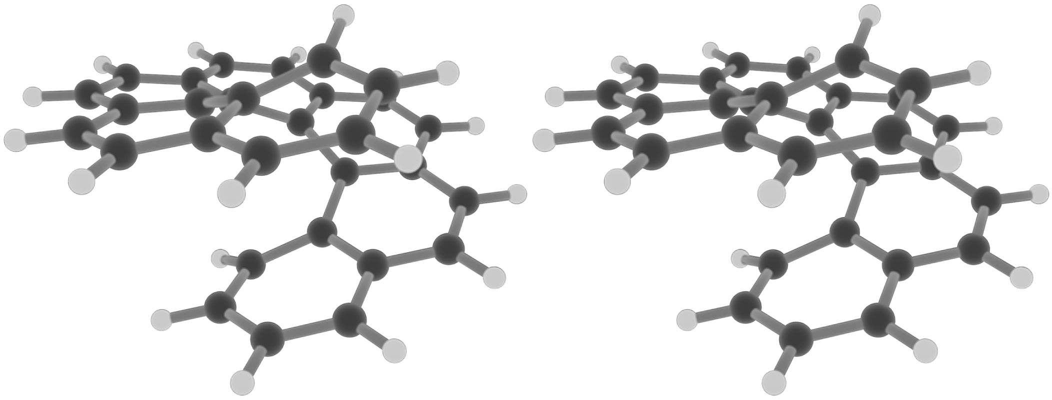

Figure 4.7: Stereoscopic cross-eyed model of helicene with $N = 7$ rings.

4.3 HELICENE

Before concluding the thesis, we end by considering a model of helicene. This molecule is simple enough that we can model it using a similar method that we used for polyacetylene, but complex enough that it is not obvious whether non-trivial effects may come into play. Crucially, however, it has been studied experimentally and therefore it serves as a testbed to see whether our observations for polyacetylene carries over to more complex molecules.

The specific molecule that we shall consider is what is generally referred to as [7]P-helicene, and is shown in cross-eye stereoscopy in Figure 4.7. This exact molecule has been studied experimentally using photoemission on different surfaces by Kettner et al.[27], and is summarised in Table 1.2. Since the planar staircase structure of the rings in the helicene molecule is rigid compared to polyacetylene, we cannot use bond twisting. Instead, in order to have a tunable parameter related to the geometry, we are going to vary the height between neighbouring rings, which we denote δz. Tuning this parameter effectively amounts to stretching and squeezing the molecule along the helical axis. In Figure 4.8, we plot the result of this variation in an energy window above the chemical potential. When compared to a relaxed structure of free standing helicene from *ab initio* calculations, a realistic value of δz is between 0.5 and $1.0\,\text{Å}$. Importantly, Figure 4.8A shows a heatmap of the magnitude of the $\vec{D}$-vector in which we see that, first of all, the structure has level crossings, and second, that near these crossings the polarisation increases. The leads are again coupled to the outermost carbon atoms at either end of the molecule, and the initial state, γ_L is not proportional to Γ_L. There is also high polarisation for some parameters away from level crossings. However, these high

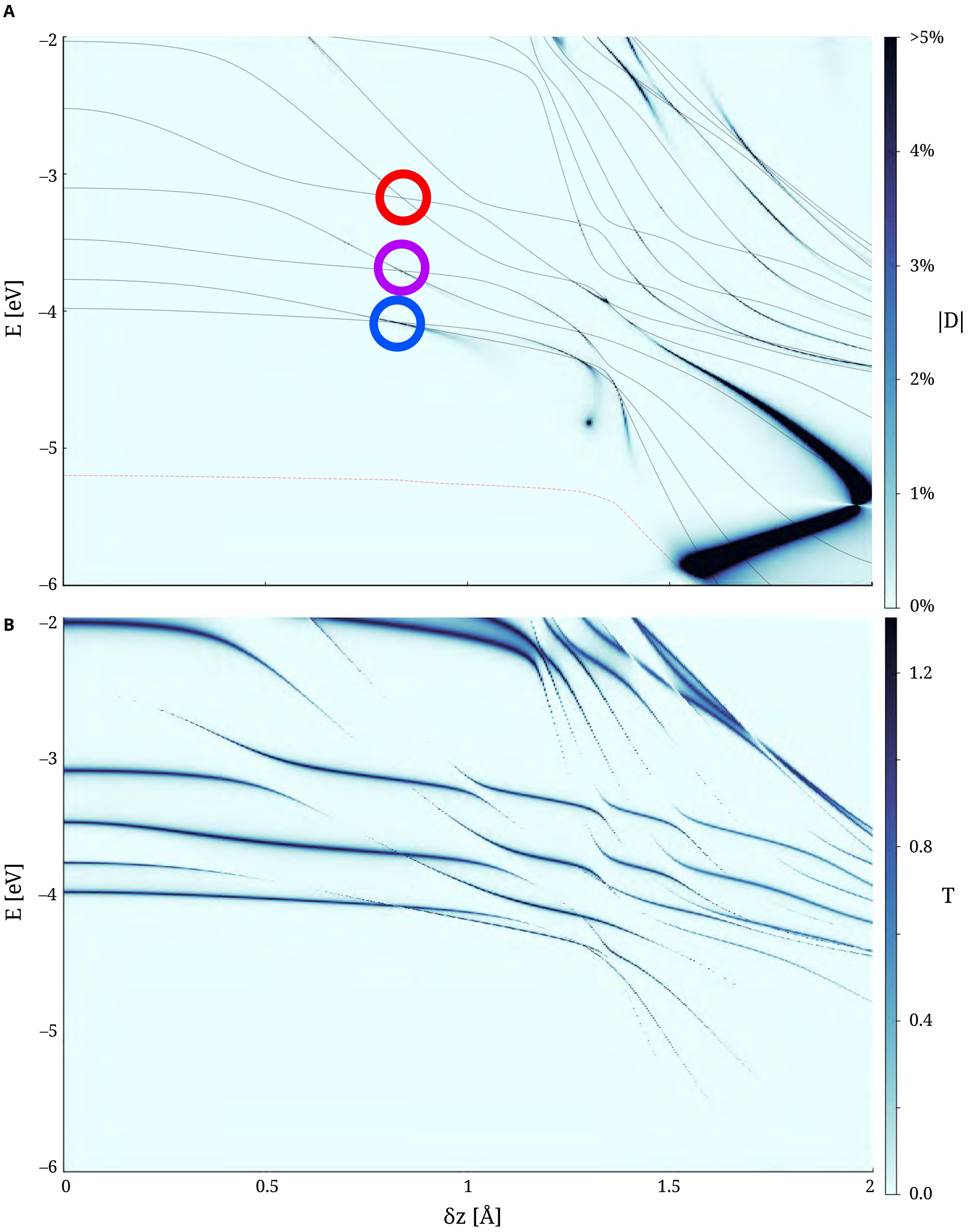

Figure 4.8: (A) Energy levels and heatmap of the magnitude of the $\vec{D}$-vector for energies above the chemical potential (dashed red line) as a function of the stretching of the molecule, δz. As with polyacetylene, we generally see peaks in the polarisation near level crossings. (B) Transmission function in the same region.

Table 4.2: $\vec{D}$- and $\vec{C}$-vectors for three selected level crossings in [7]P-helicene.

Circle	D_x (%)	D_y (%)	D_z (%)	C_x (%)	C_y (%)	C_z (%)
Blue	-3.9	6.8	-53.4	0.3	-0.3	-3.3
Purple	2.3	-4.0	-12.2	1.1	-0.8	-1.6
Red	0.1	-0.2	-4.4	0.8	-0.8	-0.7

values are artifacts of a vanishing transmission, as seen in Figure 4.8B, and thus do not contribute significantly to the spin current when integrated over.

In Table 4.2 we list the components of the $\vec{D}$- and $\vec{C}$-vectors at the level crossings marked by circles. We see that despite the fact that the molecule is more planar than polyacetylene, the $\vec{D}$-vector is still generally dominated by its component along the helical axis. The $\vec{C}$-vectors at the same points are generally an order of magnitude smaller, which was also the case for polyacetylene. It is worth noting that the projection into the two degenerate states yields the same $\vec{D}$-vectors up to the third decimal point, when compared to the full treatment.

Now, by comparison with the experiments on [7]P-helicene, we find that the polarisation is in the opposite direction. This might seem contradictory at first. However, we have in our calculation picked an initial state that is a random subset Γ_L. Since the no polarisation theorem guarantees that for γ_L proportional to Γ_L, the $\vec{D}$-vector vanishes, it follows that $\Gamma_L - \gamma_L$ leads to the opposite polarisation. Therefore, the calculations that we have done can only serve to highlight the mechanisms that are important to get a significant polarisation, rather than predict what the polarisation of a given experiment will be. In particular, we have found that the polarisation is greatly enhanced and reaches experimentally observed values only when two molecular levels are close in energy. The analysis above should therefore not be used to predict the polarisation, but to highlight the importance of these hotspots in the spectrum.

4.4 CONCLUDING REMARKS

In this thesis, we have introduced a formalism for dealing with the CISS effect in a single particle picture. This formalism allows us to capture most previous theoretical models and explain the results obtained therein. Because the CISS effect has been measured in organic molecules, where the atomic spin orbit coupling is weak, the CISS effect must be a first order effect in the SOC. This lead to a profound theorem which says that it should not be possible to measure any spin polarisation to first order, in a standard Landauer-Büttiker setup with two leads, where the electrons populate states with the same energy with equal probability. Thus, a crucial ingredient to any theory of the CISS effect must be that this symmetry is broken somehow. It is in fact broken in all experiments involving photoemission or photoexcitation, since the electrons are excited by means of a laser with selection rules that preferentially populate certain states. Moreover, in photoexcitation experiments that relied on different recombination rates for two opposite directions of spin, we indeed found that on short time scales, the theorem did not prevent one spin from escaping the molecule faster than the other. Using a similar observation for the electrochemistry experiments, we found that a similar argument could be applied to explain how magnetisation could be induced on a short time scale, when the molecule is gated. The measured magnetic fields in the experiments using a Hall probe, however, is much too large to be explained by injected polarised electrons. Thus, another mechanism must be responsible for the Hall effect measured in those experiments, which is beyond the scope of this thesis. All of the effects above could in general be reduced to two vector quantities related to the molecule, the $\vec{D}$- and $\vec{C}$-vectors. These vectors describe the polarisation and precession of an incoming electron beam, respectively.

In the case of experiments involving transport and a magnetic lead, we had to be more careful, since initial considerations using time reversal symmetry and the Ward identity lead to the result that it should not be possible to measure a difference in the current for oppositely oriented magnetic fields. A more careful analysis showed, however, that the spin current from the magnetic lead to the normal lead was non-zero. More importantly, when a chiral molecule was sandwiched between, the induced magnetisation into the normal lead was not anti-symmetric as one would usually expect. Instead, it was a combination of the magnetisation of the lead and the chirality of the molecule. Thus, any description of transport between a magnetic lead and a normal lead with a chiral molecule between must take this asymmetric effect into account.

Finally, we showed that in models of organic molecules, the spin polarisation generally only reaches a sizeable value, when two molecular levels are close in energy, i. e. are almost degenerate. At these hotspots, the polarisation in our model systems could reach values comparable to those measured in experiments. The occurence of accidental degeneracies was shown to be a general feature of idealised twisted molecules with p-like orbitals, and found to exist in both twisted polyacetylene and helicene. The points made in this thesis thus represents the foundations upon which more comprehensive treatments of molecules in relation to the CISS effect can be built. That is, the no polarisation theorem, the concept of the $\vec{D}$- and $\vec{C}$-vectors in both steady state and short time limits, the asymmetric induced magnetisation, and the enhancement of the polarisation near degeneracies.

APPENDIX

A

MATHEMATICAL IDENTITIES

A.1 VECTOR OPERATORS

A.1.1

IDENTITY

$$(\vec{A}\times\vec{B})^T = -\vec{B}^T\times\vec{A}^T \tag{A.1}$$

PROOF Writing the cross product using the anti-symmetric tensor,

$$\vec{A}\times\vec{B} = \sum_{ijk}\epsilon_{ijk}A_iB_j\hat{n}_k, \tag{A.2}$$

and the fact that the transpose changes the order of its arguments, we immediately find that

$$(\vec{A}\times\vec{B})^T = \sum_{ijk}\epsilon_{ijk}B_j^TA_i^T\hat{n}_k = -\vec{B}^T\times\vec{A}^T. \tag{A.3}$$

A.2 DISTRIBUTION FUNCTIONS

A.2.1

IDENTITY

$$n_F(E-\mu_L) - n_F(E-\mu_R) = \frac{\sinh(\beta\Delta\mu/2)}{\cosh(\beta(E-\bar{\mu}))+\cosh(\beta\Delta\mu/2)}. \tag{A.4}$$

PROOF We first plug in the definitions:

$$\begin{aligned} n_F(x) - n_F(y) &= (n_F^{-1}(y) - n_F^{-1}(x)) n_F(x) n_F(y) \\ &= \left(e^{\beta y} - e^{\beta x}\right) n_F(x) n_F(y) \\ &= e^{\beta(x+y)/2} \left(e^{\beta(y-x)/2} - e^{-\beta(y-x)/2}\right) n_F(x) n_F(y) \\ &= 2\sinh(\beta(y-x)/2) \frac{e^{\beta x/2}}{e^{\beta x}+1} \frac{e^{\beta y/2}}{e^{\beta y}+1}. \end{aligned} \tag{A.5}$$

Using:

$$\frac{e^{\beta x/2}}{e^{\beta x}+1} = \frac{1}{2\cosh(\beta x/2)}, \tag{A.6}$$

we find:

$$n_F(x) - n_F(y) = \frac{1}{2} \frac{\sinh(\beta(y-x)/2)}{\cosh(\beta x/2)\cosh(\beta y/2)}. \tag{A.7}$$

Finally, from:

$$\begin{aligned} \cosh(x)\cosh(y) &= \frac{(e^x + e^{-x})(e^y + e^{-y})}{4} \\ &= \frac{e^{x+y} + e^{-(x+y)} + e^{x-y} + e^{-(x-y)}}{4} \\ &= \frac{\cosh(x+y) + \cosh(x-y)}{2}, \end{aligned} \tag{A.8}$$

and setting $x = E - \mu_L$, $y = E - \mu_R$, and defining $\Delta\mu = \mu_L - \mu_R$, $\bar{\mu} = (\mu_L + \mu_R)/2$, we obtain the identity, Eq. (A.4).

A.2.2

IDENTITY

$$\int_{-\infty}^{\infty} (n_F(E-\mu_L) - n_F(E-\mu_R)) dE = \mu_L - \mu_R \tag{A.9}$$

PROOF Using,

$$\int_{-a}^{a} n_F(x)\, dx = \int_{-a}^{a} \frac{dx}{e^{\beta x}+1} = 2a + \frac{1}{\beta} \ln\left[\frac{1+e^{-\beta a}}{1+e^{\beta a}}\right], \tag{A.10}$$

we find:

$$\int_{-a}^{a} dE (n_F(E-\mu_L) - n_F(E-\mu_R)) = \frac{1}{\beta} \ln\left[\frac{1+e^{\beta(-a-\mu_L)}}{1+e^{\beta(a-\mu_L)}} \frac{1+e^{\beta(a-\mu_R)}}{1+e^{\beta(-a-\mu_R)}}\right]. \tag{A.11}$$

In the limit, $a \to \infty$, direct evaluation of this expression diverges. We thus have to use L'Hôpital's rule. Note that:

$$\partial_a (1 + e^{-\beta(a-\mu_L)})(1 + e^{\beta(a-\mu_R)}) = \beta \left[e^{\beta(a-\mu_R)} - e^{\beta(-a-\mu_L)} \right]. \tag{A.12}$$

Thus,

$$\lim_{a\to\infty} \frac{1 + e^{\beta(-a-\mu_L)}}{1 + e^{\beta(a-\mu_L)}} \frac{1 + e^{\beta(a-\mu_R)}}{1 + e^{\beta(-a-\mu_R)}} = \lim_{a\to\infty} \frac{e^{\beta(a-\mu_R)} - e^{\beta(-a-\mu_L)}}{e^{\beta(a-\mu_L)} - e^{\beta(-a-\mu_R)}}, \tag{A.13}$$

and by multiplying by $e^{-\beta a}$ in the numerator and denominator, we obtain:

$$\lim_{a\to\infty} \frac{e^{-\beta\mu_R} - e^{-2\beta a} e^{-\beta\mu_L}}{e^{-\beta\mu_L} - e^{-2\beta a} e^{-\beta\mu_R}} = e^{\beta(\mu_L - \mu_R)}. \tag{A.14}$$

Plugging this result back into Eq. (A.11), we arrive at the identity, Eq. (A.9).

B

TIME REVERSAL

In this appendix, we want to prove some properties and relations of systems as a consequence of time reversal and time reversal symmetry. We define, in informal terms, the time reversal operator, $\mathbb{T}$, as an operator that reverses the direction of time. To figure out its form as an operator, we consider the position operator, $\hat{x}$. Under time reversal, changing the direction of time does not affect the instantaneous position of a particle, and thus we demand that $\mathbb{T}\hat{x} = \hat{x}\mathbb{T}$. Conversely, for the momentum operator, $\hat{p} = m\partial_t\hat{x} = i[\hat{H}, m\hat{x}]/\hbar$, we expect it to change sign:

$$\mathbb{T}\hat{p} = -\hat{p}\mathbb{T} = -\frac{i}{\hbar}[\hat{H}, m\hat{x}]\mathbb{T}. \tag{B.1}$$

In real space, for a particle in a potential,

$$\hat{H} = \frac{\hat{p}^2}{2m} + \hat{V}. \tag{B.2}$$

The kinetic energy term is quadratic in $\hat{p}$ and thus does not change sign. In general, the potential can be found by considering the forces acting on the particle:

$$\vec{F} = -\vec{\nabla}V. \tag{B.3}$$

For a particle in an electromagnetic field, the force field can be found as:

$$\vec{F} = \frac{q}{m}(m\vec{E} + \vec{p} \times \vec{B}) = -\vec{\nabla}V. \tag{B.4}$$

The contribution from the electric field reads:

$$V(\vec{r}) = -q\int_{\vec{r}_0}^{\vec{r}} d\vec{r}\,' \cdot \vec{E}(\vec{r}\,'). \tag{B.5}$$

Assuming the electric field to be unaffected by time reversal, this term, like the kinetic energy, also does not change sign.

The magnetic field is different. Assuming for simplicity, that the magnetic field is constant, we get:

$$V(\vec{r}) = \frac{q}{m}\vec{r} \cdot \vec{p} \times \vec{B} = \vec{B} \cdot \underbrace{\frac{q}{m}(\vec{r} \times \vec{p})}_{\vec{\mu}}, \tag{B.6}$$

where $\vec{\mu}$ is the magnetic moment of the particle. Since $\vec{p}$ changes sign, this whole term changes sign under time reversal, and thus a magnetic field is often said to break time reversal symmetry*. Note that matrix elements of the operator $\hat{H}$ are real, if the states are real:

$$\langle\psi| \hat{H} |\phi\rangle = \int d\vec{r}\, \psi(\vec{r}) \left(-\frac{\nabla^2}{2m} + V(\vec{r})\right) \phi(\vec{r}), \tag{B.7}$$

since $V(\vec{r})$ is a real field. Consequently, going back to Eq. (B.1), it is satisfied in a real basis, if $\mathbb{T} = K$ is the complex conjugation operator.

Operators that only depend on the position of a particle and even powers of its momentum are time reversal symmetric. For such an operator, A, it thus follows that, when expressed in a real basis, $A = A^*$. Operators that depend on odd powers of momentum or momentum-like quantities of a particle are anti-symmetric under time reversal, and thus obey $A = -A^*$ instead. The latter is the case for the energy of a particle in a magnetic field, its the angular momentum and spin degrees of freedom.

B.1 SPIN

In our analysis above, we have ignored the properties of spin. Since the electron spin is also an angular momentum, we must also require $\mathbb{T}\vec{a} \cdot \vec{\sigma} = -\vec{a} \cdot \vec{\sigma}\mathbb{T}$. This is satisfied if we let the spinful representation of the time reversal operator be $\mathbb{T} = -i\sigma_y K$. To see this, we use the fact that $\sigma_x\sigma_y = -\sigma_y\sigma_x$:

$$\mathbb{T}\sigma_x = -i\sigma_y\sigma_x K = -\sigma_x(-i\sigma_y K) = -\sigma_x\mathbb{T}. \tag{B.8}$$

And similarly for σ_z. For σ_y we use the complex conjugation operator to find the same relationship:

$$\mathbb{T}\sigma_y = -i\sigma_y\sigma_y^* K = -\sigma_y(-i\sigma_y K) = -\sigma_y\mathbb{T}. \tag{B.9}$$

This proves that $\mathbb{T} = -i\sigma_y K$ is the time reversal operator in a spinful (spin-$\frac{1}{2}$) representation.

All the spinful operators we are interested in can be written on so-called quarternion form:

$$A = A_0\sigma_0 + \vec{A} \cdot \vec{\sigma}, \tag{B.10}$$

where σ_0 is the identity matrix in spin space. By applying the time reversal operators, we see that in a real basis, they must obey:

$$\mathbb{T}A = \mathbb{T}(A_0 + \vec{A} \cdot \vec{\sigma}) = (A_0^* - \vec{A}^* \cdot \vec{\sigma})\mathbb{T} = A^Q\mathbb{T}, \tag{B.11}$$

---

* In a full treatment, we want our physical laws to look identical, when we "play the movie backwards", and thus the way out of this conundrum is to let the magnetic field change sign under time reversal, which would also be the case if one considered the sources giving rise to the field in the first place.

where the superscript Q denotes the quarternion conjugate, defined by the equality. Note that because of the tracelessness of the Pauli matrices, the trace of the product of two quarternion operators is given by:

$$\mathrm{tr}\Big[(A_0 + \vec{A}\cdot\vec{\sigma})(B_0 + \vec{B}\cdot\vec{\sigma})\Big] = \mathrm{tr}[AB] + \mathrm{tr}\Big[\vec{A}\cdot\vec{B}\Big]. \tag{B.12}$$

Plugging in the definition of the quarternion conjugate and using the invariance of the trace under transposition, it is therefore trivial to show that:

$$\mathrm{tr}[AB] = \mathrm{tr}\big[A^Q B^Q\big]^* = \mathrm{tr}\big[(A^Q)^\dagger (B^Q)^\dagger\big] = \mathrm{tr}[A^\tau B^\tau], \tag{B.13}$$

for all quarternion operators, where $A^\tau = (A^Q)^\dagger$ denotes what we refer to as the quarternion transpose.

Note that, like normal conjugation,

$$(AB)^Q = A^Q B^Q. \tag{B.14}$$

To see this, the explicit calculation of the product of the two quarternion operators gives:

$$AB = A_0 B_0 + \vec{A}\cdot\vec{B} + (A_0\vec{B} + \vec{A}B_0 + i\vec{A}\times\vec{B})\cdot\vec{\sigma}, \tag{B.15}$$

while the product of their quarternion conjugates gives:

$$A^Q B^Q = A_0^* B_0^* + \vec{A}^*\cdot\vec{B}^* - (A_0^*\vec{B}^* + \vec{A}^* B_0^* + i\vec{A}^*\times\vec{B}^*)\cdot\vec{\sigma}, \tag{B.16}$$

which is exactly equal to $(AB)^Q$. This relationship can be extended to the quarternion transpose, by taking the adjoint of the expressions above. We thus find:

$$(A^Q B^Q)^\dagger = B^\tau A^\tau = B_0^T A_0^T + \vec{B}^T\cdot\vec{A}^T - (\vec{B}^T A_0^T + B_0^T \vec{A}^T + i\vec{B}^T\times\vec{A}^T)\cdot\vec{\sigma}, \tag{B.17}$$

where we have used the identity A.1.1 for transposition of cross products to cancel the sign change from the conjugation of i. Thus, we find that analogous to the normal transpose, it also holds that:

$$(AB)^\tau = B^\tau A^\tau. \tag{B.18}$$

This allows us to extend the trace identity to:

$$\mathrm{tr}[ABC] = \mathrm{tr}[C^\tau B^\tau A^\tau], \tag{B.19}$$

for all quarternion operators, which of course generalises to higher order products as well.

B.1.1 *Time reversed operators*

If the Hamiltonian is time reversal invariant, it must hold that in a real basis:

$$\mathbb{T}H = H\mathbb{T} = H^Q\mathbb{T} \quad \Rightarrow \quad H = H^Q = H^\dagger = H^\tau. \tag{B.20}$$

If we include the spin-orbit coupling, it consists of the product of two angular momenta (spin and orbital), thus it must also hold that:

$$\mathbb{T}\vec{\sigma}\cdot\vec{\Lambda} = \vec{\sigma}\cdot\vec{\Lambda}\mathbb{T}. \tag{B.21}$$

If the Hamiltonian is time reversal invariant, $\mathbb{T}H = H\mathbb{T}$, the propagator is related to its adjoint through time reversal as:

$$\mathbb{T}G^0 = \frac{1}{E\mathbb{T}^{-1} - H\mathbb{T}^{-1} + i\eta\mathbb{T}^{-1}} = \frac{1}{\mathbb{T}^{-1}E - \mathbb{T}^{-1}H - \mathbb{T}^{-1}i\eta} = (G^0)^\dagger\mathbb{T}. \tag{B.22}$$

It thus follows that for self-energies of the type:

$$\mathbb{T}\Sigma_R = \mathbb{T}H_{MR}G^0_R H_{RM} = H_{MR}(G^0_R)^\dagger H_{RM}\mathbb{T} = \Sigma^\dagger_R\mathbb{T}, \tag{B.23}$$

and therefore the time reverse partner of the full propagator is also its adjoint:

$$\mathbb{T}G = \mathbb{T}\frac{1}{E - H - \Sigma} = \mathbb{T}\frac{1}{E - H - \Sigma^\dagger}\mathbb{T} = G^\dagger\mathbb{T}. \tag{B.24}$$

Since the time reverse of any spinful operator is its quarternion conjugate, we thus find $G^Q = G^\dagger$, and $G = G^\tau$, if the whole system is time reversal invariant.

In the case of a magnetic lead, time reversal symmetry is broken. However, if the lead has magnetisation along an axis $\hat{m}$, we can write,

$$\mathbb{T}H(\hat{m}) = \mathbb{T}H_0 + \mathbb{T}\Delta H(\hat{m}\cdot\vec{\sigma}) = H_0\mathbb{T} - \Delta H(\hat{m}\cdot\vec{\sigma})\mathbb{T} = H(-\hat{m})\mathbb{T}. \tag{B.25}$$

Consequently, we find for the other operators,

$$\mathbb{T}G^0(\hat{m}) = (G^0(-\hat{m}))^\dagger\mathbb{T}, \quad \mathbb{T}\Sigma(\hat{m}) = \Sigma^\dagger(-\hat{m})\mathbb{T}, \quad \mathbb{T}G(\hat{m}) = G^\dagger(-\hat{m})\mathbb{T}, \tag{B.26}$$

or $G^Q(\hat{m}) = G^\dagger(-\hat{m})$, $G(\hat{m}) = G^\tau(-\hat{m})$, etc.

C

APPENDIX TO CHAPTER 2

C.1 PARTICLE CURRENT OF CROSS-TERMS

In the case of cross-terms in the density matrix involving the molecule subspace, it turns out to be convenient to go back to Eq. (2.54) and introduce projection operators there:

$$\mathrm{tr}[(L+R)\rho(t_0)MG^\dagger AG] = \mathrm{tr}[\rho(t_0)MG^\dagger A(GV+1)(L+R)G^0], \tag{C.1}$$

and

$$\mathrm{tr}[M\rho(t_0)(L+R)G^\dagger AG] = \mathrm{tr}[M\rho(t_0)(G^0)^\dagger(L+R)(1+VG^\dagger)AG]. \tag{C.2}$$

The cross-term density matrix is then defined as:

$$\rho_{LM}(E) = \frac{\eta}{\pi}LG^0\rho(t_0)M = \sum_{\psi kk'}\langle n_\psi\rangle\psi_{kk'}\frac{\eta/\pi}{E-E_k+i\eta}L\left|k\right\rangle\left\langle k'\right|M. \tag{C.3}$$

And similarly for ρ_{ML}, etc. Note that in the limit, $\eta\to 0^+$,

$$\rho_{LM}(E) = \sum_{\psi kk'}\langle n_\psi\rangle\psi_{kk'}\left(\mathcal{P}\frac{\eta/\pi}{E-E_k} - i\eta\delta(E-E_k)\right)L\left|k\right\rangle\left\langle k'\right|M, \tag{C.4}$$

where $\mathcal{P}$ denotes the principal value. When integrated over E, both of the terms vanish identically, in this limit. Thus, we are justified in ignoring cross-terms related to the molecule when calculating the steady state current.

For cross-terms related to the leads, we find one non-zero trace from the second and third terms of Eq. (2.60). It is:

$$\langle H_{RM}\rangle^{(2,3)}_{LR} = \int dE\,\mathrm{tr}[\rho_0^{LR}H_{RM}G_MH_{ML}] = \int dE\,\mathrm{tr}[\gamma_{LR}G_M]. \tag{C.5}$$

The terms related to ρ_0^{RL} are zero. To see this, note that due to the projections, it is not possible to find operators that "line up" under the trace:

$$\mathrm{tr}[\rho_0^{RL}H_{RM}G_MH_{MR}] + \mathrm{tr}\left[\rho_0^{RL}H_{LM}G^\dagger_{MR}H_{RM}\right] = 0. \tag{C.6}$$

Consequently, the particle current associated with these cross-terms are of the form:

$$\langle\dot{R}\rangle_{LR}^{(2,3)} = \int \frac{dE}{\hbar} 2\text{Im}\,\text{tr}[\gamma_{LR} G_M] = \int \frac{dE}{\hbar} i\,\text{tr}\left[\gamma_{RL} G_M^\dagger - \gamma_{LR} G_M\right], \tag{C.7}$$

where we have used the fact that $\gamma_{LR}^\dagger = \gamma_{RL}$. Now, in the steady state limit,

$$\gamma_{LR} = \sum_{\psi kk'} \langle n_\psi \rangle \psi_{kk'} \delta_{E_k, E'_k} L \left|k\right\rangle \delta(E - E_k) \left\langle k'\right| R, \tag{C.8}$$

in both the scattering and initial state picture. If the density matrix is time-reversal invariant, the equation above tells us that $\gamma_{LR} = \gamma_{LR}^Q$, where the superscript Q denotes the quarternion conjugate, as discussed in Appendix B. Using Eq. (B.13), we are thus left with the trace:

$$\text{tr}[\gamma_{LR} G_M] = \text{tr}[\gamma_{LR}^\tau G_M^\tau] = \text{tr}[\gamma_{RL} G_M]. \tag{C.9}$$

Here we have used the fact that in a real basis, $G_M^\tau = G_M$ for a time-reversal invariant Hamiltonian. Therefore, we finally find that the corresponding particle current is given by:

$$\langle\dot{R}\rangle_{LR}^{(2,3)} = \int \frac{dE}{\hbar} i\,\text{tr}\left[\gamma_{RL}(G_M^\dagger - G_M)\right] = -\int \frac{dE}{\hbar} \text{tr}\left[\gamma_{RL} G_M^\dagger \Gamma G_M\right]. \tag{C.10}$$

For the fourth term of Eq. (2.60), an analysis analogous to the one in section 2.4 leads to:

$$\langle\dot{R}\rangle_{LR}^{(4)} + \langle\dot{R}\rangle_{RL}^{(4)} = \int \frac{dE}{\hbar} \text{tr}\left[(\gamma_{LR} + \gamma_{RL}) G_M^\dagger \Gamma_R G_M\right], \tag{C.11}$$

and putting it all together:

$$\langle\dot{R}\rangle_{LR} + \langle\dot{R}\rangle_{RL} = \int \frac{dE}{\hbar} \left(\text{tr}\left[\gamma_{LR} G_M^\dagger \Gamma_R G_M\right] - \text{tr}\left[\gamma_{RL} G_M^\dagger \Gamma_L G_M\right]\right). \tag{C.12}$$

C.1.1 *Transient effects*

On short time scales, we consider only the issue of a molecule coupled to a single lead. In this case, we have to consider the density matrix:

$$\begin{aligned} \rho_{RM}(E) &= \frac{\hbar}{2\pi\tau} R G^0 \rho(t_0) M = \sum_{\psi kk'} \langle n_\psi \rangle \psi_{kk'} \frac{\Gamma_\tau/2\pi}{E - E_k + i\Gamma_\tau/2} R \left|k\right\rangle \left\langle k'\right| M \\ &= \frac{\Gamma_\tau}{2\pi} \sum_{\psi kk'} \langle n_\psi \rangle \psi_{kk'} \left(\frac{E - E_k - i\Gamma_\tau/2}{(E - E_k)^2 + (\Gamma_\tau/2)^2} \right) R \left|k\right\rangle \left\langle k'\right| M \end{aligned} \tag{C.13}$$

For very short time scales, Γ_τ is large, and therefore find that the density matrix tends towards a constant for finite E:

$$\rho_{RM}(E \ll \Gamma_\tau) = -\frac{i}{\pi} R \rho(t_0) M. \tag{C.14}$$

Assuming ρ is spinless and time-reversal invariant, in which case it is real, ρ_{RM} thus becomes imaginary. This might initially seem counterintuitive, but it is important to remember that ρ_{RM} represents off-diagonal elements of the density matrix. All we require is that the full density matrix is hermitian, and we indeed find by the same analysis that the corresponding ρ_{MR} comes with an opposite sign. Thus the form of the density matrix is consistent.

Now, to calculate the particle current into the lead, we again have to consider two kinds of traces. The first trace is of the type:

$$\langle H_{RM}\rangle^{(1)}_{MR} = \int dE\,\mathrm{tr}[\rho_{MR}H_{RM}G_M] = \int dE\,\mathrm{tr}[\gamma_{\tau R}G_M], \tag{C.15}$$

where we have defined $\gamma_{R\tau} = H_{MR}\rho_{RM}$, analogous to our usual definitions. The current from this term thus yields:

$$\langle \dot{\bar{R}}\rangle^{(1)}_{\tau R} = \int \frac{dE}{\hbar} 2\mathrm{Im}\,\mathrm{tr}[\gamma_{\tau R}G_M] = \int \frac{dE}{\hbar} i\,\mathrm{tr}\Big[\gamma_{R\tau}G^{\dagger}_{M} - \gamma_{\tau R}G_M\Big]. \tag{C.16}$$

Joining it with the remaining term, analogous to the fourth term in Eq. (2.60), we finally obtain:

$$\langle \dot{\bar{R}}\rangle_{MR} = \int \frac{dE}{\hbar}\left(\mathrm{tr}\Big[(\gamma_{R\tau}+\gamma_{\tau R})G^{\dagger}_{M}\Gamma_R G_M\Big] + \mathrm{tr}\Big[\gamma_{R\tau} iG^{\dagger}_{M} - \gamma_{\tau R} iG_M\Big]\right). \tag{C.17}$$

Unfortunately, unlike in the steady state case, $\gamma_{R\tau}$ is now complex, and thus time reversal invariance of the initial state does not ensure time reversal invariance of $\gamma_{R\tau}$. Thus we cannot simplify the last term under the integral above, without further assumptions about the whole system.

C.2 THE PRECESSION TERM IN EQUILIBRIUM

Note: this derivation depends on quantities and notation introduced in chapter 3. Expanding the propagators to first order in the SOC, $\vec{H}_M = \vec{\Lambda}$, we get:

$$\begin{aligned}
\mathrm{tr}\Big[\gamma G^{\dagger}_{M}\hat{n}\times\vec{\Lambda}\cdot\vec{\sigma}G_M\Big] &= \mathrm{tr}\Big[\gamma g^{\dagger}_{M}(\vec{\Lambda}\cdot\vec{\sigma})g^{\dagger}_{M}(\hat{n}\times\vec{\Lambda})\cdot\vec{\sigma}g_M\Big] \\
&\quad + \mathrm{tr}\Big[\gamma g^{\dagger}_{M}(\hat{n}\times\vec{\Lambda})\cdot\vec{\sigma}g_M(\vec{\Lambda}\cdot\vec{\sigma})g_M\Big] \\
&= 2\,\mathrm{tr}\left[\left(g_M\gamma g^{\dagger}_{M}\right)\left(\sum_{ijk}\epsilon_{ijk}n_i\Lambda^k(g_M - g^{\dagger}_{M})\Lambda^j\right)\right].
\end{aligned} \tag{C.18}$$

Now, since in a real basis:

$$g = g^T, \quad \vec{\Lambda} = -\vec{\Lambda}^T, \tag{C.19}$$

we find:

$$\Lambda^k g^\dagger \Lambda^j = (\Lambda^j g^\dagger \Lambda^k)^T. \tag{C.20}$$

Additionally, in the equilibrium situation where $\gamma \propto \Gamma$, we can make use of the Ward identity to find that $g_M \Gamma g_M^\dagger = (g_M \Gamma g_M^\dagger)^T$. From the property of the trace,

$$\mathrm{tr}[AB] = \mathrm{tr}[A^T B^T], \tag{C.21}$$

and (C.20) above, we thus end up with:

$$\begin{aligned}
&\mathrm{tr}\left[\left(g_M \Gamma g_M^\dagger\right)\left(\sum_{ijk} \epsilon_{ijk} n_i \Lambda^k (g_M - g_M^\dagger)\Lambda^j\right)\right] \\
&\quad = \mathrm{tr}\left[\left(g_M \Gamma g_M^\dagger\right)^T \left(\sum_{ijk} \epsilon_{ijk} n_i \Lambda^k (g_M - g_M^\dagger)\Lambda^j\right)^T\right] \\
&\quad = \mathrm{tr}\left[\left(g_M \Gamma g_M^\dagger\right)\left(\sum_{ijk} \epsilon_{ijk} n_i \Lambda^j (g_M - g_M^\dagger)\Lambda^k\right)\right].
\end{aligned} \tag{C.22}$$

Note that in the last equality, the indices j and k have been reversed. Using the fact that the anti-symmetric tensor, ϵ_{ijk} changes sign under such an interchange, the trace must be zero. In other words, in equilibrium, there is no net spin polarisation of the system in steady state up to second order in the atomic SOC.

Using the quarternion notation of Appendix B, this can be shown to hold more generally. In a spinful representation, $G_M = G_M^\tau = (G_M^Q)^\dagger$. Consequently, if Γ is time-reversal symmetric, since it is hermitian, $\Gamma = \Gamma^Q = \Gamma^\dagger = \Gamma^\tau$. Thus we have the analogous quarternion transpose identity, using the Ward identity, Eq. (2.79): $G_M \Gamma G_M^\dagger = (G_M \Gamma G_M^\dagger)^\tau$. Consequently:

$$\begin{aligned}
\mathrm{tr}\left[(G_M \Gamma G_M^\dagger)(\hat{n} \times \vec{\Lambda}) \cdot \vec{\sigma}\right] &= \mathrm{tr}\left[(G_M \Gamma G_M^\dagger)^\tau ((\hat{n} \times \vec{\Lambda}) \cdot \vec{\sigma})^\tau\right] \\
&= -\,\mathrm{tr}\left[G_M \Gamma G_M^\dagger (\hat{n} \times \vec{\Lambda}) \cdot \vec{\sigma}\right] = 0.
\end{aligned} \tag{C.23}$$

In the last equality, we have used the fact that $\vec{\Lambda}$ and $\vec{\sigma}$ are hermitian, and the fact that the quarternion conjugation yields:

$$((\hat{n} \times \vec{\Lambda}) \cdot \vec{\sigma})^Q = -(\hat{n} \times \vec{\Lambda}) \cdot \vec{\sigma}. \tag{C.24}$$

D

APPENDIX TO CHAPTER 3

D.1 THE TWENTY TERMS

Inserting the spin-resolved propagators and Γ-matrix, the transmission function takes the form:

$$
\begin{aligned}
T_{i\to j} = \mathrm{tr}[&\gamma_i(\bar{g}_M^\dagger + (\hat{m}\cdot\vec{\sigma})\Delta g_M^\dagger)(\vec{\Lambda}\cdot\vec{\sigma})(\bar{g}_M^\dagger + (\hat{m}\cdot\vec{\sigma})\Delta g_M^\dagger) \\
&\times (\bar{\Gamma}_j + (\hat{m}\cdot\vec{\sigma})\Delta\Gamma_j)(\bar{g}_M + (\hat{m}\cdot\vec{\sigma})\Delta g_M)]
\end{aligned}
\tag{D.1}
$$

Applying the rules listed in Table 3.1, only the following terms involved in the pertubative expansion of the transmission function survive:

$$
\begin{aligned}
T_{i\to j} = {} & 2\,\mathrm{tr}\Big[\gamma_i\bar{g}_M^\dagger\bar{\Gamma}_j\bar{g}_M\Big] + 2\,\mathrm{tr}\Big[\gamma_i\Delta g_M^\dagger\Delta\Gamma_j\bar{g}_M\Big] \\
& + 2\,\mathrm{tr}\Big[\gamma_i\bar{g}_M^\dagger\Delta\Gamma_j\Delta g_M\Big] + 2\,\mathrm{tr}\Big[\gamma_i\Delta g_M^\dagger\bar{\Gamma}_j\Delta g_M\Big] \\
& + 2\,\mathrm{tr}\Big[\gamma_i\Delta g_M^\dagger(\vec{\Lambda}\cdot\hat{m})\bar{g}_M^\dagger\bar{\Gamma}_j\bar{g}_M\Big] + 2\,\mathrm{tr}\Big[\gamma_i\bar{g}_M^\dagger(\vec{\Lambda}\cdot\hat{m})\Delta g_M^\dagger\bar{\Gamma}_j\bar{g}_M\Big] \\
& + 2\,\mathrm{tr}\Big[\gamma_i\bar{g}_M^\dagger(\vec{\Lambda}\cdot\hat{m})\bar{g}_M^\dagger\Delta\Gamma_j\bar{g}_M\Big] + 2\,\mathrm{tr}\Big[\gamma_i\bar{g}_M^\dagger(\vec{\Lambda}\cdot\hat{m})\bar{g}_M^\dagger\bar{\Gamma}_j\Delta g_M\Big] \\
& + 2\,\mathrm{tr}\Big[\gamma_i\bar{g}_M^\dagger(\vec{\Lambda}\cdot\hat{m})\Delta g_M^\dagger\Delta\Gamma_j\Delta g_M\Big] + 2\,\mathrm{tr}\Big[\gamma_i\Delta g_M^\dagger(\vec{\Lambda}\cdot\hat{m})\bar{g}_M^\dagger\Delta\Gamma_j\Delta g_M\Big] \\
& + 2\,\mathrm{tr}\Big[\gamma_i\Delta g_M^\dagger(\vec{\Lambda}\cdot\hat{m})\Delta g_M^\dagger\bar{\Gamma}_j\Delta g_M\Big] + 2\,\mathrm{tr}\Big[\gamma_i\Delta g_M^\dagger(\vec{\Lambda}\cdot\hat{m})\Delta g_M^\dagger\Delta\Gamma_j\bar{g}_M\Big]. \\
& + 2\,\mathrm{tr}\Big[\gamma_i\Delta g_M^\dagger\bar{\Gamma}_j\bar{g}_M(\vec{\Lambda}\cdot\hat{m})\bar{g}_M\Big] + 2\,\mathrm{tr}\Big[\gamma_i\bar{g}_M^\dagger\Delta\Gamma_j\bar{g}_M(\vec{\Lambda}\cdot\hat{m})\bar{g}_M\Big] \\
& + 2\,\mathrm{tr}\Big[\gamma_i\bar{g}_M^\dagger\bar{\Gamma}_j\Delta g_M(\vec{\Lambda}\cdot\hat{m})\bar{g}_M\Big] + 2\,\mathrm{tr}\Big[\gamma_i\bar{g}_M^\dagger\bar{\Gamma}_j\bar{g}_M(\vec{\Lambda}\cdot\hat{m})\Delta g_M\Big] \\
& + 2\,\mathrm{tr}\Big[\gamma_i\bar{g}_M^\dagger\Delta\Gamma_j\Delta g_M(\vec{\Lambda}\cdot\hat{m})\Delta g_M\Big] + 2\,\mathrm{tr}\Big[\gamma_i\Delta g_M^\dagger\bar{\Gamma}_j\Delta g_M(\vec{\Lambda}\cdot\hat{m})\Delta g_M\Big] \\
& + 2\,\mathrm{tr}\Big[\gamma_i\Delta g_M^\dagger\Delta\Gamma_j\bar{g}_M(\vec{\Lambda}\cdot\hat{m})\Delta g_M\Big]. + 2\,\mathrm{tr}\Big[\gamma_i\Delta g_M^\dagger\Delta\Gamma_j\Delta g_M(\vec{\Lambda}\cdot\hat{m})\bar{g}_M\Big]
\end{aligned}
\tag{D.2}
$$

Table D.1: Incoming polarisations for photoemission experiments.

Year	Author(s)	Molecule	Substrate	ccw.	lin.	cw.
2011	Göhler et al.[22]	50-bp dsDNA	Au(111)	22	0	−22
		40-bp dsDNA	Au(poly.)	−4	2	6
		50-bp dsDNA		−4	2	6
		78-bp dsDNA		−4	2	6
2013	Mishra et al.[30]	Bacteriorhodopsin	Au(poly.)[a]	−4	2	6
			Al(poly.)	0	0	0
2015	Kettner et al.[31]	AL5 oligopeptide	Au(poly.)[a]	−4	2	6
		AL6 oligopeptide		−4	2	6
		AL7 oligopeptide		−4	2	6
2018	Kettner et al.[27]	M-helicene	Cu(332)	0	0	0
		P-helicene		0	0	0
		M-helicene	Ag(110)	3	0	−3
		P-helicene		3	0	−3
		M-helicene	Au(111)	27	0	−24
		P-helicene		27	0	−24
2019	Ghosh et al.[32]	L-CuO film (20 nm)	Au(111)	–	0	–
		D-CuO film (20 nm)		–	0	–

[a] The values were not reported and have been assumed similar to the experiments on dsDNA above.

BIBLIOGRAPHY

[1] S. Dalum and P. Hedegård, “Theory of Chiral Induced Spin Selectivity”, Nano Lett. **19**, 5253–5259 (2019).

[2] W. T. Kelvin, *The molecular tactics of a crystal*, in collab. with University of Michigan (Oxford, Clarendon Press, 1894), 65 pp.

[3] H. D. Flack, “Louis Pasteur’s discovery of molecular chirality and spontaneous resolution in 1848, together with a complete review of his crystallographic and chemical work”, Acta Cryst A **65**, 371–389 (2009).

[4] R. S. Cahn, C. Ingold, and V. Prelog, “Specification of Molecular Chirality”, Angewandte Chemie International Edition in English **5**, 385–415 (1966).

[5] L. Pasteur, “Memoires sur la relation qui peut exister entre la forme crystalline et al composition chimique, et sur la cause de la polarization rotatoire”, Compt. rend. **26**, 535–538 (1848).

[6] T. L. V. Ulbricht and F. Vester, “Attempts to induce optical activity with polarized β-radiation”, Tetrahedron **18**, 629–637 (1962).

[7] A. S. Garay, “Origin and Role of Optical Isomery in Life”, Nature **219**, 338–340 (1968).

[8] W. A. Bonner, M. a. V. Dort, and M. R. Yearian, “Asymmetric degradation of DL-leucine with longitudinally polarised electrons”, Nature **258**, 419–421 (1975).

[9] L. A. Hodge, F. B. Dunning, G. K. Walters, R. H. White, and G. J. Schroepfer, “Degradation of DL -leucine with longitudinally polarised electrons”, Nature **280**, 250–252 (1979).

[10] P. S. Farago, “Spin-dependent features of electron scattering from optically active molecules”, J. Phys. B: At. Mol. Phys. **13**, L567–L571 (1980).

[11] M. J. M. Beerlage, P. S. Farago, and M. J. V. d. Wiel, “A search for spin effects in low-energy electron scattering from optically active camphor”, J. Phys. B: At. Mol. Phys. **14**, 3245–3253 (1981).

[12] D. M. Campbell and P. S. Farago, “Electron optic dichroism in camphor”, J. Phys. B: At. Mol. Phys. **20**, 5133–5143 (1987).

[13] S. Mayer and J. Kessler, “Experimental Verification of Electron Optic Dichroism”, Phys. Rev. Lett. **74**, 4803–4806 (1995).

[14] C. Nolting, S. Mayer, and J. Kessler, "Electron dichroism - new data and an experimental cross-check", J. Phys. B: At. Mol. Opt. Phys. **30**, 5491–5499 (1997).

[15] I. M. Smith, D. G. Thompson, and K. Blum, "Chiral effects in electron scattering by molecules using a continuum multiple scattering method", J. Phys. B: At. Mol. Opt. Phys. **31**, 4029–4058 (1998).

[16] R. Naaman, "Autobiography of Ron Naaman", J. Phys. Chem. C **117**, 22173–22174 (2013).

[17] K. Ray, S. P. Ananthavel, D. H. Waldeck, and R. Naaman, "Asymmetric Scattering of Polarized Electrons by Organized Organic Films of Chiral Molecules", Science **283**, 814–816 (1999).

[18] I. Carmeli, V. Skakalova, R. Naaman, and Z. Vager, "Magnetization of Chiral Monolayers of Polypeptide: A Possible Source of Magnetism in Some Biological Membranes", Angewandte Chemie International Edition **41**, 761–764 (2002).

[19] I. Carmeli, Z. Gefen, Z. Vager, and R. Naaman, "Alternation between modes of electron transmission through organized organic layers", Phys. Rev. B **68**, 115418 (2003).

[20] M. Eckshtain-Levi, E. Capua, S. Refaely-Abramson, S. Sarkar, Y. Gavrilov, S. P. Mathew, Y. Paltiel, Y. Levy, L. Kronik, and R. Naaman, "Cold denaturation induces inversion of dipole and spin transfer in chiral peptide monolayers", Nature Communications **7**, 10744 (2016).

[21] S. G. Ray, S. S. Daube, G. Leitus, Z. Vager, and R. Naaman, "Chirality-Induced Spin-Selective Properties of Self-Assembled Monolayers of DNA on Gold", Phys. Rev. Lett. **96**, 036101 (2006).

[22] B. Göhler, V. Hamelbeck, T. Z. Markus, M. Kettner, G. F. Hanne, Z. Vager, R. Naaman, and H. Zacharias, "Spin Selectivity in Electron Transmission Through Self-Assembled Monolayers of Double-Stranded DNA", Science **331**, 894 (2011).

[23] Z. Xie, T. Z. Markus, S. R. Cohen, Z. Vager, R. Gutierrez, and R. Naaman, "Spin Specific Electron Conduction through DNA Oligomers", Nano Lett. **11**, 4652–4655 (2011).

[24] A.-M. Guo and Q.-f. Sun, "Spin-Selective Transport of Electrons in DNA Double Helix", Phys. Rev. Lett. **108**, 218102 (2012).

[25] R. Gutierrez, E. Díaz, R. Naaman, and G. Cuniberti, "Spin-selective transport through helical molecular systems", Phys. Rev. B **85**, 081404 (2012).

[26] E. Medina, F. López, M. A. Ratner, and V. Mujica, "Chiral molecular films as electron polarizers and polarization modulators", EPL **99**, 17006 (2012).

[27]M. Kettner, V. V. Maslyuk, D. Nürenberg, J. Seibel, R. Gutierrez, G. Cuniberti, K.-H. Ernst, and H. Zacharias, "Chirality-Dependent Electron Spin Filtering by Molecular Monolayers of Helicenes", J. Phys. Chem. Lett. **9**, 2025–2030 (2018).

[28]N. F. Mott and N. H. D. Bohr, "The scattering of fast electrons by atomic nuclei", Proceedings of the Royal Society of London. Series A, Containing Papers of a Mathematical and Physical Character **124**, 425–442 (1929).

[29]N. F. Mott and H. S. W. Massey, *The theory of atomic collisions*, 3rd ed, International series of monographs on physics (Clarendon Press, Oxford, 1965).

[30]D. Mishra, T. Z. Markus, R. Naaman, M. Kettner, B. Göhler, H. Zacharias, N. Friedman, M. Sheves, and C. Fontanesi, "Spin-dependent electron transmission through bacteriorhodopsin embedded in purple membrane", PNAS **110**, 14872–14876 (2013).

[31]M. Kettner et al., "Spin Filtering in Electron Transport Through Chiral Oligopeptides", J. Phys. Chem. C **119**, 14542–14547 (2015).

[32]K. B. Ghosh et al., "Controlling Chemical Selectivity in Electrocatalysis with Chiral CuO-Coated Electrodes", J. Phys. Chem. C **123**, 3024–3031 (2019).

[33]P. C. Mondal, P. Roy, D. Kim, E. E. Fullerton, H. Cohen, and R. Naaman, "Photospintronics: Magnetic Field-Controlled Photoemission and Light-Controlled Spin Transport in Hybrid Chiral Oligopeptide-Nanoparticle Structures", Nano Lett. **16**, 2806–2811 (2016).

[34]P. Roy, N. Kantor-Uriel, D. Mishra, S. Dutta, N. Friedman, M. Sheves, and R. Naaman, "Spin-Controlled Photoluminescence in Hybrid Nanoparticles Purple Membrane System", ACS Nano **10**, 4525–4531 (2016).

[35]J. M. Abendroth, N. Nakatsuka, M. Ye, D. Kim, E. E. Fullerton, A. M. Andrews, and P. S. Weiss, "Analyzing Spin Selectivity in DNA-Mediated Charge Transfer via Fluorescence Microscopy", ACS Nano **11**, 7516–7526 (2017).

[36]K. S. Kumar, N. Kantor-Uriel, S. P. Mathew, R. Guliamov, and R. Naaman, "A device for measuring spin selectivity in electron transfer", Phys. Chem. Chem. Phys. **15**, 18357–18362 (2013).

[37]I. Carmeli, K. S. Kumar, O. Heifler, C. Carmeli, and R. Naaman, "Spin Selectivity in Electron Transfer in Photosystem I", Angewandte Chemie International Edition **53**, 8953–8958 (2014).

[38]O. Ben Dor, N. Morali, S. Yochelis, L. T. Baczewski, and Y. Paltiel, "Local Light-Induced Magnetization Using Nanodots and Chiral Molecules", Nano Lett. **14**, 6042–6049 (2014).

[39]B. P. Bloom, V. Kiran, V. Varade, R. Naaman, and D. H. Waldeck, "Spin Selective Charge Transport through Cysteine Capped CdSe Quantum Dots", Nano Lett. **16**, 4583–4589 (2016).

[40]V. Kiran, S. R. Cohen, and R. Naaman, "Structure dependent spin selectivity in electron transport through oligopeptides", J. Chem. Phys. **146**, 092302 (2016).

[41]V. Kiran, S. P. Mathew, S. R. Cohen, I. Hernández Delgado, J. Lacour, and R. Naaman, "Helicenes—A New Class of Organic Spin Filter", Adv. Mater. **28**, 1957–1962 (2016).

[42]A. C. Aragonès et al., "Measuring the Spin-Polarization Power of a Single Chiral Molecule", Small **13**, 1602519 (2017).

[43]H. Al-Bustami, G. Koplovitz, D. Primc, S. Yochelis, E. Capua, D. Porath, R. Naaman, and Y. Paltiel, "Single Nanoparticle Magnetic Spin Memristor", Small **14**, 1801249 (2018).

[44]F. Tassinari, D. R. Jayarathna, N. Kantor-Uriel, K. L. Davis, V. Varade, C. Achim, and R. Naaman, "Chirality Dependent Charge Transfer Rate in Oligopeptides", Advanced Materials **30**, 1706423 (2018).

[45]G. Bullard, F. Tassinari, C.-H. Ko, A. K. Mondal, R. Wang, S. Mishra, R. Naaman, and M. J. Therien, "Low-Resistance Molecular Wires Propagate Spin-Polarized Currents", J. Am. Chem. Soc. **141**, 14707–14711 (2019).

[46]S. P. Mathew, P. C. Mondal, H. Moshe, Y. Mastai, and R. Naaman, "Non-magnetic organic/inorganic spin injector at room temperature", Appl. Phys. Lett. **105**, 242408 (2014).

[47]P. C. Mondal, N. Kantor-Uriel, S. P. Mathew, F. Tassinari, C. Fontanesi, and R. Naaman, "Chiral Conductive Polymers as Spin Filters", Advanced Materials **27**, 1924–1927 (2015).

[48]V. Varade, T. Markus, K. Vankayala, N. Friedman, M. Sheves, D. H. Waldeck, and R. Naaman, "Bacteriorhodopsin based non-magnetic spin filters for biomolecular spintronics", Phys. Chem. Chem. Phys. **20**, 1091–1097 (2018).

[49]H. Einati, D. Mishra, N. Friedman, M. Sheves, and R. Naaman, "Light-Controlled Spin Filtering in Bacteriorhodopsin", Nano Lett. **15**, 1052–1056 (2015).

[50]P. C. Mondal, C. Fontanesi, D. H. Waldeck, and R. Naaman, "Field and Chirality Effects on Electrochemical Charge Transfer Rates: Spin Dependent Electrochemistry", ACS Nano **9**, 3377–3384 (2015).

[51]T. J. Zwang, S. Hürlimann, M. G. Hill, and J. K. Barton, "Helix-Dependent Spin Filtering through the DNA Duplex", J. Am. Chem. Soc. **138**, 15551–15554 (2016).

[52]M. Gazzotti, S. Arnaboldi, S. Grecchi, R. Giovanardi, M. Cannio, L. Pasquali, A. Giacomino, O. Abollino, and C. Fontanesi, "Spin-dependent electrochemistry: Enantioselectivity driven by chiral-induced spin selectivity effect", Electrochimica Acta **286**, 271–278 (2018).

[53]A. Kumar, E. Capua, K. Vankayala, C. Fontanesi, and R. Naaman, "Magnetless Device for Conducting Three-Dimensional Spin-Specific Electrochemistry", Angewandte Chemie **129**, 14779–14782 (2017).

[54]S. Mishra, V. S. Poonia, C. Fontanesi, R. Naaman, A. M. Fleming, and C. J. Burrows, "Effect of Oxidative Damage on Charge and Spin Transport in DNA", J. Am. Chem. Soc. **141**, 123–126 (2019).

[55]A. Kumar, E. Capua, M. K. Kesharwani, J. M. L. Martin, E. Sitbon, D. H. Waldeck, and R. Naaman, "Chirality-induced spin polarization places symmetry constraints on biomolecular interactions", PNAS **114**, 2474–2478 (2017).

[56]E. Z. B. Smolinsky, A. Neubauer, A. Kumar, S. Yochelis, E. Capua, R. Carmieli, Y. Paltiel, R. Naaman, and K. Michaeli, "Electric Field-Controlled Magnetization in GaAs/AlGaAs Heterostructures–Chiral Organic Molecules Hybrids", J. Phys. Chem. Lett. **10**, 1139–1145 (2019).

[57]T. Dietl, A. Haury, and Y. Merle d'Aubigné, "Free carrier-induced ferromagnetism in structures of diluted magnetic semiconductors", Phys. Rev. B **55**, R3347–R3350 (1997).

[58]O. Ben Dor et al., "Magnetization switching in ferromagnets by adsorbed chiral molecules without current or external magnetic field", Nature Communications **8**, 14567 (2017).

[59]O. B. Dor, S. Yochelis, S. P. Mathew, R. Naaman, and Y. Paltiel, "A chiral-based magnetic memory device without a permanent magnet", Nat Commun **4**, 1–6 (2013).

[60]R. Gutierrez, E. Díaz, C. Gaul, T. Brumme, F. Domínguez-Adame, and G. Cuniberti, "Modeling Spin Transport in Helical Fields: Derivation of an Effective Low-Dimensional Hamiltonian", J. Phys. Chem. C **117**, 22276–22284 (2013).

[61]A.-M. Guo, E. Díaz, C. Gaul, R. Gutierrez, F. Domínguez-Adame, G. Cuniberti, and Q.-f. Sun, "Contact effects in spin transport along double-helical molecules", Phys. Rev. B **89**, 205434 (2014).

[62]A.-M. Guo and Q.-F. Sun, "Spin-dependent electron transport in protein-like single-helical molecules", PNAS **111**, 11658–11662 (2014).

[63]H.-N. Wu, Y.-L. Zhu, X. Sun, and W.-J. Gong, “Spin polarization and spin separation realized in the double-helical molecules”, Physica E: Low-dimensional Systems and Nanostructures **74**, 156–159 (2015).

[64]S. Matityahu, Y. Utsumi, A. Aharony, O. Entin-Wohlman, and C. A. Balseiro, “Spin-dependent transport through a chiral molecule in the presence of spin-orbit interaction and nonunitary effects”, Phys. Rev. B **93**, 075407 (2016).

[65]T.-R. Pan, A.-M. Guo, and Q.-F. Sun, “Spin-polarized electron transport through helicene molecular junctions”, Phys. Rev. B **94**, 235448 (2016).

[66]S. Matityahu, A. Aharony, O. Entin-Wohlman, and C. A. Balseiro, “Spin filtering in all-electrical three-terminal interferometers”, Phys. Rev. B **95**, 085411 (2017).

[67]E. Díaz, F. Domínguez-Adame, R. Gutierrez, G. Cuniberti, and V. Mujica, “Thermal Decoherence and Disorder Effects on Chiral-Induced Spin Selectivity”, J. Phys. Chem. Lett. **9**, 5753–5758 (2018).

[68]M. Geyer, R. Gutierrez, V. Mujica, and G. Cuniberti, “Chirality-Induced Spin Selectivity in a Coarse-Grained Tight-Binding Model for Helicene”, J. Phys. Chem. C (2019).

[69]E. Medina, L. A. González-Arraga, D. Finkelstein-Shapiro, B. Berche, and V. Mujica, “Continuum model for chiral induced spin selectivity in helical molecules”, J. Chem. Phys. **142**, 194308 (2015).

[70]K. Michaeli and R. Naaman, “Origin of spin dependent tunneling through chiral molecules”, arXiv:1512.03435 [cond-mat], arXiv: 1512.03435 (2015).

[71]S. Varela, V. Mujica, and E. Medina, “Effective spin-orbit couplings in an analytical tight-binding model of DNA: Spin filtering and chiral spin transport”, Phys. Rev. B **93**, 155436 (2016).

[72]E. Díaz, A. Contreras, J. Hernández, and F. Domínguez-Adame, “Effective nonlinear model for electron transport in deformable helical molecules”, Phys. Rev. E **98**, 052221 (2018).

[73]D. Nürenberg and H. Zacharias, “Evaluation of spin-flip scattering in chirality-induced spin selectivity using the Riccati equation”, Phys. Chem. Chem. Phys. **21**, 3761–3770 (2019).

[74]X. Yang, C. H. van der Wal, and B. J. van Wees, “Spin-dependent electron transmission model for chiral molecules in mesoscopic devices”, Phys. Rev. B **99**, 024418 (2019).

[75]J. C. Slater and G. F. Koster, “Simplified LCAO Method for the Periodic Potential Problem”, Phys. Rev. **94**, 1498–1524 (1954).

[76] P. Löwdin, “On the Non-Orthogonality Problem Connected with the Use of Atomic Wave Functions in the Theory of Molecules and Crystals”, J. Chem. Phys. **18**, 365–375 (1950).

[77] M. Elstner, D. Porezag, G. Jungnickel, J. Elsner, M. Haugk, T. Frauenheim, S. Suhai, and G. Seifert, “Self-consistent-charge density-functional tight-binding method for simulations of complex materials properties”, Phys. Rev. B **58**, 7260–7268 (1998).